NOTES

NR 21 (21) 2014

News of Science and Education

Sheffield
SCIENCE AND EDUCATION LTD
2014

News of Science and Education

Editor in chief: SERGIY YEKIMOV

Editorial board:
prof. Vaclav Helus, CSc.
prof. Jan Kuchar, CSc.
prof. Karel Hajek, CSc.
prof. Alena Svarcova, CSc.
prof. Jiri Cisar, CSc.
prof. Vera Winterova, CSc.
doc. PhDr. David Novotny, Ph.D.
doc. PhDr. Zdenek Salac, Ph.D.
prof. Pavel Suchanek, CSc.
prof. Katarzyna Hofmannova, CSc.
prof. Vaclav Grygar, CSc.
prof. Zuzana Syllova, CSc.
prof. Alena Sanderova, CSc.
prof. Marek Jerabek, CSc.
prof. Vera Perinova, CSc.
prof. Ing. Karel Marsalek, M.A., Ph.D.
prof. Ing. Jiri Smolik, M.A., Ph.D.

Technical editor:

Mgr. Helena Krzyzankova

Editorial address:

OFFICE 1, VELOCITY TOWER,
10 ST. MARY'S GATE, SHEFFIELD, S
YORKSHIRE, ENGLAND, S1 4LR

e-mail: praha@rusnauka.com

Date signed for printing , 10.12.2014
Publisher : Science and education LTD
Registered Number: 08878342
OFFICE 1, VELOCITY TOWER,10 ST. MARY'S GATE, SHEFFIELD, S YORKSHIRE, ENGLAND, S1 4LR

Common depth can't be increased.

Is not difficult to see, that there are no other cases.

Now the proof of Main Theorem follows from the fact, that common depth for every axiom of considered Frege system is no more than some constant and results of Lemma 2:

$$t^{F}_{\varphi_n} = \Omega(2^{3n}) = \Omega(\frac{n2^{2n}\sqrt{n2^{2n}}}{\sqrt{n^3}}) = \Omega(|\varphi_n|\sqrt{\frac{|\varphi_n|}{n^3}}) = \Omega(|\varphi_n|\sqrt{\frac{|\varphi_n|}{(\log_2(n)+2n)^3}}) = \Omega(|\varphi_n|\sqrt{\frac{|\varphi_n|}{\log_2{}^3(|\varphi_n|)}})$$

Note that & and $\vee$ in φ_n will be changed accordingly to $\neg(A \supset \neg B)$ and $\neg A \supset B$ during proof, which doesn't change common depth values of formulas.

4. Conclusion

In this paper the super linear lower bound is obtained for some sequence of formulas in a Frege system. It will be interesting to prove the same result for the other Frege systems.

Acknowledgment

This work is supported by Grant 13-1B246 of SSC of Goverment of RA.

References

1. S.A.Cook, A.R.Reckhow: The relative efficiency of propositional proof systems, Journal of Symbolic Logic, vol. 44, 2000, 21-29.
2. A.Nurijanyan: On the some condition of proofs in Intuitionistic and Minimal propositional calculi, Sbornik ?Molodoy nauchnij sotrudnic?, YGU, Yerevan, vol. 2(34), 1981, 42-50.
3. A.Chubaryan, H.Nalbandyan: Comparison of proof sizes in Frege systems and substitution Frege systems, International Journal "Information Theories and Applications", Vol. 17, Number 2, 2010, 146-153.
4. A.A.Chubaryan: Comparison of proof sizes in systems and substitution systems of Frege, Izvestiya NAN Armenii, Matematika, vol. 35, No. 5, 2002, 71-84.

CONTENT

TECHNICAL SCIENCES

MATHEMATICS

It is not possible to use modus ponens when small premise is axiom 2 and big premise is axiom 3.

Case 6. B = $Des_1(3,1)$.

Small premise: $(\neg A \supset B) \supset ((\neg A \supset \neg B) \supset A)$

Big premise:

$((\neg A \supset B) \supset ((\neg A \supset \neg B) \supset A)) \supset (C \supset ((\neg A \supset B) \supset ((\neg A \supset \neg B) \supset A)))$

Descendant: $C \supset ((\neg A \supset B) \supset ((\neg A \supset \neg B) \supset A))$

There are two common essential subformulas $\neg A \supset B$ and $\neg A \supset \neg B$. Each of them increased by 1 in depth, so common depth increased by 2. The prove can't have formula like $Des_2(3,1)$, because in that case its big premise will be $Des_1(3,1)$ and as descendant we will have already proven formula.

Case 7. B = $Des_1(3,2)$.

Small premise: $(\neg A \supset B) \supset ((\neg A \supset \neg B) \supset A)$

Big premise:

$((\neg A \supset B) \supset ((\neg A \supset \neg B) \supset A)) \supset (((\neg A \supset B) \supset (((\neg A \supset \neg B) \supset A) \supset C)) \supset ((\neg A \supset B) \supset C))$

Descendant: $((\neg A \supset B) \supset (((\neg A \supset \neg B) \supset A) \supset C)) \supset ((\neg A \supset B) \supset C)$

There are two common independent essential subformulas $\neg A \supset B$ and $\neg A \supset \neg B$. First's depth increased from 1 to 2, other's depth increased from 2 to 4. Common depth increased by 3.

Invalid case. B = $Des_1(3,3)$.

It is not possible to use modus ponens when small and big premises are both axiom 3.

Case 8. B = $Des_2(1,2)$.

Small premise: $A \supset ((B \supset A) \supset C))$

Big premise $Des_1(1,2)$: $((A \supset ((B \supset A) \supset C)) \supset (A \supset C))$

Descendant: $A \supset C$

Common depth can't be increased.

Case 9. B = $Des_2(1,3)$.

Small premise: $(\neg A \supset \neg(B \supset \neg A)$

Big premise $Des_1(1,3)$: $((\neg A \supset \neg(B \supset \neg A)) \supset A)$

Descendant: A

Common depth can't be increased.

Case 10. B = $Des_2(2,2)$.

Small premise: $((A \supset B) \supset (((A(B \supset C)) \supset (A \supset C)) \supset D)$

Big premise: $(((A \supset B) \supset (((A(B \supset C)) \supset (A \supset C)) \supset D)) \supset ((A \supset B) \supset D))$

Descendant: $(A \supset B) \supset D)$

Common depth can't be increased.

Case 11. B = $Des_2(3,2)$.

Small premise: $(\neg A \supset B) \supset (((\neg A \supset \neg B) \supset A) \supset C)$

Big premise: $((\neg A \supset B) \supset (((\neg A \supset \neg B) \supset A) \supset C)) \supset ((\neg A \supset B) \supset C)$

Descendant: $(\neg A \supset B) \supset C$

Big premise: $(A \supset (B \supset A)) \supset (C \supset (A \supset (B \supset A)))$,

Descendant: $(C \supset (A \supset (B \supset A)))$

Small premise has only one independent essential subformula $B \supset A$, which is not essential in Descendant formula. The prove can't have formula like $Des_2(1,1)$, because in that case its big premise will be $Des_1(1,1)$ and as result we will have useless formula $A \supset (B \supset A)$, which was already proven before.

Case 2. B = $Des_1(1,2)$.

Small premise: $A \supset (B \supset A)$,

Big premise: $(A \supset (B \supset A)) \supset ((A \supset ((B \supset A) \supset C)) \supset (A \supset C))$,

Descendant: $((A \supset ((B \supset A) \supset C)) \supset (A \supset C))$

It is easy to see that $B \supset A$ is independent essential both in small premise and descendant. In small premise it has depth equal to 1 and in descendant equal to 3. So difference will be 2 in this case. As there are no other common essential subformulas common depth will be changed by 2.

Case 3. B = $Des_1(1,3)$.

Small premise: $\neg A \supset (B \supset \neg A)$,

Big premise: $(\neg A \supset (B \supset \neg A)) \supset ((\neg A \supset \neg(B \supset \neg A)) \supset A)$,

Descendant: $((\neg A \supset \neg(B \supset \neg A)) \supset A)$

$(B \supset \neg A)$ is independent essential both in small premise and descendant. In small premise it has depth equal to 1 and in descendant equal to 2. So difference will be 1 in this case. As there are no other common independent essential subformulas common depth will be changed by 1.

Case 4. B = $Des_1(2,1)$.

Small premise: $(A \supset B) \supset ((A \supset (B \supset C)) \supset (A \supset C))$,

Big premise:

$((A \supset B) \supset ((A \supset (B \supset C)) \supset (A \supset C))) \supset (D \supset ((A \supset B) \supset ((A \supset (B \supset C)) \supset (A \supset C))))$

Descendant: $(D \supset ((A \supset B) \supset ((A \supset (B \supset C)) \supset (A \supset C))))$

There are three ($A \supset B$, $B \supset C$, $A \supset C$) common independent essential subformulas in small premise and descendant. Depth of each of them increased by 1 in descendant subformula, so the common depth will be increased by 3 in descendant formula.

Case 5. B = $Des_1(2,2)$.

Small premise: $((A \supset B) \supset ((A \supset (B \supset C)) \supset (A \supset C)))$

Big premise:

$((A \supset B) \supset ((A \supset (B \supset C)) \supset (A \supset C))) \supset (((A \supset B) \supset (((A(B \supset C)) \supset (A \supset C)) \supset D)) \supset ((A \supset B) \supset D))$

Descendant: $(((A \supset B) \supset (((A(B \supset C)) \supset (A \supset C)) \supset D)) \supset ((A \supset B) \supset D))$

There are 3 common independent essential subformulas with 1 increase in depth. Common depth will be increased by 3.

Invalid case. B = $Des_1(2,3)$.

Aleksander A. Sirota
Ph. D. (Tech.), Associate Professor
Yuri G. Shcherbak
Ph. D. (Tech.), Associate Professor
Petro Mohyla Black Sea State University,Ukraine

FUEL ECONOMY OF MARINE MEDIUM-SPEED DIESEL ENGINE USING SMALL ADDITIVES OF HYDROGEN TO THE DIESEL FUEL, THAT PERFORMANCE ACCORDING TO THE SCREW CHARACTERISTIC

Abstract

Results of a pilot study influence of small hydrogen additives to the main fuel are given in work on profitability the medium-speed of diesels with pressurization of the small power, that performance according to the screw characteristic. It is defined that small hydrogen additions to basic fuel (0.04 to 0.12 %) in medium-speed supercharged diesel engine 1ЧН 20/27 result in improved fuel efficiency of the engine; in such a case the absolute fuel saving can reach 14.5 g/(kW·h), and relative fuel saving can be up to 6 %.

Key words: *medium-speed of diesels, hydrogen additions; specific fuel consumption; economy of diesel fuel; screw characteristic*

I. INTRODUCTION

Atmospheric air condition, which affects climate and biosphere of the Earth, is crucial for human life and survival of flora and fauna. Under the current conditions of human society development, increasingly greater attention is paid to qualitative improvement of the atmospheric air resource and its protection. Generation of various kinds of energy causes pollution of the atmosphere. Today, internal combustion engines (ICE) are the most common source of mechanical energy for means of transport. When running, these engines besides exhaust gases (EG) discharge a number of toxic compounds to the atmosphere thus causing considerable changes to the biosphere.

Significant effect on the atmospheric air pollution is exerted by diesel engines which are presently the most energy efficient heat engines. For instance, combustion of 1 kg diesel oil causes emission of 80 to 100 g toxic components [1]. Having much lower CO and hydrocarbon emissions vs gasoline engines, the diesel engine EG have sufficiently high toxicity due to high NOx, soot and aldehyde content.

The harmful components are extremely hazardous for human and animal health, and result in reduced yields and livestock farming productivity, failure of construction

materials, and elevated concentration of hazardous substances in domestic environment and work spaces.

At present, the issues associated with environmental safety of transport facilities are among the top priority ones.

One of the ways to reduce toxic content of diesel engine EG is improvement of the cylinder combustion process due to small (in weight) hydrogen additions to diesel oil.

Several authors have researched working processes of four-stroke high-speed naturally-aspirated engines (2ЧН 10.5/13, 2ЧН 13.5/14), with hydrogen supplied to the air intake system.

The researches have shown that even minor hydrogen addition makes the combustion process different. For instance, hydrogen supply amounting to 0.5 to 2.0 % of diesel fuel weight improves efficient specific fuel consumption by 2 to 9 % [2 – 7]. At the same time, EG soot content decreases by 35 % and NOx content decreases by 30 to 40 % [8]; while 5 % hydrogen supply can 2.4 times reduce NOx content [9]. However, hydrogen supply of over 5 to 9 % impairs its efficiency as an activating agent.

It is common knowledge that rather good results in improvement of diesel engine environmental performance and fuel efficiency can be achieved by alternate methods, not only through hydrogen additions to fresh charge of air:

– hydrogen gas supply to diesel engine cylinders via injection valve within compression stroke in the period after valves closing and before diesel oil supply [9];

– hydrogen gas supply via a special dual-fuel injector [8];

– hydrogen gas supply via a special mixing unit upstream a fuel injector [10].

The above alternate methods of hydrogen adding to diesel oil will have ambiguous effect onto energy efficiency of an updated engine (engine with hydrogen additive supply into cylinders).

Using one of the above hydrogen supply methods for marine diesel engines will, on the one hand, sophisticate the fuel supply system and subsequently increase a price for an updated engine; on the other hand, this will result in significantly decreased amount of hydrogen addition (tens of times) and therefore in lower operating expenses for hydrogen accumulation or production.

For example, according to the data [1], direct adding only 0.1 % hydrogen to diesel oil gives decrease in engine expenditures by 5 to 7 % on the average, NOx emission by 30 to 40 %, and soot content by 30 to 50 %.

All literature data known to us, as well as researches by various authors in hydrogen adding to fuel both with fresh air charge [2 – 7], and directly into cylinders [8], cover diesel engines with relatively small cylinder output (about 7 to 15 kW) installed on board small crafts and boats. However, in actual practice, e.g. on board small and medium fishing and cargo ships, the main and auxiliary engines are generally four-stroke medium-speed supercharged engines with 50 to 120 kW cylinder output.

Besides, there are no literature data on researches in effect of small hydrogen additions to basic fuel on basic operating parameters of the above engines. Therefore, aiming to study applicability of small hydrogen additions to basic fuel for such engines,

$$\varphi_n = \&_{j=1}^{2^n-1}\ \psi_{\sigma^1}^{j} \vee (\&_{j=1}^{2^n-1}\ \psi_{\sigma^2}^{j} \vee (\ldots \vee \&_{j=1}^{2^n-1}\ \psi_{\sigma^{2^n}}^{j})\ldots)$$

Where:

$$\&_{j=1}^{2^n-1}\ \psi_{\sigma^k}^{j} = (\psi_{\sigma^k}^{1}\ \&\ (\psi_{\sigma^k}^{2}\ \&\ (\ldots\ \&\ \psi_{\sigma^k}^{2^n-1})\ldots)$$

So the depth of $\psi_{\sigma^k}^{j}$ will be:

$$depth(\psi_{\sigma^k}^{j}) = k + j$$

And common depth for all independent essential sub formulas will be:

$$Cd(\varphi_n) = \sum_{k=1}^{2^n}\sum_{j=1}^{2^n-1} k + j = \sum_{k=1}^{2^n}(k + (2^n - 1)2^{n-1}) =$$

$$= 2^{n-1}(2^n + 1) + 2^n(2^n - 1)2^{n-1} = \Theta(2^{3n})$$

3. Main result

The main result of the paper is the following statement.

Main Theorem.

$$t_{\varphi_n}^{\mathsf{F}} = \Omega(|\varphi_n| \sqrt{\frac{|\varphi_n|}{\log_2^3(|\varphi_n|)}})$$

To prove the theorem let us in addition introduce some notions and prove some auxiliary statements.

If formula B is inferred from formulas A and $\mathsf{A} \supset \mathsf{B}$ by modus ponens, then A is called small premise, $\mathsf{A} \supset \mathsf{B}$ - big premise and B is called descendant.

We denote by $Des_1(i, j)$ every formula, which is descendant of axioms number i ($i = 1,2,3$) as small premise and number j ($j = 1,2,3$) as big premise, and as $Des_2(i, j)$ every formula, which is descendant of some formula as small premise and $Des_1(i, j)$ as big premise.

Lemma 1. Every formula, which is big premise in some right-chopping proof, must be or axiom, or $Des_1(i, j)$, or $Des_2(i, j)$.

Proof. follows from the definition right-chopping proof.

Lemma 2. If some formula B is inferred from formulas A and $\mathsf{A} \supset \mathsf{B}$ by modus ponens in right-chopping proof, then $Cd(\mathsf{B}) \le max(Cd(\mathsf{A}), Cd(\mathsf{A} \supset \mathsf{B})) + 3$

Proof. Note, that every essential subformula of B must be or essential subformula of A, or essential subformula of $\mathsf{A} \supset \mathsf{B}$. If it is essential subformula of $\mathsf{A} \supset \mathsf{B}$, then it is not essential in A and in this case $Cd(\mathsf{B}) \le Cd(\mathsf{A} \supset \mathsf{B})$. Therefore we can consider only the cases, when essential subformula of B is essential subformula of A. From Lemma 1 we can say that B has one of following 11 forms. Lets discuss them one by one.

Case 1. $\mathsf{B} = Des_1(1,1)$. This means that both small and big premises have form of first axiom:

Small premise: $A \supset (B \supset A)$,

The analogous statement for classical Hilbert style systems is not valid, but for above mentioned Frege system F the following statement is proved in [3].

Proposition 1. Every F-proof of a formula φ can be transformed into right-chopping proof of φ, the t-complexity of which is no more than t-complexity of original proof.

For proving the main results we use also the notion of *essential subformulas*, introduced in [4].

Let F be some formula and $Sf(F)$ is the set of all non-elementary subformulas of formula F.

For every formula F, for every $\varphi \in Sf(F)$ and for every variable p by F_{φ}^{p} is denoted the result of the replacement of the subformulas φ everywhere in F by the variable p. If $\varphi \notin Sf(F)$, then F_{φ}^{p} is F.

We denote by $Var(F)$ the set of variables in F.

Definition 1. Let p be some variable that $p \notin Var(F)$ and $\varphi \in Sf(F)$ for some tautology F. We say that φ is an ***essential subformula*** in F iff F_{φ}^{p} is non-tautology.

We denote by $Essf(F)$ the set of essential subformulas in F.

If F is minimal tautology, i.e. F is not a substitution of a shorter tautology, then $Essf(F) = Sf(F)$.

In [4] the following statement is proved.

Proposition 2. Let F be a minimal tautology and $\varphi \in Essf(F)$, then in every F-proof of F subformula φ must be essential at least in some axiom, used in proof.

Definition 2. The essential subformula of tautology F is called ***independent essential subformula*** of F, if no other essential subformula of F is the subformula of it.

We denote by $IndEssf(F)$ the set of independent essential subformulas in F.

The total number of symbols, appearing in a formula φ, we call size of φ and denote by $|\varphi|$.

Definition 3. Let φ be some tautology. The total sum of maximum depths of occurrences in φ for different independent essential subformulas is called **common depth** of φ.

We denote by $Cd(\varphi)$ the common depth of φ. For future consideration the key role play tautologies $\varphi_n = TTM_{n,2^{n-1}}$, where

$$TTM_{n,m} = \vee_{(\sigma_1,\ldots,\sigma_n)\in E^n} \ \&_{j=1}^{m} \ \vee_{i=1}^{n} p_{ij}^{\sigma_i}$$

It is not difficult to see that $|\varphi_n| = n2^{2n}$ and $Cd(\varphi_n) = \Theta(2^{3n})$. It is easy to see that each $\vee_{i=1}^{n} p_{ij}^{\sigma_i}$ subformula is independent essential for φ_n. Lets denote $\psi_{\sigma}^{j} = \vee_{i=1}^{n} p_{ij}^{\sigma_i}$, where $\sigma = (\sigma_1,\ldots,\sigma_n)$. φ_n will look like this:

$$\varphi_n = \vee_{\sigma\in E^n} \ \&_{j=1}^{2^n-1} \ \psi_{\sigma}^{j}$$

In tree like form it will be:

we have developed a test bed on the basis of a four-stroke medium-speed supercharged engine, type 1ЧН 20/27, with about 60 kW cylinder output [10].

The purpose of this research is to identify effect of small hydrogen additions to basic fuel on efficiency of medium-speed supercharged small-power engines, with engine performance being propeller and hull dependent.

II. EXPERIMANTAL STADY OF 1ЧН 20/27 DIESEL ENGINE RUNNING WITH HYDROGEN ADDITIONS, AND REVIEW OF RESULTS

The first set of experiments has been conducted for 1ЧН 20/27 engine under constant temperature of compressor inlet air $T_{в}$ =314 K.

With engine performance being propeller and hull dependent, the engine has been tested with crankshaft speeds of 476, 546, 580 and 600 rpm, i.e. with relative load within 0.5 to 1.0.

Efficient specific consumption of diesel oil has been determined for all running conditions of diesel engine both without hydrogen additions g_e, g/(kW·h), and with hydrogen additions $g_e^{H_2}$, g/(kW·h).

Mass additions of hydrogen under various conditions have been determined as a ratio of hydrogen specific consumption g_{H_2}, g/(kW·h) to the value g_e, g/(kW·h), i.e.

$$m_{H_2} = \frac{g_{H_2}}{g_e} \cdot 100, \quad \%.$$

The size of these additions has been widely varied (within 0.04 to 0.12 %), and value of efficient specific fuel consumption $g_e^{H_2}$, g/(kW·h) has been determined.

The resulting test data have enabled calculation of the engine below key parameters under every running condition:

– absolute and relative saving of diesel oil with hydrogen being supplied into diesel engine cylinder, respectively:

$$\Delta g_e^{H_2} = g_e - g_e^{H_2}, \ \text{g/(kW·h)}, \tag{1a}$$

$$\Delta \bar{g}_e^{H_2} = \frac{\Delta g_e^{H_2}}{g_e} \cdot 100, \ \%; \tag{1b}$$

– effective efficiency of diesel engine without hydrogen additions and with hydrogen additions, respectively:

$$\eta_e = \frac{3600 \cdot 10^5}{g_e \cdot 42700}, \% \ ; \quad \eta_e^{H_2} = \frac{3600 \cdot 10^5}{b_e \cdot 42700}, \% \ , \tag{2}$$

where b_e is corrected specific fuel consumption of a diesel engine including hydrogen additions, which is calculated by the formula

$$b_e = g_e^{H_2} + 2{,}83 \cdot g_{H_2}, \text{ g/(kW·hr)}. \quad (3)$$

The factor 2.83 in the formula (3) is a ratio of hydrogen calorific value $Q_H^{H_2}$ to diesel oil calorific value $Q_H^{ДТ}$, i.e. $Q_H^{H_2} / Q_H^{ДТ}$=2.83. For this purpose the following values have been assumed $Q_H^{H_2}$=121000 kJ/kg and $Q_H^{ДТ}$= 42700 kJ/kg;

– absolute and relative change in diesel engine effective efficiency

$$\Delta \eta_e^{H_2} = \eta_e^{H_2} - \eta_e, \% \quad (4)$$

$$\Delta \bar{\eta}_e^{H_2} = \Delta \eta_e^{H_2} / \eta_e, \% \quad (5)$$

Diesel oil consumption by engine using hydrogen additions can be calculated by means of influence coefficient K_{H_2} determined as a ratio

$$K_{H_2} = g_e^{H_2} / g_e, \quad (6)$$

then

$$g_e^{H_2} = K_{H_2} \cdot g_e, \text{ g/(kW·h)}. \quad (7)$$

The test data acquired by us has enabled calculation of the coefficient K_{H_2} as a function of diesel engine relative load, size of hydrogen additions m_{H_2}, crankshaft speed n, rpm, and engine running performance. With diesel engine performance being propeller and hull dependent, the below empirical dependence has been obtained:

$$K_{H_2} = 1 - \frac{1{,}045 \cdot m_{H_2}}{n^{0.707}\left(0{,}0125 + m_{H_2}^2\right)}. \quad (8)$$

The formula (8) describes relationship $K_{H_2} = f(m_{H_2}, n)$ for 1ЧН 20/27 diesel engine with error within 3 % and is true for m_{H_2} = (0.04…0.12) and n = 476…600 rpm.

Fig. 1 shows influence coefficient K_{H_2} as a function of diesel engine crankshaft speed n and size of hydrogen additions m_{H_2}.

. We prove that in some Frege system the proof steps for some sequence of tautologies φ_n are at least $|\varphi_n| \sqrt{\frac{|\varphi_n|}{\log_2^3(|\varphi_n|)}}$ by order.

2. Preliminary

We shall use well known notions of propositional formula, tautology and depth of subformula occurrence in formula.

We shall use also generally accepted concepts of Frege system. A Frege system F uses a denumerable set of propositional variables, a finite, complete set of propositional connectives; F has a finite set of inference rules defined by a *figure* of the form $\frac{A_1 A_2 \ldots A_m}{B}$ (the rules of inference with zero hypotheses are the axioms schemes); F must be sound and complete, i.e. for each rule of inference $\frac{A_1 A_2 \ldots A_m}{B}$ every truth-value assignment, satisfying $A_1 A_2 \ldots A_m$, also satisfies B, and F must prove every tautology.

We assume further that F is a Frege system, whose language contains only the connectives $\supset$ and $\neg$.

The axiom-schemas are:

1. $A \supset (B \supset A)$
2. $(A \supset B) \supset ((A \supset (B \supset C)) \supset (A \supset C))$
3. $(\neg A \supset B) \supset ((\neg A \supset \neg B) \supset A)$

and inference rule is Modus ponens $\frac{A \quad A \supset B}{B}$.

We use also the well-known notions of proof and proof complexities. The proof in any system Φ (Φ-proof) is a finite sequence of such formulas, each being an axiom of Φ, or is inferred from earlier formulas by one of the rules of Φ. Note that every Φ-proof has an associated graph with nodes, labeled by formulas, and edges from A to B if formula B is the result of applying of some inference rule to A (perhaps with another formulas).

We define **t - complexity of proof** to be its length (= the total number of different proof formulae). The minimal **t - complexity of a formula** φ in a proof system Φ we denote by $t_\varphi \Phi$.

Let us recall the notion of right-chopping proof, introduced in [2]. For Intuitionistic and Minimal (Johansson's) Logic is proved the following statement:

If the axiom $F_1 \supset (F_2 \supset (\ldots \supset (F_m \supset G)\ldots)$ and the formulas $F_1, F_2, \ldots, F_m$ are used in the minimal (by steps) derivation of formula G by the successive applying of the rule modus ponens, then $m \le 2$, i.e. the length of branch, going to right and upwards from every node of the corresponding graph, is no more than 2. Such graph and hence the corresponding proof are called **right-chopping**.

Anahit Chubaryan
Doctor of Sciences, Full Professor of the Department of Informatics and Applied Mathematics, Yerevan State University, Yerevan, Armenia
Armen Mnatsakanyan
PhD Student of the Department of Informatics and Applied Mathematics, Yerevan State University, Yerevan, Armenia

SUPER LINEAR LOWER BOUNDS FOR STEPS OF PROOFS IN SOME FREGE SYSTEM

Abstract

It is known that in Frege systems together with trivial exponential upper bounds there are only $\Omega(n^2)$ bounds of proof size and $\Omega(n)$ bounds of proof steps for tautologies with the length n. We prove that in some Frege system for some sequence of tautologies φ_n the proof steps are at least $|\varphi_n|\sqrt{\frac{|\varphi_n|}{\log_2^3(|\varphi_n|)}}$ by order.

Keywords: Frege system, proof complexity, depth of occurrence of subformula, essential subformula.

ACM Classification Keywords: F.4.1 Mathematical Logic and Formal Languages, Mathematical Logic, Proof theory

1. Introduction

It is well known that the investigations of the propositional proof complexity are very important due to their relation to the main problem of the complexity theory: $P \stackrel{?}{=} NP$.

One of the most fundamental problems of the proof complexity theory is to find an efficient proof system for propositional calculus. There is a wide spread understanding that polynomial time computability is the correct mathematical model of feasible computation. According to the opinion, a truly "effective" system must have a polynomial size $p(n)$ proof for every tautology of size n. In [1] Cook and Reckhow named such a system a *super system*. They showed that if there exists a super system, then $NP = coNP$.

It is well known that many systems are not super. This question about Frege system, the most natural calculi for propositional logic, is still open. It is known that in Frege systems together with trivial exponential upper bounds there are only $\Omega(n^2)$ bounds of proof size and $\Omega(n)$ bounds of proof steps for tautologies with the length n

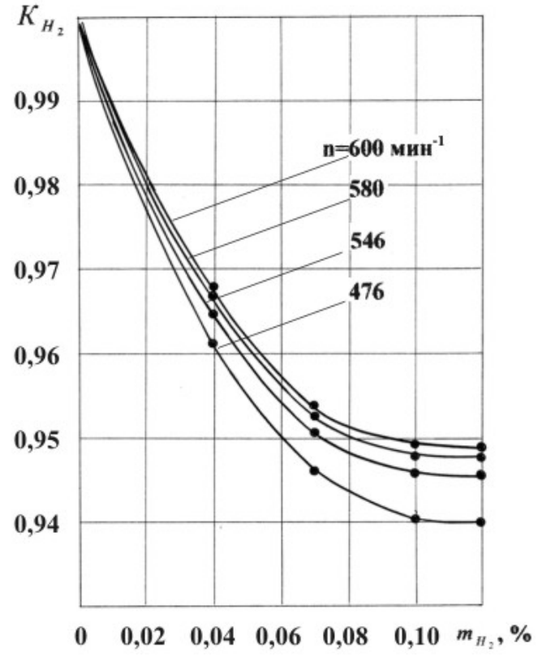

Fig. 1. Coefficient K_{H_2} dependence on size of hydrogen addition m_{H_2} to basic fuel and crankshaft speed n for 1ЧН 20/27 diesel engine, with engine performance being propeller and hull dependent

For instance, with m_{H_2} increasing from 0 to 0.12 %, value K_{H_2} decreases down to about 0.95 at the engine rated load (n = 600 rpm) and down to about 0.94 at 0.5 load of the rated one (n = 476 rpm). The dependencies shown imply that m_{H_2} increasing more than 0.1 % has nearly no effect on further decrease in K_{H_2}.

Fig. 2 shows results of experimental research in effect of crankshaft speed n and size of hydrogen additions m_{H_2} onto 1ЧН 20/27 diesel engine running efficiency.

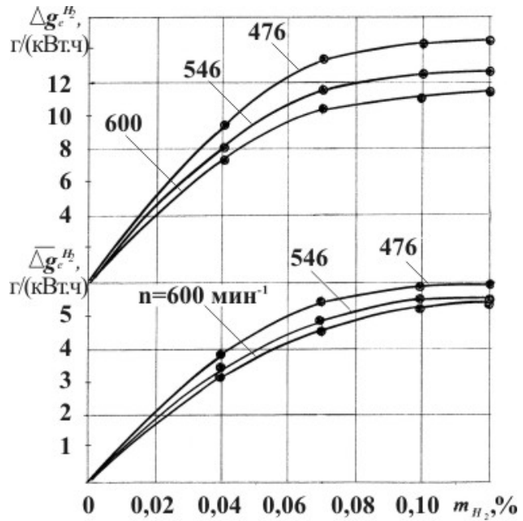

Fig. 2. Fuel saving indicators $\Delta g_e^{H_2}$ and $\Delta \overline{g}_e^{H_2}$ for 1ЧН 20/27 diesel engine, with engine performance being propeller and hull dependent, as a function of hydrogen addition size m_{H_2} to basic fuel and crankshaft speed *n*

For instance, increase in hydrogen addition m_{H_2} up to 0.12 % results in absolute fuel saving up to 14 g/(kW·h), and relative fuel saving up to 6 %. In this case, nearly no further growth in fuel saving is observed starting with m_{H_2} = 0.1 %.

It is worthy of note that hydrogen additions to diesel engine basic fuel under partial (shared) load conditions lead to more effect than under rated loads. For instance, addition m_{H_2} = 0.1 % under rated conditions (n = 600 rpm) enables about 11 g/(kW·h) saving, and with the same value of m_{H_2} and *n* = 476 rpm decrease in efficient specific fuel consumption can reach about 15 g/(kW·h).

Fig. 3 compares efficiency of 1ChN 20/27 diesel engine running with and without hydrogen additions to basic fuel. The data presented show that increase in hydrogen additions up to 0.12 % gives increase in engine absolute effective efficiency by $\Delta \eta_e^{H_2}$ up to 2.0 %, and relative value $\Delta \overline{\eta}_e^{H_2}$ increase up to 6.0 %. In this case better efficiency of diesel engine is observed during m_{H_2} growing up to about 0.1 %, and afterwards increase in hydrogen additions has no effect onto diesel engine performance.

It is worthy of note that hydrogen additions to diesel engine basic fuel gave better effect under partial (shared) load conditions of the engine. For instance, with *n* = 476 rpm and m_{H_2} = 0.1 %, the change $\Delta \overline{\eta}_e^{H_2}$ is about 6. 0 %, while under rated load (*n* = 600 rpm) $\Delta \overline{\eta}_e^{H_2}$ = 5 % .

REFERENCES

[1] Tanenbaum, T. Austin, Structured Computer Organization (6th Edition), Prentice Hall, 2012.
[2] W. Stallings, Operating Systems: Internals and Design Principles, Pearson Education, 2011.
[3] Hamacher, et. al., Computer Organization and Embedded Systems, McGraw-Hill Science/Engineering/Math, 2011.
[4] Orlov, S.P. Computer systems organization /S.P. Orlov, N.V. Efimushkina. – Samara: Samara State Technical University, 2011.

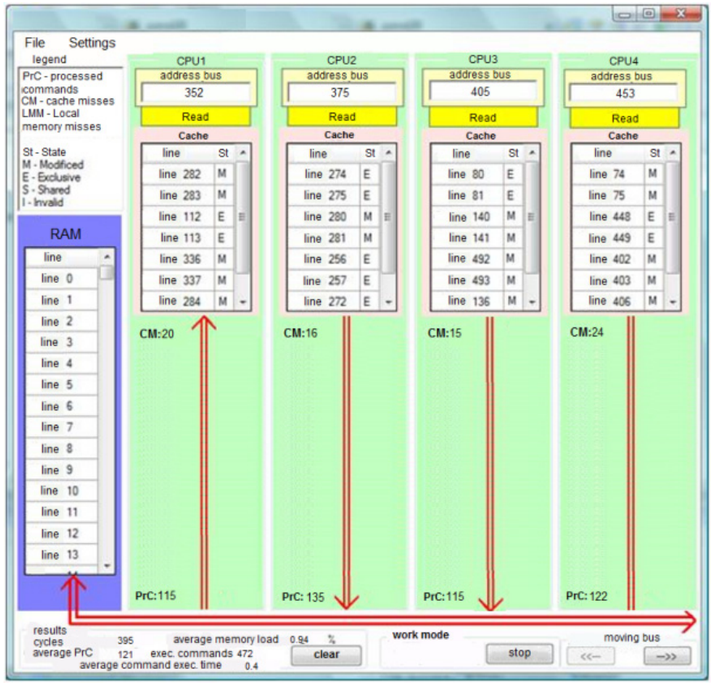

Fig. 7 System without local memory structure

The model allows researching the influence of the following system characteristics: the number of processors, the memory structures, and also the programming structure (the access memory instructions ratio). There is an opportunity to define effective conditions for the system operation, and also the maximum number of processors for similar structures.

V. CONCLUSION

The program complex contains three typical multiprocessor systems models. It is used in laboratory classes on subject «Architecture of the high-performance computing systems». Simulation models are developed with use of the universal environments (Delphi and C ++). Models were simplified to reproduce the functioning of main computer elements, their structures and operational states, and visualized to make material more understandable for the student. The experiments that can be conducted using the models help to analyze the computer parameters and find out the optimal operating modes with provided input information.

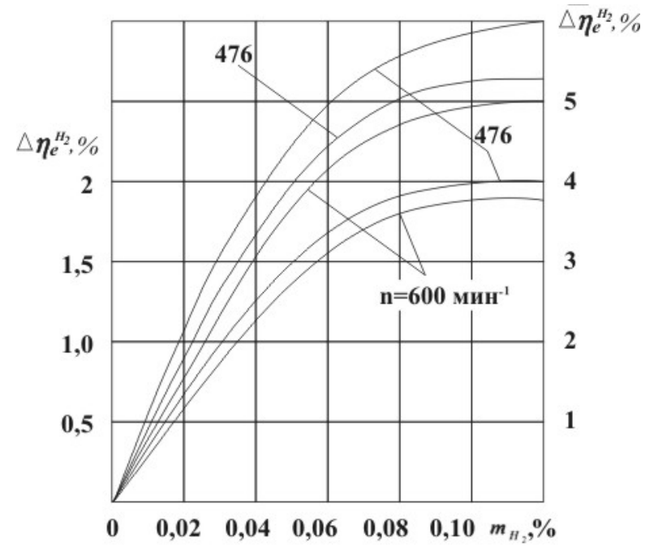

Fig. 3. 1ЧН 20/27 diesel engine running efficiency, with engine performance being propeller and hull dependent, as a function of m_{H_2} size of hydrogen addition to basic fuel and crankshaft speed *n*

III. CONCLUSIONS

1. Small hydrogen additions to basic fuel (0.04 to 0.12 %) in medium-speed supercharged diesel engine result in improved fuel efficiency of the engine; in such a case the absolute fuel saving can reach 14.5 g/(kW·h), and relative fuel saving can be up to 6 %.

2. Hydrogen additions of 0.04 to 0.12 % to diesel engine basic fuel improve the engine performance efficiency. For instance, the value $\Delta\eta_e^{H_2}$ increases up to 2.0 % at m_{H_2} = 0.1 %, and $\Delta\overline{\eta}_e^{H_2}$ increases up to 6.0 %.

REFERENCES

1. http://www.dissland.com/catalog/snizhenie_vrednih_vibrosov_prieksplu-atasii_dizel...
2. Sirota A.A.: Improving Fuel Efficiency of Marine Diesel Engines through Using Hydrogen as a Fuel Additive //Internal Combustion Engines. – Kharkov: NTU «KHPI», 2006. – № 1. – Pages 63-67.
3. Sirota A.A., A.I. Churakov A.I., O.A. Golikov O.A., Radchenko N.I. Hydrogen Additions to Carbon Fuel As the First Stage of Marine High-Speed ICE Conversion to Clean Hydrogen Fuel // Works of Electrodynamics Institute, National Academy of Sciences of Ukraine: Collection of Studies. – K.: Printing House of National Academy of Sciences of Ukraine. –2006. – Pages 111-114.

4. Syrota A., Radchenko N., Churacov A.: Increasing the Efficiency of High Speed Internal Combustion Engines by Hydrogen Adding to Fuel//Heat Transfer and Renewable Sources of Energy 2006. Szeczecin (Poland). – 2006. – Pages 207-211.
5. Syrota A.A., Radchenko N.I., Churacov A.I.: Improving Environmental Safety and Energy Efficiency of Marine High-Speed Internal Combustion Engines through Adding Hydrogen to Fuel // Collection of Studies National Shipbuilding University. – Mykolaiv: NUK, 2006. –№ 1 (406). – Pages 181- 186.
6. Syrota A.A., Radchenko N.I., Churacov A.I.: Hydrogen Additions to Fuel As a Way to Improve Efficiency of Marine High-Speed Diesel Engines // Collection of Studies, National Shipbuilding University. – Mykolaiv: NUK, 2006. – № 3 (408). – Pages 121- 127.
7. Sirota A.A.: Optimum Running Conditions of Trigeneration Marine Diesel Installations // Aerospace Engineering and Technology. – Kharkov: NTU «KHPI», 2007. – № 4(40). – Pages 29-34.
8. http://aomai.secna.ru:8080/Books/Files/Vestn_2000_02/10/10.htm.
9. http://elib.altstu.ru/elib/books/Filles/va2000_2/pages/14/14.htm.
10. Syrota O.A., Shcherbak Yu.G.: Test Bed to Research Effect of Hydrogen Additions on Running Performance of a Marine Medium-Speed Supercharged Engine // Materiály X mezinárodní vědecko-praktická konference «Věda a technologie – 2014». – Dil 33. Technicke vědy.: Praha. Publishing House «Education and Science» s.r.o. – Pages 28-34.
11. http://www.magistral-uz.com.ua./articles/vodorodnyj-koktejl-dlja-lokomotiva. html.

7) The number of lines copied in a cache and local memory for once (quantity of lines in the block).

There is an opportunity to change number of the processors from 4 to 32.

The model results are represented as:

1) The executed instruction and cycles quantities;
2) The average time of executed instruction;
3) The system bus average efficiency;
4) The processors cache misses quantity;
5) The local memory misses quantity;
6) The executed instruction average quantity.

The model uses the principle «locality of references». In it information census from the bottom level in the top is carried out by the consecutive addresses blocks of lines. The general structure of a subsystem is represented on the screen in the fig. 6.

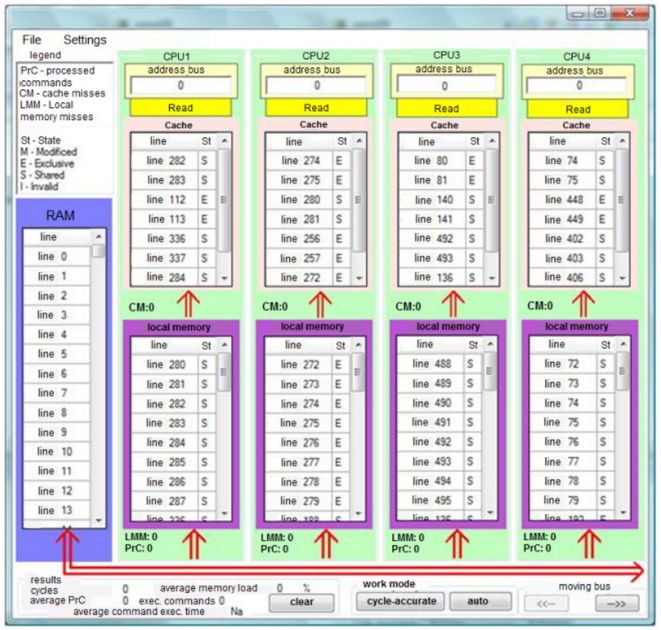

Fig. 6 General memory subsystem structure

The system without local memory screen form is given in fig. 7.

3) The efficiency coefficient;
4) The number of conflicts.

The modeling process screen form is presented in fig. 5.

The described model provides to research the influence of the number of processors and the RAM, and also parameters of tasks on the system characteristics.

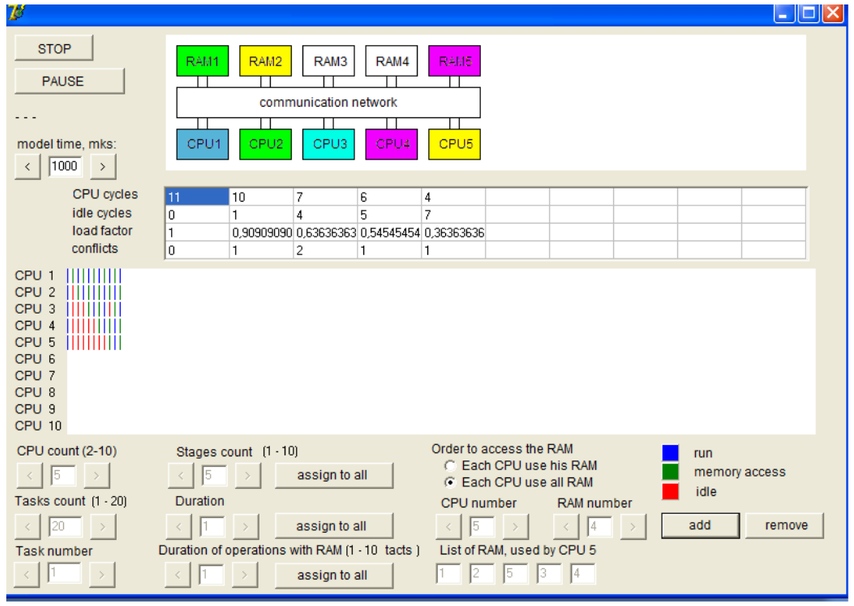

Fig. 5 The modeling process screen form

In a latest model the architecture of the multiprocessor UMA SMP computer system with the bus organization, the memory subsystem containing following main devices is investigated:

a) The main memory (RAM);
b) The cache memory;
c) The local memory.

Input data for modeling are:

1) The number of processors;
2) Total the number of memory access instruction;
3) Rate of read/write operations in the general mix;
4) The multiprocessor computer system configuration:
- Without cache and local memory;
- With cache memory;
- With cache and local memories.
5) RAM, local and cache memory capacities in lines;
6) RAM, local and cache memories read and write latencies in clock cycles;

Turymbetov T.A[1]., Aitkulov A.U[1]., Azhikhanov N.T[2]., Aimeshov Zh.A[2].
[1]Caspian State University of Technologies and Engineering named after Sh. Yessenov, Kazakhstan
[2]Kh.Yasavi International Kazakh-Turkish University, Kazakhstan

EVALUATION OF THE LIMIT CHANGES OF DEBIT WELLS AT PRESENCE IN THE FORMATION VERTICAL CRACKS

Abstract. *Ones of first crack which will form by hydraulic fracturing, this cracks in vertical plane, so-called vertical cracks. In this paper were obtained the formulas with by which to define maximum and minimum flow rates to the wells granting in the presence of formation of a crack in view of change of plasticity and elasticity of the reservoir formation fluids.*

Keywords: *well, debit, fracturing, plasticity, elasticity*

I. Introduction

The practice of developing oil and gas fields shows that when during the hydraulic fracturing on the formation in the around wellbore, in the wells primarily formed crack in the vertical plane, i.e. vertical cracks. To make a decision on doing hydrofracturing in the formation [1], with a view to undertake such work, for to increase productivity of the reservoir near the wellbore formation you must perform evaluation process calculations. In this regard, this paper is devoted research by evaluation of technological efficiency vertical fracture during hydraulic fracturing. To perform the work is considered a circular formation with radius supply circuit R_k.

II. The setting of the problem

If the radius of the external boundary $R_k \geq R_0$, that radius supply and cracks without much error can be taken for two confocal ellipse (Fig. 1).

If we take $K_2 = \infty$, i.e. assume that the pressure in the fracture $P_{cr} = P_w$, then for determining q_l and q_h (respectively low and high values of debit wells) you can use the solution outlined in the I.A. Charny [2]

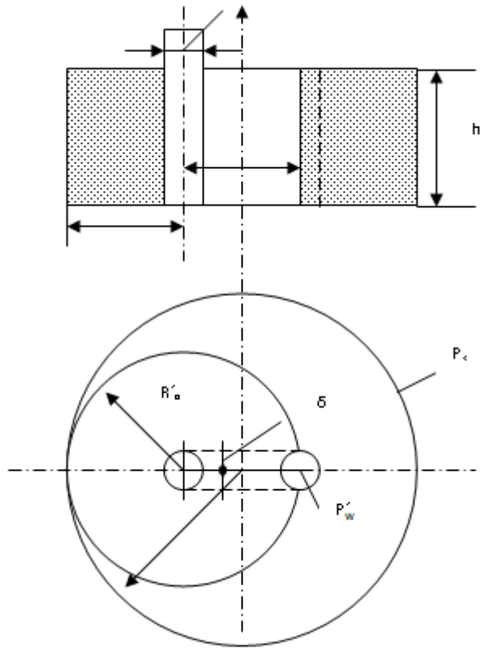

Fig. 1. Scheme of Arrangement of a vertical crack in a circular formation

Assuming that the inflow of liquid takes place not only to fracture (as adopted for the ellipse) but as well as the impact of self-wells on inflow will be considered a phenomenon inflow through not breach of the formation, then this stream will be much more inflow to the wellbore and fracture, i.e. will be more well production.

According to the decision, given in [2], inclusive of the results of [4], inflow to the crack (to ellipse) is given by:

$$q_l = \frac{2\Pi K_1 \cdot h \cdot \rho}{\mu} \cdot \frac{1 - \exp\left[-\alpha_{\kappa_1}\left(P_\kappa - P_w\right)\right]}{\alpha_{\kappa_1} \cdot \ln \frac{R_\kappa}{\frac{1}{4}\left(R_o + \delta\right)}} \qquad (1)$$

In that $\delta << R_o$, then the formula (29) has the form:

$$q_l = \frac{2\Pi K_1 \cdot h \cdot \rho}{\mu} \cdot \frac{1 - \exp\left[-\alpha_{\kappa_1}\left(P_\kappa - P_w\right)\right]}{\alpha_{\kappa_1} \cdot \ln \frac{R_\kappa}{\frac{1}{4}R_o}} \qquad (2)$$

From equation (2) shows that the flow is equivalent to a crack flow to the well with a radius $r_{eq} = \frac{1}{4}R_o$.

4) The execute stages quantity;
5) Duration of execution;
6) The access latency of memory;
7) The order of accesses to memory unit.

The model allows receiving the following results:
1) The processors operation clock cycles quantity;
2) Their idle time clock cycles quantity;
3) The processor efficiency coefficients;
4) Each processor conflicts quantity.

It is possible to change number of the processors and number of RAM modules from 2 to 10. The number of the tasks varies from 100 to 1000. The quantity of the execute stages, the execute times and the access memory times change from 1 to 10 steps. Initial data set screen form for complex containing the five processors and RAM is provided on fig. 4.

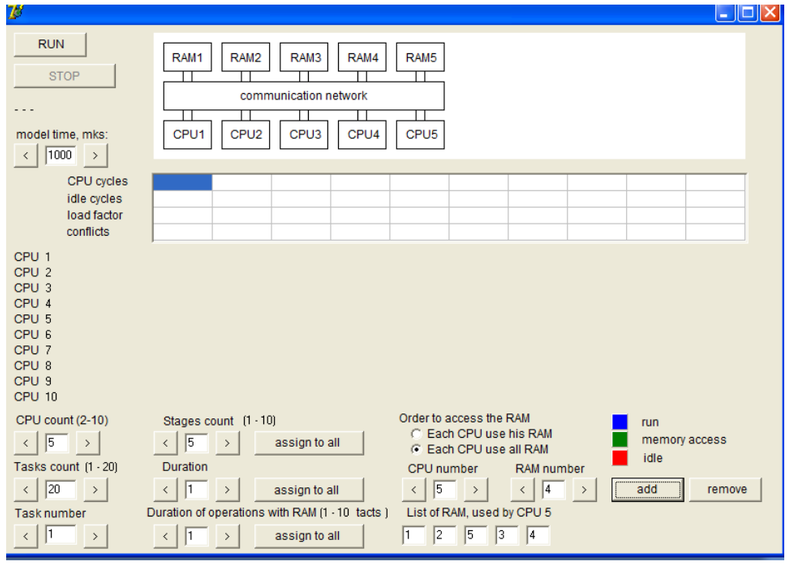

Fig. 4 Initial data set screen for five processors and RAM

The functioning processor is painted on the model scheme by its own the color. If the processor stands idle, it is signed by red color. The addressed RAM is painted over by the corresponding processor color. If the RAM is free, its color is white.

After model start in the form center the chart showing a condition of each processor in each step begins being under construction: blue color designates the account, green – the memory access and red – idle time.

During modeling the next statistics is obtained:
1) The processor operation cycles quantity;
2) The idle time cycles quantity;

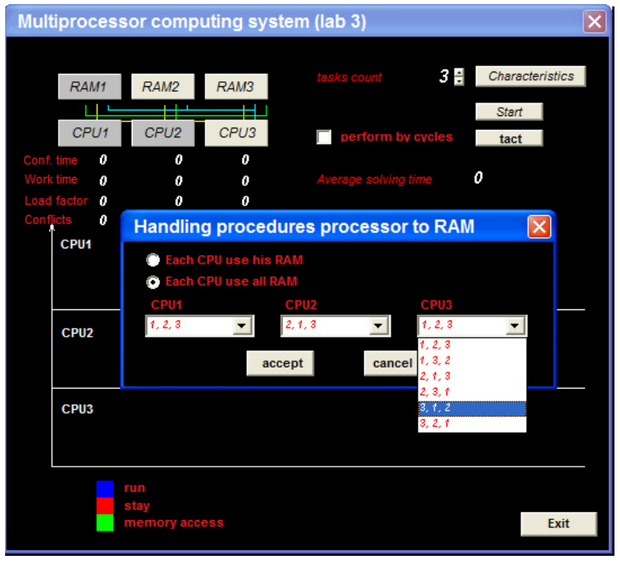

Fig. 2 The screen form for setting an order of CPU – RAM accesses

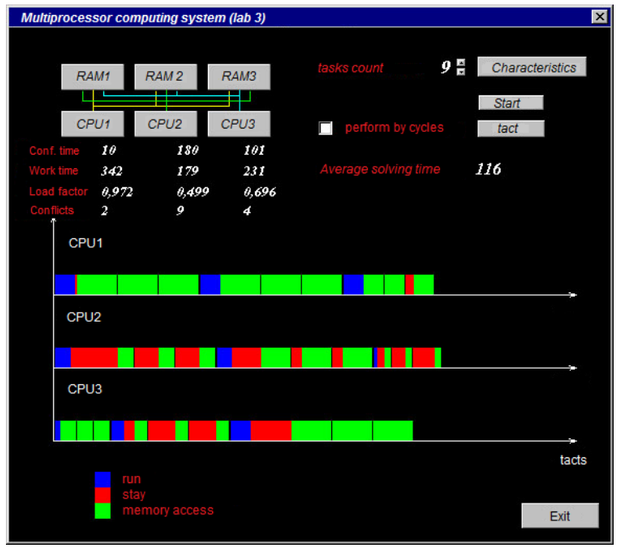

Fig. 3 The model results

Input modeling data are:
1) The number of processors;
2) The number of RAM modules;
3) The number of tasks;

According to Figure 1, it follows that the left side of the wellbore axis at the distance of radius R'_o in a porous structure is moving to the bottom of wells fluid with debit equal, inclusive of [2,4]

$$q_w = \frac{2\Pi K_1 \cdot h \cdot \rho}{\mu} \cdot \frac{1 - \exp\left[-\alpha_{\kappa_1}\left(P_\kappa - P_w\right)\right]}{\alpha_{\kappa_1} \cdot \ln \frac{R'_o}{r_w}} \tag{3}$$

Then, the total production well rate will be determined by the formula

$$q_{w.tot.} = \frac{2\Pi K_1 \cdot h \cdot \rho}{\mu} \cdot \frac{1 - \exp\left[-\alpha_{\kappa_1}\left(P_\kappa - P_w\right)\right]}{\alpha_{\kappa_1}} \cdot \left(\frac{1}{\ln \frac{R'_o}{r_w}} + \frac{1}{\ln \frac{R_\kappa}{\frac{1}{4} R_o}} \right) \tag{4}$$

Well production without fracture is determined by the well-known formula Dupy [2].

Then the relative maximum increase in the q_h compared with q_w determined by the ratio

$$\varphi_h = \frac{q_{h.w\,tot}}{q_w} = \left(\frac{1}{\ln \frac{R'_o}{r_w}} + \frac{1}{\ln \frac{R_\kappa}{\frac{1}{4} R_o}} \right) \cdot \ln \frac{R_\kappa}{r_w} + c \tag{5}$$

Determination of minimal increase well production is carried out in the following way. Inflow to the ellipse, which is completely written well and crack (see Figure 1) will be less than the inflow only into the well and crack if you take the pressure on the contour of the ellipse $P=P_w'$ and also $P_w'>P_w$. If you use this assumption, then this may be an ellipse with semiaxes $\frac{R_o}{2} + r_w$ and $\sqrt{R_o \cdot r_w + r_w^2}$ (see Fig. 1). Then the value of inflows, i.e. productivity of fluid to this ellipse according to [2,3] is defined by the formula

$$q_l = \frac{2\Pi K_1 \cdot h \cdot \rho}{\mu} \cdot \frac{1 - \exp\left[-\alpha_{\kappa_1}\left(P_\kappa - P'_w\right)\right]}{\alpha_{\kappa_1} \cdot \ln \frac{R_\kappa}{\frac{1}{4}\left(R_o + 2r_w + 2\sqrt{R_o \cdot r_w + r_w^2}\right)}} \tag{6}$$

Relative increase q_l as compared with q_w will be determined by the following formula

$$\varphi_l = \frac{q_l}{q_w} = \frac{1-\exp\left[-\alpha_{\kappa_1}\left(P_\kappa - P_w{}'\right)\right]}{1-\exp\left[-\alpha_{\kappa_1}\left(P_\kappa - P_w\right)\right]} \cdot \frac{\ln\frac{R_\kappa}{r}+c}{\ln\frac{R_\kappa}{\frac{1}{4}\left(R_o+2r_w+2\sqrt{R_o\cdot r_w+r_w{}^2}\right)}} \qquad (7)$$

Thus, by obtained formulas (5), (6) and (7) can determine the boundaries, between which is the actual value of flow rate in the presence of a vertical crack in the reservoir.

For example, take the following data:

a) the radius of the external boundary $R_\kappa = 1000\ m.$

b) wells radius $r_w = 0.1\ m.$

c) coefficient imperfections wells as by extent thus by characteristic $c = 2{,}1$

d) thickness reservoir $h_1 = 10\ m.$

e) permeability reservoir $K_{1.0} = 0.25\ d = 0{,}25\cdot 10^{-12}\ m^2.$

f) permeability cracks $K_2 = 83300\cdot\delta^2.$

g) radius cracks $R_o = 25\ m.$

h) the value of the crack opening $\delta = 1\ mm.$

i) pressure on the feed supply contour $P_\kappa = P_o = 25\ MPa.$

j) pressure on the bottom of the well $P_w = 18\ MPa.$

k) coefficient meterage hydroconductivity of reservoir $\alpha_{\kappa_1} = 0.117\frac{1}{MPa}.$

l) pressure magnitude $P_c{}' = 21\ MPa.$

According to the formula (7) is determined by the low value of the relative increase well production φ_l, which equals:

$$\varphi_l = \frac{1-\exp\left[-0{,}117(25-21)\right]}{1-\exp\left[-0{,}117(25-18)\right]} \cdot \frac{\ln\frac{1000}{0{,}1}+2{,}1}{\ln\frac{1000}{\frac{1}{4}\left(25+2\cdot 0{,}1+2\sqrt{25\cdot 0{,}1+0{,}1^2}\right)}} = 1{,}53$$

По формуле (5) определяется максимальный прирост параметра φ_h

$$\varphi_h = \left(\frac{1}{\ln\frac{20}{0{,}1}}+\frac{1}{\ln\frac{1000}{\frac{25}{4}}}\right)\cdot\ln\frac{1000}{0{,}1}+2{,}1 = 4{,}36$$

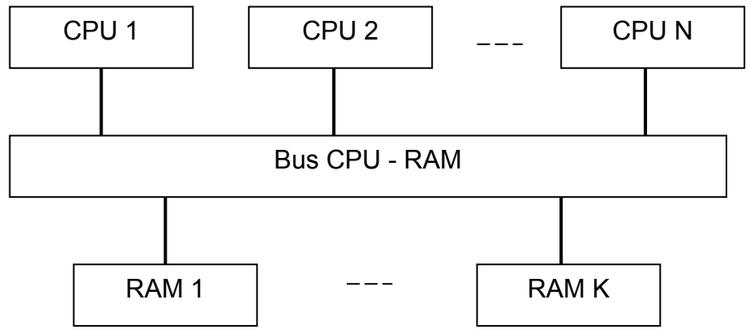

Fig .1 The structure of multiprocessor system

1. The trace of tasks executions for the each processor;
2. Total processors waiting times and task holding times which are shown near each processor during modeling;
3. The processors efficiency coefficients.

The model allows to research two main operating modes:

a) Each processor works only with the own RAM;

b) Each processor works with the all RAMS.

The first mode doesn't cause the conflicts and is an etalon for the second one. If the processors work with the all RAMS, it is necessary to set an order of their accesses to the memory modules. At three processors and the RAM the order can be set in six different ways. In the model it appears by the revealing lists. The screen form for such operation is given in fig. 2.

Several tasks service is imitated in the model. For each of them the execute stage of processor and the memory access is carried out. Thus the temporary charts of processors employment are under construction and all above characteristics are counted, as shown in fig. 3.

The model allows revealing an optimum order of the processors accesses to the RAM, and also influencing on the system characteristics a ratio of the execute time and the access memory time.

The variable structure computing system model provides studying the work of such systems at different number of processors and the RAM. It also allows tasks characteristics variation which can repeatedly address to memory as it happens in virtual memory systems.

systems productivity. The software provides an assessment of the temporary characteristics. It includes simulation models for such systems as:

1) The fixed structure multiprocessor system;
2) The multiprocessor system with a variable structure;
3) The multilevel memory subsystem.

The multiprocessor systems are based under construction on the identical devices: processors, RAM modules, etc. They work under control of the general operating system. The central part of such systems consists of several processors and the memory modules connected by a communication network (as shown in fig. 1) [1, 2].

Nowadays, the various structures of such networks are developed. In offered article connection «everyone with everyone» is considered.

One of the most important problems of the multiprocessor systems is the conflicts in the central part, arising at the access of two and more processors to one memory unit. Such access, as we know, can lead to the information distortion in the RAM and data mistakes. The semaphore principle is used for their elimination. The first processor addressed to memory, takes it and sets a flag. All the other processors requests are put in the queue. Such queue service is carried out with using some of known disciplines. From the point of the whole system the conflicts lead to increase the task solution time and decrease the processors efficiency due the resources (RAM) release waiting.

Research conflicts in the computer systems are one of the important problems of the computing systems theory. Analytical methods of this problem solution are based on the closed stochastic networks theory and are characterized by the complex expressions and valuable errors [3]. The system simulation model working in a multiprogramming mode, allows researching her behavior at any structure and any service discipline. Such a model is also realized in offered creation. Three processors and three RAMS are presented in it. The bigger amount of the devices will complicate model and system studying.

Input data for modeling are:

1. The number of the tasks processed by the system;
2. Each task parameters:
2.1. The number of tasks processing stages (execution and RAM access).
2.2. The execute time and RAM access time.
They can have the following ratios:
2.2.1. The execute time is more in 2, 5, 10 times the RAM access time;
2.2.2. The execute time is equal RAM access time;
2.2.3. The execute time is less in 1, 5, 2, 3 times the RAM access time;
3. Order of the processors accesses to the RAM.
The following modes are investigated:
3.1. Each processor works only with the own RAM (the RAM has the same number, as the processor);
3.2. Each task works with the all RAMS in the set order.
Model results are presented as (fig.1):

Mean value equals $\varphi_m = \frac{1{,}53 + 4{,}36}{2} = 2{,}95$.

III. The results

The calculation results indicate that the increase in well production in the formation of a vertical crack is mainly dependent on changes in the size of the cracks and hydrodynamic parameters formed by vertical channels.

Graph dependent on the variation of the parameter φ from R_o by formation of vertical cracks, built at different values R_o' shown in Figure 2.

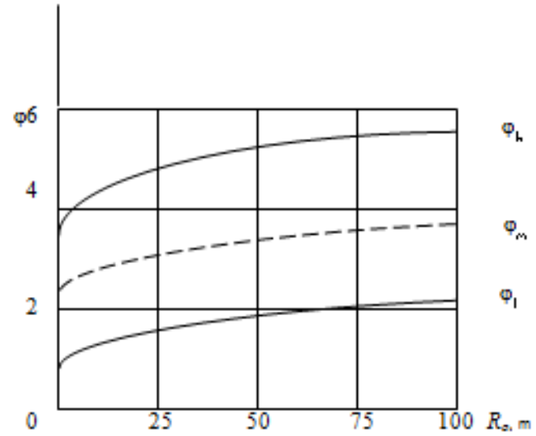

Fig. 2. The dependence φ_h and φ_l от R_o when K_1 = 0,25 mkm^2 in circumstances where formation of a vertical crack

IV. Conclusions

Of the constructed graphics dependence φ and R_o seen, that the upper and lower limits to increase production wells at formation a horizontal and a vertical cracks due to hydraulic fracturing in the near-wellbore are significant differences between them. This is apparently due to the influence on the process of hydro fracturing, plasticity formation and elastic fluid which greatly affect the formation of cracks.

From results of analysis calculated data shows that the smaller the width of the crack, the correspondingly and reduced efficiency hydraulic fracturing, formed in the horizontal plane and also with increases a parameter R_o decreases the growth rate coefficient φ.

References:

1. Malyshev A.G., Malyshev G.A., Jurba V.N., Salnikova N.N. Analysis of the technology of hydraulic fracturing in the fields of «Surgutneftegas». «Oil Industry». 1997. 9. P. 46-51.
2. Shchelkachev V.N. Fundamentals of application and theory of unsteady filtration. M .: Oil and Gas, 1995 – V.I.- 586 p., V. 2.- 493 p.
3. Basniev K.S., Dmitriev N.M., Kanevskaya R.D., Maksimov B.M. Underground gidromehanika.-Moscow-Izhevsk: Institute of Computer Science, 2006.-488 p.
4. Gorbunov A.T. Development of abnormal oil fields. M: Nedra, 237p. 1981.

method more valuable and understandable for students, simulation models should be visualized by implemented user interfaces.

The correct choice of parameters and attributes which should be used to describe the structure and the possible states of the objects inside the model is the core problem of its development. The chosen attributes should provide the basic properties of computers' functioning on the one hand and to reduce the number of secondary factors which complicate the perception of the model on the other hand.

III. PROBLEM SOLUTION

The number of problems had been solved while developing models:

1) Choosing the basic elements of the system which have to be displayed in the model;

2) Definition the specification level of the object parameters;

3) Assessment of the model adequacy.

During for the solution of the first problem as the research objects were chosen:

a) The central part of the multiprocessor system containing the central processors and memory modules;

b) The multilevel memory subsystem.

It was necessary to display the basic elements of the systems which define the features of their functioning. For example, in the multiprocessor systems the major elements are the processors and the related random access memory modules. The conflicts arising at the access of the several processors to one memory module, can significantly affect system productivity. The memory subsystem has a hierarchical multilevel structure. Such a structure also is investigated in the considered models.

The choice of the set objects parameters was another problem in developing models. They have to provide the explanation of the main functioning features of the high-performance computing systems and their devices. Thus, it is necessary to reject the minor factors which complicate the perception.

Described approach has led to use the simplified models of the systems. So, peripheral devices aren't displayed. Models contain the minimum quantity of the elements which are enough for explanation of object work.

IV. THE DESCRIPTION OF MODELS FOR STUDYING THE MULTIPROCESSOR SYSTEMS

Models represent the software package of the various structure computer systems simulation models. It is intended for carrying out the laboratory classes on the subject «Architecture of the high-performance computing systems» for the computer science bachelors. The software can be useful for the similar architecture real computer systems research. It allows studying the organization of computing processes in the central part of the multiprocessor systems, and also in their memory subsystem. There is an opportunity to research the most various factors influencing on these devices and

Orlov S.P., Efimushkina N.V.[1]
Samara State Technical University
Samara, Russia

SIMULATION MODELS OF THE MULTIPROCESSOR SYSTEMS

Abstract – *The paper describes the computing systems simulation models, such as the multiprocessor systems of different structures, as well as the subsystem of memory of these systems. The sets of input and output data are given. The samples of the screen form for the simulation models are shown.*

Key-words – *multiprocessor system, memory, simulation*

I. INTRODUCTION

Modern computers and systems are characterized by the complex architectures and sophisticated operating modes. Methods of the computing systems theory are applied to study the specifics of the systems. The most reliable results might be obtained by the experiments on the computing systems functioning under the real or close to real conditions. High complexity of the real computer architectures makes the process of learning very hard for the student.

II. PROBLEM FORMULATION

The most perspective methods of simulation modeling are the methods which are based on the functional specification of the system presented in the form of algorithm called as simulation (algorithmically) model. The program contains the procedures that imitate the states of the system and the processes for evaluation of the system requirements. Simulation models reproduce the work of the system according to the foregone properties of the elements which models in their turn are also combined into corresponding structure. Scalability is one of the most important properties of simulation modeling. Proposed approach allows studying the systems of any complexity considering the impacts of different factors and reproducing the most typical situations.

Simulation models provide qualitative information about the system properties to make reasonable design decisions. In order to make the application of the described

[1] Sergey P. Orlov – head of the Computer technology department, Samara State Technical University, Doctor of Technical Sciences, Professor,
Nataliya V. Efimushkina - Associate professor of the Computer technology department, Samara State Technical University

Sharapov V.M., Trembovetskaja R.V., Tychkov V.V., Kisil T.Ju.
Cherkasy State Technological University, Ukraine

THE PROCESSES DESIGN IN MECHANICAL SIZES TRANSDUCERS WITH DOMEN-DISSIPATION PIEZOELEMENTS IN ELECTRIC HIGH-PASSES CHARTS

Abstract

The paper proposes an equivalent circuit of the transducer mechanical quantities with piezo in the scheme of passive high-pass filter with a T-shaped and double-T connection diagram. Obtained by frequency converters transfer coefficient. The modeling and study of the frequency response of piezoelectric transducers with computer simulation package Multisim (EWB). In this case, according to the theory bimorph electromechanical analogies presented series-parallel oscillatory RLC – circuit. Shows the correspondence of computer and mathematical model of a real converter converter, which is confirmed by the coincidence of the frequency and amplitude characteristics. The information generated by the computer model response transducers correspond to response, and based on mathematical models. Found that the nonlinearity of frequency and amplitude-frequency error converters depends on the angle between the polarization vector and the electric field vector of the output voltage. For converters based on a modified schemes of high pass filters with increasing angle between the polarization vector and the electric field vector of the output voltage from 0 to 40˚ resonance peak amplitude-frequency converter error and decreases.

KEY WORDS: piezoelectric preobrazazovatel, bimorph, domain-dissipative converter, computer simulation, the frequency gain, frequency response

Introduction

Piezoelectric transducers are widely used for measuring mechanical quantities (force, pressure, acceleration, weight, angular velocity, torque, strain, etc.) [1]. Piezoelectric transducers are widely used in medical technology, particularly in ultrasound imaging, in urology for creating strong ultrasonic fields in physiotherapy for creating aerosols, etc.

Bimorph (BPE) is one of the most promising elements are widely used in instrumentation and automation [4]. On this basis can be synthesized various transducers and arrangements.

Consist of a piezoelectric bimorph dvuhchastey – two piezoelectric elements are connected to each other (symmetrical bimorph elements) or a piezoelectric element and a metal plate also interconnected by means of epoxy resin or low-melting solder (asymmetric bimorph elements).

Material and methods

The authors in [1-4] the possibility of the creation of the transducers of mechanical quantities from a domain-dissipative piezo elements included in the chain of electrical filters.

According to the classification of piezoelectric transducers [1] to the domain-dissipative converters are converters in which the electric field vector of the output signal constitutes a polarization vector angle α, where $0 << \alpha \leq 90^0$. As the angle α between the polarization vector and the electric field vector the output signal is a degeneration of the vibrational properties of the converter in an aperiodic differentiating circuit, this increases the sensitivity and extended operating frequency range.

The reason for the transformation of the vibrational level in the aperiodic based on the anisotropic properties of piezoelectric ceramics and the associated increase in the resistance of the piezoelectric element's own sensor (internal friction) in the formation of the angle between the vectors **E** and **F**. Change your own resistance due to the influence of the ordered domain structure polarized piezoceramic on the motion of charge carriers [1].

The aim of this work is to create a mathematical and computer models and analysis of response transducers mechanical variables with domain-dissipative piezoelements based on modified schemes of high pass filters with the help of electrical circuits modeling and analysis.

Results and discussion

As was shown in [1], frequency response converter using a conventional bimorph has resonance peaks in the operating frequency range of the converter.

The authors suggest transducers of mechanical quantities with piezoelements in the scheme of the high pass filter [2]. In this case, the piezoelectric elements filter uses the domain-dissipative piezoelectric [3, 4].

We use the well-known domain-dissipative bimorph transducer [5], which is composed of the piezoelectric element of the piezoceramic PZT-19 30 mm in diameter and 0.3 mm thick, and the plates of fiberglass ∅37 and 0.5 mm thick, glued together with epoxy resin based epoxy resin ED-20 (Fig. 1).

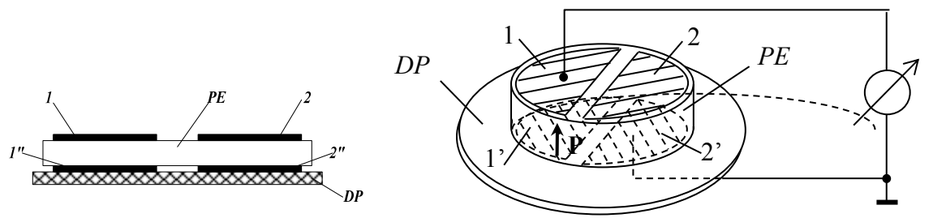

Fig. 1. Bimorph piezoelectric transducer: PE – piezo, DP – dielectric plate [1, 5]

IV. Conclusion

We have considered a method based on a semi-splitting finite-difference scheme. Its implementation in a code was verified and validated.

We calculated a problem on the propagation of a surface wave in the ocean and compared calculated results with those obtained by Mader [6].

The semi-splitting finite-difference scheme is quite applicable to numerical calculations where the equations of shallow water theory hold.

It is shown that the proposed method is also applicable to the problem of wave run-up on the coast. Further work implies the development of a 2D code for surface wave propagation simulation.

References

1. Fletcher, C., Computational techniques for fluid dynamics. V. 2 / C. Fletcher. – Moscow, MIR Publishers, 1991. – 552 P.
2. Kuropatenko, V.F., Shock capture methods / V.F. Kuropatenko // Far Eastern Mathematical Journal. – 2001. – V. 2, No. 2. – P. 45-59
3. Simonenko, V.A., Numerical simulation of mega-tsunami / V.A. Simonenko, N.A. Skorkin, V.P. Elsukov, A.S. Uglov // South-Ural State University News, Mathematics, Physics and Chemistry Series – 2008. – No. 22, Is. 11 – P. 58-65
4. Stanyukovich, K.P., Unsteady continuum motions / K.P. Stanyukovich – Moscow, Nauka Publishers, 1971
5. Sedov, L.I., Similarity and dimensionality methods in mechanics / L.I. Sedov – Moscow, Nauka Publishers, 1972. – P. 440
6. Mader, Charles L., Numerical Simulation of Tsunami / Charles L. Mader // Journal of Physical Oceanography. – 1974. V.4. – P. 74-82
7. Marchuk, Andrey G.A., Method for Numerical Modeling of Tsunami Run-up on the Coast of Arbitrary Profile / Andrey G.A. Marchuk, A.A. Anisimov // ITS 2001 Processing, Session 7, Number 7-27, P. 933-940
8. Mazova, R.K., Linear run-up theory / R.K. Mazova, E.N. Pelinovsky // USSR Academy of Sciences' Institute of Applied Physics Preprint, 1981. – No. 3.

A similar problem with boundary condition (16) was calculated by TMB. Calculated results agree well with data from [6], specifically, the wave height increases from 1 m to 1,5 m and then remains unchanged. Figure 9 shows wave profiles for the varied shelf depth which was zero at $X = 459,0$ km.

It is thus shown that TMB and SWAN calculations for similar problems agree well.

Run-up on coast

The problem is calculated with equations (15). The calculation is run till the time when the wave reaches the coastal line R_0. As in [7], for the region $R > R_0$, i.e., on land, we introduce a «height» $\overline{h}(R) < 0$, which is the height of land above the unperturbed ocean surface, taken with the negative sign. For the region $R > R_0$, the height of the unperturbed «water» surface (before the wave reaches the coast) equals the height of land above the unperturbed ocean surface, taken with the positive sign: $\eta(R) = -\overline{h}(R) > 0$. At the water-land interface we assume $\eta(R) = \overline{h}(R) = 0$. Then, for $0 < R < R_0$, $H(R,t=0) \neq 0$, and for $R > R_0$, $H(R,t=0) = 0$. We obtain a problem of strong shock propagation in water and ground, which is solved with the modified homogeneous semi-splitting finite-difference scheme described above.

The method we use for calculating wave run-up on coast is tested through comparison between numerical results and analytical solutions (see Figure 10), which were taken from [7] with reference to [8].]. Figure 3.10 shows the wave profile $Z(R,t)$ at different times during its travel to the coast sloped 32˚. The dotted line shows the initial position of the wave; the dashed one shows its position at next time; and the solid line shows its maximal run-up on the coast which is shown by the line with circular markers. The analytical solution [8] is shown by the line with triangle markers. The results are seen to agree well.

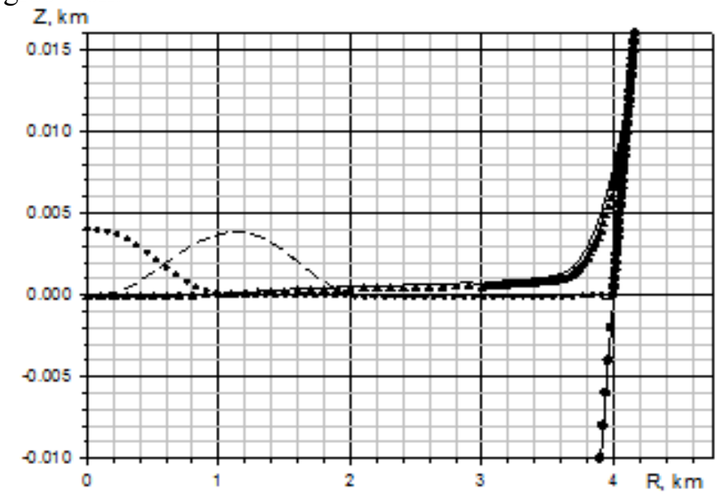

Figure 10 – Wave evolution to the coast

Each electrode in a piezoelectric element is divided into two half-disks so on piezoelectric element 4 to be in the form of half-disks of the electrode, each electrode on the lower end surface of a projection of the electrode on the upper end surface.

Resistance and capacitance between the electrodes $(1-1')$, $(1-2')$, and (1-2) are shown in Tab. 1 [1].

Table 1

	1-1/	1-2/	1-2
α, º	0	82,3	90
R, kOm	6,3	169	172
C, pF	3210	107	109

Connecting electrodes $(1-1')$ corresponds to the known transducer which represents an oscillating system with a high Q factor. For a traditional transducer characterized by a pronounced peak frequency response.

When connected to the electrodes $(1-2')$ obtain domain-dissipative circuit converter with an angle α between the polarization vector and the vector of the field intensity of the output signal equal 82˚. As seen from Tab. 1, the resistance transducer increases, capacity – is reduced while oscillating unit degenerates into aperiodic circuit.

Finally, when connected to the electrodes (1-2), we obtain a domain-dissipative circuit converter with an angle α=90˚. This differentiating inertia component. Frequency response of the converter is almost linear, and sensitivity – increased [1, 5, 6].

Fig. 2 shows a diagram of the T-bar of the proposed converter, and Fig. 2b converter circuit in a double T-shaped pattern with the domain HPF – dissipative converter.

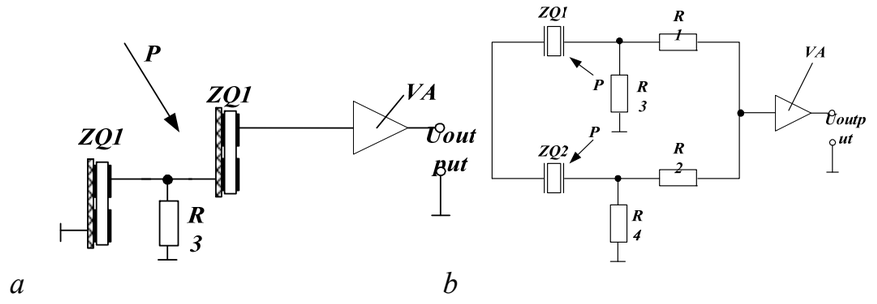

Fig. 2. The inverter mechanical variables with domain-dissipative piezoelectric) in the modified T – HPF scheme; b) in the modified double-T – HPF scheme

To create a mathematical model of the converter, i.e. transfer function and frequency response for the converter according to Fig. 2 a, we use the formula of frequency coefficient voltage transmission [7-10]:

$$W(j\omega) = \frac{Z_н}{A_{11} \cdot Z_н + A_{12}}$$

where Zn – load impedance (matching voltage amplifier);

A_{11} – the coefficient of the four-pole, showing the ratio of the input voltage to the quadrupole voltage output at idle. Obtain a coefficient taking into account the resistance of the piezoelectric element; $A_{11} = 1 + \frac{ZQ}{R3} = \frac{R3 \cdot R_m \cdot P \cdot \omega_c \cdot C_m + R_m}{(R_m \cdot P \cdot \omega_c \cdot C_m + 1) \cdot R3}$,

A_{12} – the coefficient of the quadrupole showing the ratio of the voltage at the input of the quadrupole to the current output at idle. Obtain a coefficient taking into account the resistance of the piezoelectric element.

$$A_{12} = ZQ + ZQ + \frac{ZQ \cdot ZQ}{R3} = R_m \cdot \left(\frac{2 \cdot R3 \cdot R_m \cdot P \cdot \omega_c \cdot C_m + R_m + 2 \cdot R3}{(R_m \cdot P \cdot \omega_c \cdot C_m + 1)^2 \cdot R3} \right).$$

ZQ – impedance of the piezoelectric element domain-dissipative.

As a result, we obtain the frequency converter transfer coefficient:

$$W(j\omega) = \frac{a_0 + \frac{j\omega}{\omega_c} \cdot a_1 + \left(\frac{(j\omega)^2}{\omega_c^{\,2}} \right) \cdot a_2}{b_0 + \frac{j\omega}{\omega_c} \cdot b_1 + \left(\frac{(j\omega)^2}{\omega_c^{\,2}} \right) \cdot b_2}$$

where $a_0 = Z_н \cdot R3; a_1 = 2 \cdot Z_н \cdot R3 \cdot R_m \cdot \omega_c \cdot C_m; a_2 = Z_н \cdot R3 \cdot R_m^2 \cdot \omega_c^2 \cdot C_m^2$ the coefficients of the polynomial A_{11} quadrupole, depending on the design parameters of the converter;

$$b_0 = Z_н \cdot R3 + Z_н \cdot R_m + 2 \cdot R3 \cdot R_m + R_m^2; b_1 = 2 \cdot Z_н \cdot R3 \cdot R_m \cdot \omega_c \cdot C_m +$$
$$+ Z_н \cdot R_m^2 \cdot \omega_c \cdot C_m; b_2 = Z_н \cdot R3 \cdot R_m^2 \cdot \omega_c^2 \cdot C_m^2$$

coefficients of A_{12} of polynomial of quadripole, depending on the structural parameters of transformer.

To create a mathematical model of the converter (Fig. 2 b) frequency transfer coefficient determined by the formula:

Analyze once more calculations from [6]. They show that after reaching the underwater wall inclined 1:15, the solitary wave (boundary condition (16)) increases its height from 0,96 m to 1,50 m. And then in its further propagation along the shelf to the right boundary (rocky wall) the wave height remains constant. This fact is shown in Figure 7 by a dashed envelope line at the top right-hand corner.

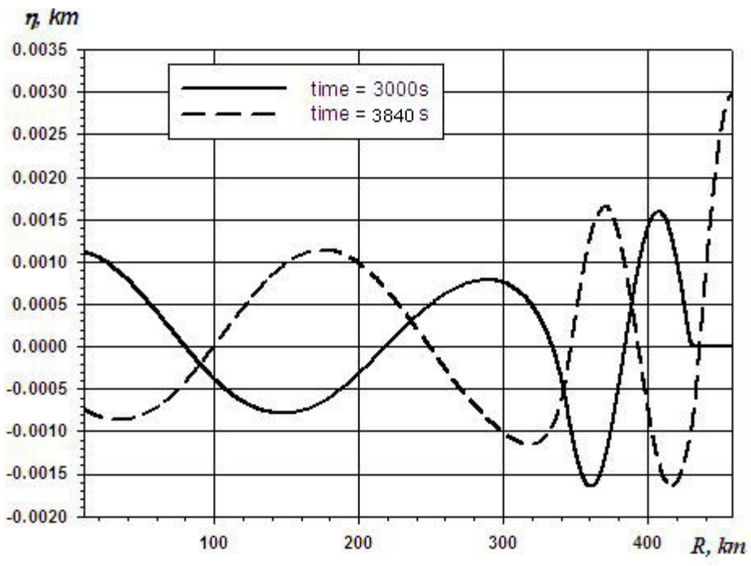

Figure 8 – Wave profiles at times 3000 and 3840 seconds

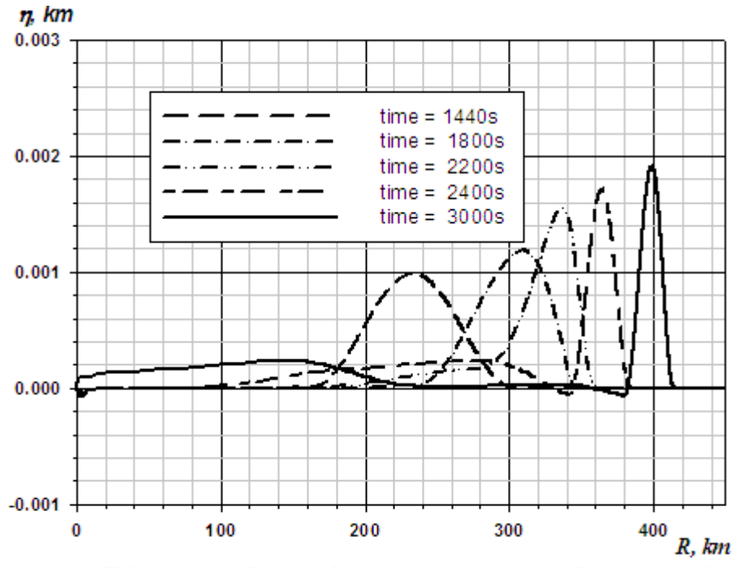

Figure 9 – Wave profiles at different times for the inclined wall

Mader [6] provides numerical results for solitary wave propagation in the ocean of depth 4,55 km. The source of waves is 460,0 km from a rocky coast, i.e., a sinusoidal wave source is set at the left boundary:

$$u = \begin{cases} 0{,}04666 \cdot \sin^2\left(0{,}004713 \cdot t\right) \text{ m/s}, & \text{if } t < 660 \text{ s} \\ 0 \text{ m/s}, & \text{if } t > 660 \text{ s} \end{cases} \quad (16)$$

This source generates a solitary wave 1 m high and 140 km wide, which moves to the right at a velocity of 210 m/s. On the right boundary the velocity of water particles is set to be zero, i.e., the coast is assumed to be a rigid wall.

The author also provides calculations for the boundary condition

$$0{,}04666 \cdot \sin^2\left(0.004713t\right) \text{ m/s}, \quad (17)$$

meaning that the source generates a train of waves with amplitudes from –1 m to 1 m and width 280 km, moving to the right at 210 m/s.

Two codes, SWAN and ZUNI (SOLA), were used for calculations presented in [6]. The computational domain is shown in Figure 7 (left). The ocean depth is $Y = 4{,}55$ km. At a distance $X = 283{,}50$ km from the source, there is a wall inclined 1:15. At a distance of $344{,}25$ km, there starts a shelf 500 m thick.

Figure 7 (right), which was taken from [6], presents SWAN and ZUNI calculations – wave heights at two times – for the boundary condition (17).

A similar problem was calculated by TMB. Calculated results satisfactorily agree with data from [6]. This can be seen from comparison between Figure 7 (right) depicting SWAN and ZUNI results, and Figure 8 which shows TMB calculations.

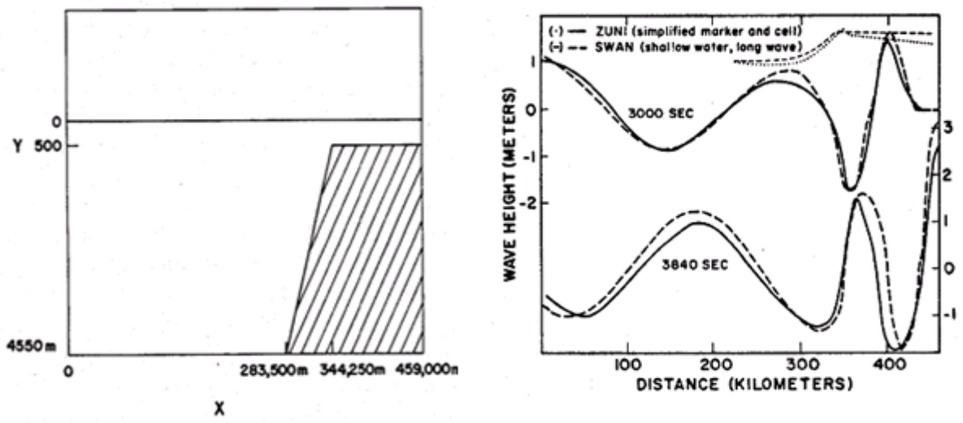

Figure 7 – Computation domain (left) and wave profiles at times 3000 and 3840 seconds [6] (right)

$$W(j\omega) = \frac{-Z_н \cdot Z_{21}}{Z_{12} \cdot Z_{21} - Z_{11} \cdot (Z_н + Z_{22})} = \frac{-Z_н \cdot Y_{21} \cdot Y}{\left(-Y_{12} \cdot Y_{21} + Y_{22} \cdot Y \cdot Z + Y_{22} \cdot Y_{11}\right)}$$

where Y_{11}, Y_{12}, Y_{21}, Y_{22} – general transformerconductivity

$$Y_{11} = \frac{R2 + R4}{ZQ \cdot R4 + R2 \cdot R4 + ZQ \cdot R2}; \quad Y_{12} = \frac{-R4}{ZQ \cdot R4 + R2 \cdot R4 + ZQ \cdot R2};$$

$$Y_{21} = -Y_{12}; Y_{22} = -Y_{11};$$

Y – coefficients matrix determinant.

As a result we will get the frequency transmitivity of transformer :

$$W(j\omega) = \frac{a_0 + \frac{j\omega}{\omega_c} \cdot a_1}{b_0 + \frac{j\omega}{\omega_c} \cdot b_1}$$

where $a_0 = -Z_н \cdot R4; a_1 = -Z_н \cdot R4 \cdot R_m \cdot \omega_c \cdot C_m$- the coefficients of the four-pole, depending on the design parameters of the transmitter;

$b_0 = 2 \cdot R2 \cdot R4 + 2 \cdot R_m \cdot R2 + 2 \cdot R_m \cdot R4 - Z_н \cdot R4 - Z_н \cdot R_m;$

$b_1 = 2 \cdot R2 \cdot R4 \cdot R_m \cdot \omega_c \cdot C_m - Z_н \cdot R4 \cdot R_m \cdot \omega_c \cdot C_m$ - coefficients of polynomial of quadripole, depending on the structural parameters of transformer.

Amplitude – frequency response is determined by the modulus of the frequency transfer function: $A(\omega) = |W(j\omega)|$. The results of computer simulation based on the frequency response of the piezoelectric transducer highpass filter using a conventional piezoelectric element (PE) and bimorph domain-dissipative polyethylene made with the following parameters converter

Table 2 Using for a design transformer parameters

corner	α= 0 degrees	α= 20 degrees	α= 40 degrees	α= 82 degrees
chart Fig. 1				
$R_m, k\hat{I}m$	3	8	33,3	1440
C_m	27 nF	1,2 nF	1,9 nF	230 pF
$R3, k\hat{I}m$	55	43	11	1000
chart Fig. 2				
$R_m, k\hat{I}m$	2	4	8	1440
C_m	27 nF	19 nF	10 nF	230 pF
$R3, k\hat{I}m$	6	8	16	1000

A result is presented on Fig. 3, 4.

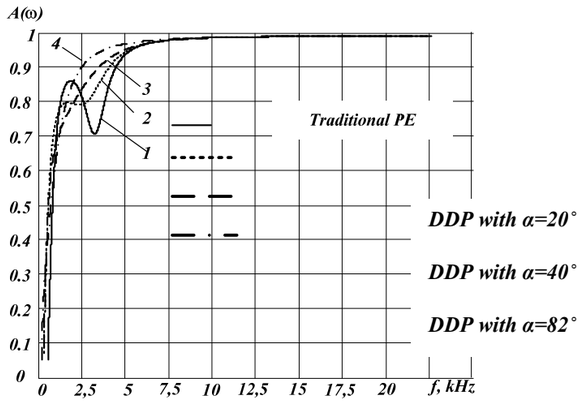

Fig. 3. AFC converter mechanical variables with domain-dissipative piezo elements in the modified T – shaped pattern highpass filter with a cutoff frequency of 500 Hz

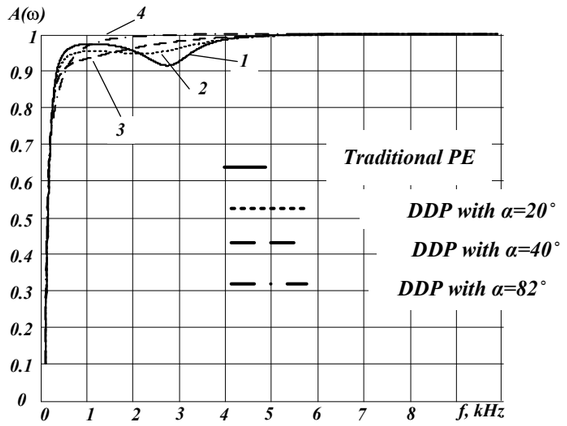

Fig. 4. AFC converter mechanical variables with domain-dissipative piezo elements in the modified T – shaped pattern highpass filter with a cutoff frequency of 125 Hz

Results of studies with the transducer response cutoff frequency of 500 Hz and with a cutoff frequency of 125 Hz show that by increasing the angle between the polarization vector of the electric field vector of the output voltage from 0 to the peak resonant converter 40° reduced 5-15 times, as occurs degeneracy of the vibrational properties of the converter in an aperiodic differentiating circuit. Wherein the amplitude-frequency error decreases 1.2-2.6 times.

Comparison between three difference schemes allows the following inferences. The scheme by Kuropatenko agrees well with the exact solution, but uses Lagrangian coordinates which limits its application to large deformations. The scheme by MacCormack has a stronger smoothing effect than the scheme we propose.

So, the semi-splitting scheme seems to fit best the numerical modeling of surface wave propagation in the ocean.

Surface wave propagation in shallow water

A cylindrically diverging wave and its impact on the coast with allowance for the shelf profile were simulated with a code which implements the shallow water approximation.

In shallow water theory, the equations which describe the propagation of a 1D circular surface wave read as

$$\begin{aligned} &\frac{\partial u}{\partial t}+u\frac{\partial u}{\partial R}=g\frac{\partial \eta}{\partial R},\\ &\frac{\partial \xi}{\partial t}+u\frac{\partial \xi}{\partial R}+\xi\left(\frac{\partial u}{\partial R}+\frac{u}{R}\right)=0, \end{aligned} \qquad (15)$$

where R is distance from the origin of coordinates (the point where a body impacts on water) on the unperturbed ocean surface, t is time, g is gravity, $u=u(R,t)$ is particle velocity on the wave surface, $\eta=\eta(R,t)$ is the surface wave profile, $h(R)$ is the ocean bed profile, and $\xi=h(R)+\eta(R,t)$.

Equations (15) are hyperbolic and can be approximated by finite differences.

The problem we are going to solve has a peculiar feature – a very large distance ($\square$ 1000 km) the wave covers. The time it takes the wave to reach the cost is about tens of thousand seconds. This means that the numerical solution of the equations will require a large number of cycles over time. That is why the finite-difference equations which approximate equations (15) need to have a minimal smoothing effect.

To solve the problem we tested the schemes by MacCormack, Lax and Wendroff, and Neumann. None of them satisfied us because of strong smoothing by viscosity.

Worthy of consideration seems the $\lambda-$scheme by Moretti [1], which approximates differential equations with use of information on the characteristics of equations (15). The scheme requires no artificial viscosity. It gives monotone profiles with almost no numerical dissipation. However, its straightforward use for equations (15) gives unphysical solutions.

So, we modified the $\lambda-$scheme, leaving its positive features intact. Our modification implements the above described semi-splitting scheme. A 1D code TMB was written for solving equations (15). It was verified through comparison with wave propagation calculations by the code SWAN [6].

Figure 5 shows velocities $U(x,t)$ along the x axis at $t = 0{,}9$ s. They are seen to agree well with the exact solution.

Figure 6 shows pressures.

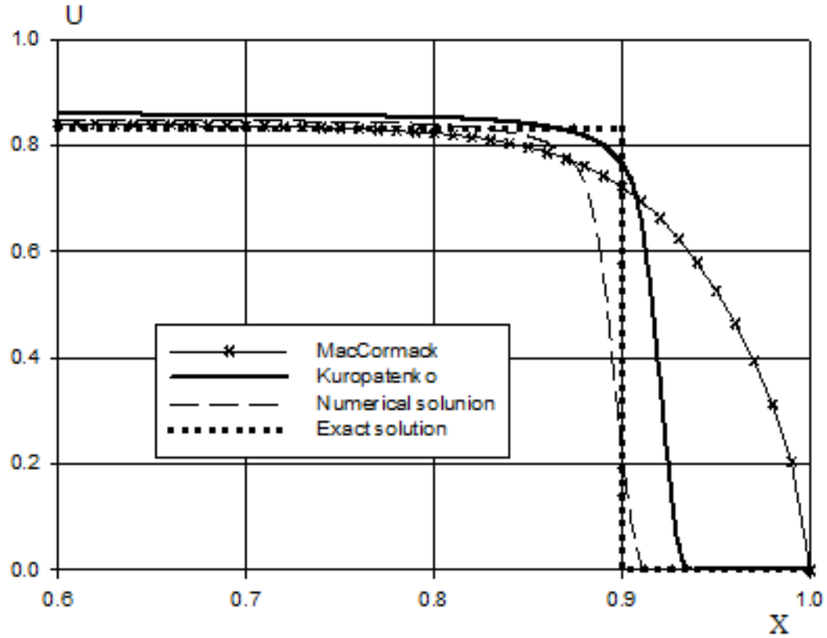

Figure 5 – Velocity $U(x,t)$ at $t = 0{,}9$ s

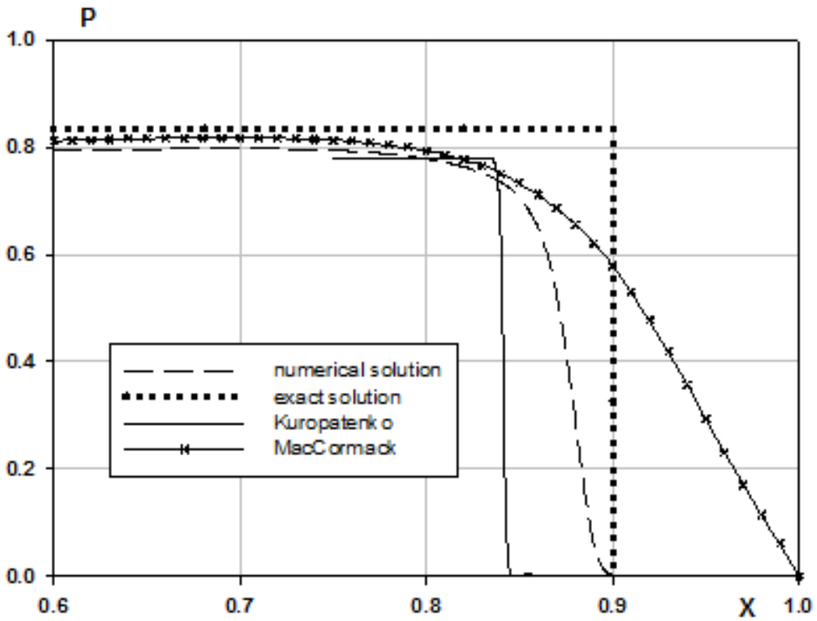

Figure 6 – Pressures at $t = 0{,}9$ s

Tab. 3 shows the comparative characteristics of the transducers from the resonance peak and the amplitude-frequency error.

Table 3 Comparison table converters mechanical variables with domain-dissipative piezo

Chart of transformer	Cut frequency, kHz	Resonance peak, relative unit				Amplitude-frequency error, %			
		α, °				α, °			
		0	20	40	82	0	20	40	82
Fig. 1	0,5	0,15	-	-	-	5,5	2,9	2,1	1,9
	0,125	0,07	-	-	-	3,7	3,4	3,0	1,9
Fig. 2	0,5	0,048	0,01	0,005	-	10	4,2	3	2,2
	0,125	0,01	0,005	-	-	4,3	4,0	3,2	2

One way to study the frequency response of the piezoelectric transducer is the use of computer modeling using modern software packages. [11]

The package program Multisim (EWB) studied the equivalent circuit of the transducer mechanical variables with domain-dissipative piezoelectric element in the scheme of passive high-pass filter with a T – shaped diagram. In this case, according to the theory bimorph electromechanical analogies presented series-parallel oscillatory RLC – circuit.

The equivalent circuit of the converter is shown in Fig. 5, and the result of a computer circuit simulation response at different angles between the electric field vector and the vector of the output signal in Fig. 6.

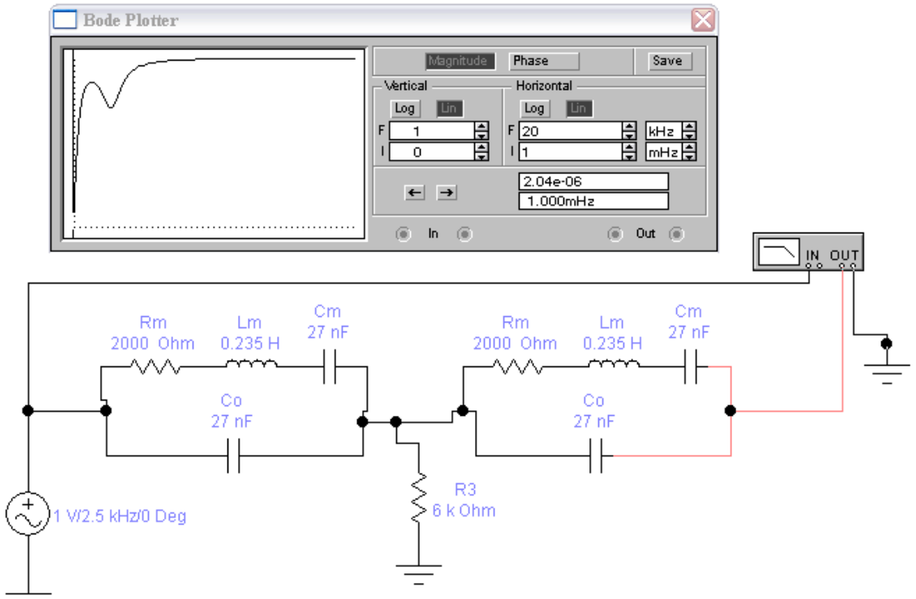

Fig. 5. The equivalent circuit of the transducer mechanical quantities with piezo in the scheme of a highpass filter with T – shaped scheme

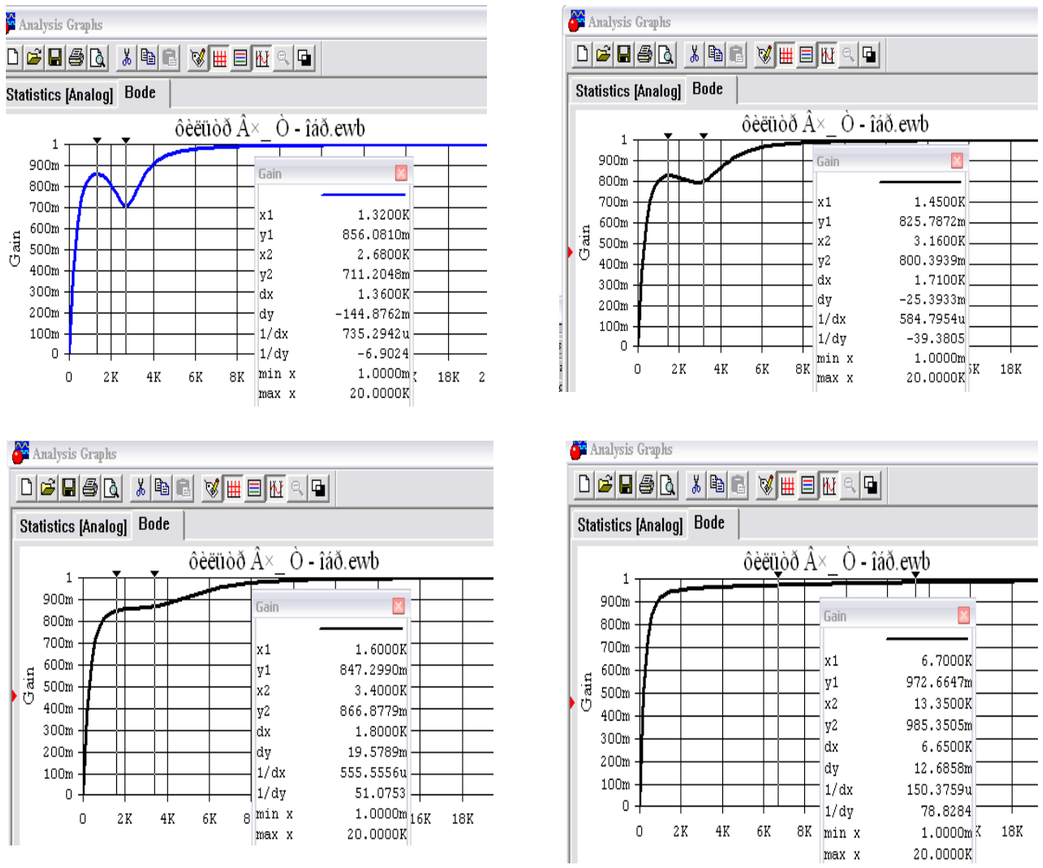

Fig. 6: The results of computer simulation of the frequency response at the transmitter: a) $\alpha = 0^\circ$**; b)** $\alpha = 20^\circ$**; c)** $\alpha = 40^\circ$**; d)** $\alpha = 82^\circ$

Fit of the model to real converter device (bimorph piezoceramic element PZT-19 diameter 27 mm, thick 0.2 mm with a metal plate with a diameter of 30 mm and a thickness of 0.2 mm made of steel 40X) and a mathematical model is confirmed by the coincidence of the frequency and amplitude characteristics.

Conclusions

1. With the system modeling and analysis of electrical circuits obtained model transducers of mechanical quantities.

2. These converters AFC match AFC, and based on mathematical models.

3. Non-linearity and frequency response amplitude-frequency error converters depends on the angle between the polarization vector and the electric field vector of the output voltage;

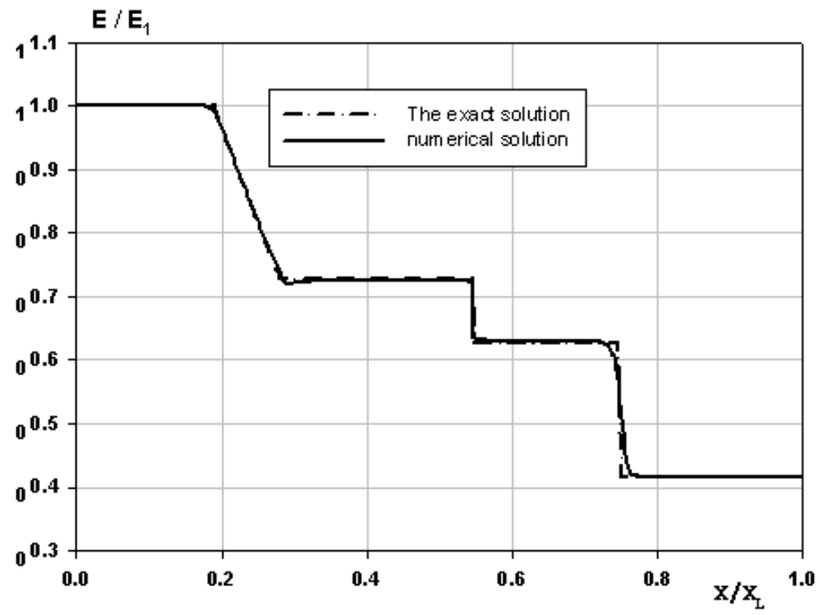

Figure 4 – Relative internal energies

The figures demonstrate good agreement between numerical and exact solutions.

Problem 2: piston

Problem statement with initial and boundary conditions is as follows:

– 1D formulation: In a gas of volume $0 \le x \le 1$, a piston instantaneously starts to move as $x(t)$ at a constant velocity U. The initial position of the piston is $x(0) = 0$ (left boundary). Its motion causes a strong shock to move at a constant velocity W through the gas.

– If assume that the gas is initially at rest with hydrodynamic parameters $U_0 = 0, P_0 = 0, \rho = \rho_0 = \text{const}$, then the values of these parameters behind the shock can be calculated with formulas from [5]:

$$U_1 = \frac{2}{\gamma+1} W,\ \rho = \frac{\gamma+1}{\gamma-1}\rho_0,\ P_1 = \frac{2}{\gamma+1}\rho_1 W^2.$$

This is the Hugoniot condition for strong shocks.

Numerical results at $t = 0{,}9$ s in comparison with the exact solution are shown in Figures 5 and 6.

The computational domain was broken into identical cells with length $\Delta x = 0{,}01$. The Courant number K in (14) for the MacCormack and Kuropatenko methods was taken to be $0{,}5$. For our semi-splitting method the stability condition was to be stronger: $K = 0{,}25$.

Numerical results obtained with (13) in comparison with the exact solution are shown in Figures 2 – 4.

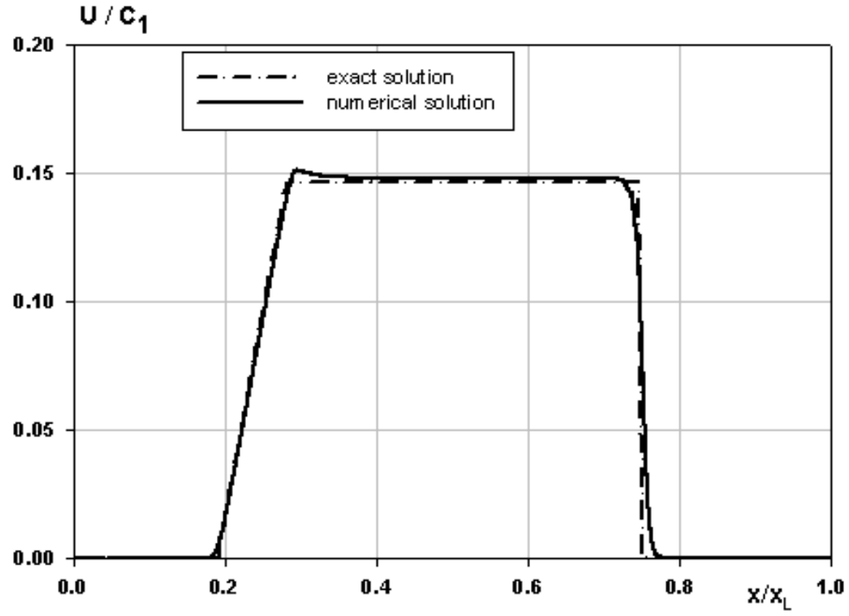

Figure 2 – Relative velocities

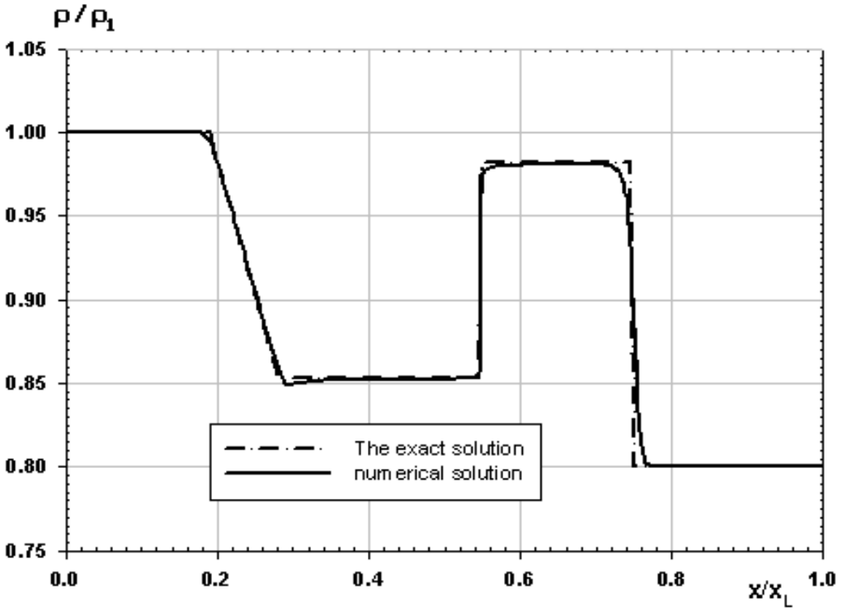

Figure 3 – Relative densities

4. Converters based on modified schemes of high pass filters with increasing angle between the polarization vector and the electric field vector of the output voltage from 0 to 40˚ resonance peak inverter decreases 5-15 times. In this case, the amplitude-frequency error is reduced to 1.2-3 times.

References

1. Piezoelectric transformers (Certificate manual) / Sharapov V.M., Mysienko M.P., Sharapova Ye.V. // Editor V.M. Sharapov. – M.: Technosphere, 2006. – 632 p. [in Russian]
2. Sharapov V.M., Trembovetskaya R.V. and other. The Piezoelectric transformer of mechanical sizes with piezoelement in the chart of high-pass // Bulletin of the Cherkasy State Technological University. – 2005. – №2. – P. 32-35 [in Russian]
3. Sharapov V.M., Trembovetskaya R.V., Shavaleva V.I. Raevskiy N.V. Application of domain-dissipative piezokeramic transformers in the charts of the electric filters // Bulletin of the Cherkasy State Technological University. – 2005. – №3. – P. 69-71 (Special issue).
4. Sharapov V.M., Trembovetskaya R.V. Domain-dissipative bimorph piezoelectric sensors in the modified charts of the electric filters of the lower frequencies // Bulletin of the Cherkasy State Technological University. – 2006. – №. – P. 274-277. (Special issue).
5. Patent Ukraine № 64316. G 01L1/16. Piezoelectric transuder mechanical sizes / Sharapov V.M., Mysienko M.P., and others. Publ. 16.02.2004. Bul. № 2. [in Ukrainian]
6. Sharapov V.M., Balkovskaja Ju.Ju., Mysienko M.P. Linearizing of gain-frequency characteristic of piezoelectric transformers with a monomorf or bimorph pickoff. // Bulletin of the Cherkasy State Technological University. – 2002. – №1. – P. 41-45. [in Russian]
7. Bobrovnikov L.Z. Radio engineering and electronics: Studies for institutions of higher learning. – M.: Nedra, 1990. – 374c. [in Russian]
8. Baskakov S.I. Radiotechnical chains and signals : Studies for institutions of higher learning on special «Radiotehnika». – M.: Vushaja shkola., 1988 – 448 p. [in Russian]
9. Makarov I.M., Menskij B.M. Linear automatic systems (elements of theory, methods of calculation and reference source). – M.: Mashinostrojenije, 1982. [in Russian]
10. Titse U., Shenk K. Semiconductor circuit technology. – M.: Mir, 1983. [in Russian]
11. Karlaschuk V.I. Electronic laboratory on IBM PC. Laboratory practical work on ElectonicsWorkbench and VisSim on by the elements of the telecommunication systems. – M.: Solon-press, 2005. – 480 p [in Russian]

Gorelik S.I., Butenko O.S., Krasovsky G.Y.
National aerospace university – Kharkov aviation institute (KhAI)

METHOD OF CREATING A COMPREHENSIVE GEO-MODEL OF POTENTIALLY UNDERFLOODABLE ZONES WITH LIMITED A PRIORI INFORMATION

Annotation

This article presents the feasibility of developing a method of creating a comprehensive geo-model of potentially underfloodable zones with limited a priori information. It is presented a method of assessing the impact of underflooding factors, determined by means of expert assessments and membership functions for the detection and localization of potentially underfloodable zones. In case of insufficient a priori information a base of production rules is established, which allows to determine the degree of danger of underflooded and potentially underfloodable areas. The main steps of creating the geo-model, resulting from overlay of cartographic models based on Shuttle Radar Topography Mission (SRTM) data and satellite image interpretation considering the technogenic impact on the analyzed area are shown. Adequacy verification of applying the proposed method has shown an 86.5% accuracy of matching the geo-model developed geometric characteristics with real data.

Keywords: underflooding, model, remote sensing, soil moisture, subterranean water, interpretation.

I Introduction

Due to the increasing pace of urbanization, activation of subterranean underflooding processes has recently been observed. They lead to deformation of buildings, poor sanitary and epidemiological conditions of people's lives, etc. According to [1], an annual expenditure of 5-6 billion dollars is required to prevent the consequences.

Rapid identifications of potentially underfloodable zones will enable to timely predict the negative consequences, associated with shallow subterranean water stratification. Typically, studying the characteristics and particularities of underflooded areas was, and is, mainly practiced using contact methods. Only in the second half of the 20th century aerospace methods for solving similar problems in this field began to evolve.

Thus, only a comprehensive approach to building geo-models for potentially underfloodable zones, which take into account the estimates obtained under conditions of limited a priori information, will improve the determination accuracy of projected changes in the geometric characteristics of the analyzed area.

– region s – $\left(x_0+\left(U^*-C_s\right)t=x_s\le x\le x^*=x_0+U^*t\right)$:

$$U\left(x,t\right)=U^*=\frac{P_1-P_2}{\rho_1C_1+\rho_2C_2},\quad C\left(x,t\right)=C_s=\left(C_1-\frac{\gamma_1-1}{2}U^*\right);$$

– region $2a$ – $\left(x_0+U^*t=x^*\le x\le x_2=x_0+\left(U^*+C_2\right)t\right)$:

$$U\left(x,t\right)=U^*,\quad C\left(x,t\right)=C_{2a}=\left(C_2+\frac{\gamma_2-1}{2}\right);$$

– region 2 – $\left(x_0+\left(U^*+C_2\right)t=x_2\le x\le x_{\mathrm{L}}\right)$.

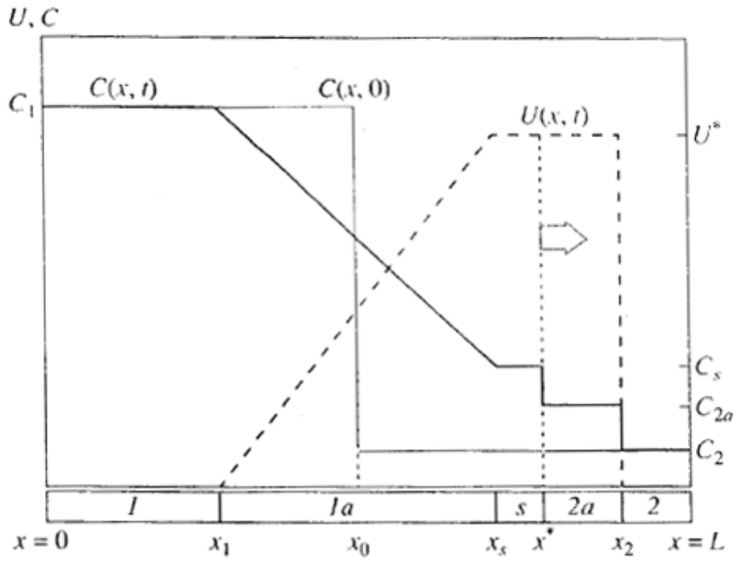

Figure 1 – Regions $1, 1a, s, 2a, 2$

The change to variables ρ,P,E is made on the left (right) from the contact discontinuity with coordinate x^* by

$$\rho\left(x,t\right)=\rho_{1(2)}\left(1-\frac{\gamma-1}{2}\frac{U\left(x,t\right)}{C_{1(2)}}\right)^{\frac{2}{\gamma-1}},$$

$$P\left(x,t\right)=P_{1(2)}\left(1-\frac{\gamma-1}{2}\frac{U\left(x,t\right)}{C_{1(2)}}\right)^{\frac{2\gamma}{\gamma-1}},$$

$$E\left(x,t\right)=\frac{C^2\left(x,t\right)}{\gamma\left(\gamma-1\right)}.$$

For the equation of state $p=(\gamma-1)\rho E$ we are considering, in node $i+0,5$, as per [2], the expression for pressure takes the form

$$\overline{p}_{i+0,5}^{n+1}=p_{i+0,5}^{n}+b(\Delta u)^2+\sqrt{\left(b(\Delta u)^2\right)^2+\left(a_{i+0,5}^{n}\right)^2},$$

where $b=\frac{\gamma+1}{4}\rho_{i+0,5}^{n}$, $a=(\rho c)^2$, $\Delta u=u_{i+1}-u_i$, $c^2=\gamma\frac{p}{\rho}$, and n is time layer.

Code verification

Finite-difference equations (13) were implemented in a code which was tested through comparison between numerical and analytical solutions to two problems.

Problem 1: shock in ideal gas

The statement of the problem and its analytical solution were taken from [4].

Problem statement:

– problem domain $x_0<x<x_{\mathrm{L}}$ with $x=0$ on the left and $x=x_{\mathrm{L}}=0{,}1$ m on the right

– at $t=0$ parameters on the left from the contact surface are: density $\rho_1=1{,}5\cdot10^3$ kg/m^3, pressure $P_1=3\cdot10^{-4}$ Pa, velocity $U_1=0$, $\gamma_1=3$;

– the same on the right are: density $\rho_2=1{,}2\cdot10^3$ kg/m^3, pressure $P_2=1\cdot10^{-4}$ Pa, velocity $U_2=0$, $\gamma_2=3$;

– at $t=0$ both on the left and on the right: $P=(\gamma-1)\rho E$, $C^2=\gamma\frac{P}{\rho}$, $\gamma=3$;

– the contact surface is initially at $x_{\mathrm{K}}=\frac{x_0+x_{\mathrm{L}}}{2}$.

The computational domain is broken into 500 intervals. The computation stability condition is

$$C_{i+0,5}=\frac{\Delta t}{\min\limits_i(x_i-x_{i-1})}<K, \qquad (14)$$

where $C_{i+0,5}$ is sound velocity, K is Courant number (taken to be $K=0{,}5$).

Write the exact solution from [4] for $u=f(x)$ and $c=\varphi(x)$ in each of the regions $1, 1a, s, 2a, 2$ – see Figure 1:

– region 1 – $\left(0\le x\le x_1=x_0-C_1(t)\right)$:

$U(x,t)=0,\quad C(x,t)=C_1;$

– region $1a$ – $\left(x_0-C_1t=x_1\le x\le x_s=x_0+\left(U^*-C_s\right)t\right)$:

$$U(x,t)=\frac{2}{\gamma_1+1}\left(C_1-\frac{x_0-x}{t}\right),\quad C(x,t)=\left(C_1+\frac{\gamma_1-1}{2}U(x,t)\right);$$

II Statement of the problem

Currently, the main methods which allow detecting the features of territories subject to underfloods are contact and Earth remote sensing.

Contact research methods of underflooded territories are based on conducting field and office work [2]. The following are practiced as field work:

- Route surveying of underflooded territories and subterranean water level measurements in wells, basements, cellars, trenches, etc.
- Population survey
- Measurement the levels in a stationary or hydrogeological wells.

According to the data produced by subterranean water monitoring, a hydroisohypses map is created using interpolation and contour map of stratification depths of the subterranean water, and using the contour map, the underflooded territories are extracted.

A propos office work, it is primarily related to baseline data collection, field data compilation and preparation of accounting materials on the underflooded territories.

Considering separately both, field work and office work, each has a set of advantages and disadvantages. An advantage of contact methods is subterranean water measurement precision. Nonetheless, numerous disadvantages exist. The most significant of those are:

- High cost of establishing a hydrogeological wells network, their maintenance and monitoring.
- Considerable time spent on field work.
- Significant effort of searching, gathering and processing various materials.
- Slow decision making on predicting or elimination of the hazardous consequences.

Utilization of remote sensing methods is based on defining the indirect interpretive attributes, implying underflood. Currently, three main directions are being considered: studying soil moisture in the visible, infrared and microwave bands, ground penetration radar and visual interpretation of indirect attributes.

Increased soil moisture may indirectly imply shallow subterranean water stratification. Localization of highly moist areas on satellite images is based on determining the contrast of the dry and moist soils' spectral brightness coefficients. The contrast increases with increasing wavelength, attaining a maximum in the near infrared range. Furthermore, it might be taken into account that besides moisture the spectral brightness coefficient is significantly affected by humus content, iron oxides, mineral composition, the predominance of sandy or clay particles, surface evenness [3, 4]. Consequently, the determination of these parameters requires additional time and material costs. The complexity of soil moisture determination is associated with presence of vegetation, therefore, it is necessary to conduct the surveying only when vegetation and snow covers are absent. The months which correspond to this period are March to early May and late September to November.

During these periods, usually, the soil has the largest humidity value, associated with periods of heavy precipitation and low evaporation. Accordingly, this factor does not necessarily indicate an underflood. An important drawback is the determination depth, which does not exceed 2.5-5cm [5].

Radioluminous temperature (T_l), registered in the thermal infrared and microwave bands, allows to extract the anomalous areas. Extraction of the anomalies requires determining the exact difference between max T_l and min T_l. Negative anomalies might indicate excess of moisture in the soil and positive anomalies – lack of it [6].

Herewith, the method depth may reach 40 cm in homogenous soils. A clear disadvantage of the method is dependence of T_l on weather conditions, as well as possibility of surveying in airplane version only. The spatial resolution and image reception interval of the data received from satellites are insufficient.

Active methods allow determining soil moisture and subterranean water stratification depth. Presence of soil layers with different moisture, which arises due to capillary rise above subterranean water level, reduces the radiothermal radiation intensity. The arising radioluminous contrast becomes more significant as the moistened horizon approximates to the surface and as the registered radiation wavelength increases. Sustainable relationship between the radiation coefficient and the subterranean water level in different soil-climatic zones differ by general patterns and can be traced down to depths of 1-3 meters [7, 8].

It should be pointed out, that subterranean water level is determined based on ground penetration radar using radiation of ultra-wideband pulses in the ultra-high and very-high frequencies range and reception of signals reflected from interfaces between layers of the remotely sensed area, having various electro-physical properties, associated with water saturation and lithological composition of the rocks. A parameter determining the depth and accuracy of measurements is frequency – 50-100MHz, at which a sufficiently high resolution of layer differentiation of the upper section is observed up to depths of 10-15 meters. The layer separation accuracy varies within the first few centimeters, which fully satisfactory for geo-engineering problems [9]. Given a sub-horizontal column structure, if the common-mode axis morphology of the waves, reflected from subterranean water level and from lithological boundaries is identical, a difficulty to determine the subterranean water level arises, and in the given scenario additional data is needed. Sometimes there's a difficulty to define the moistening boundary for geo-radiolocational profiles, which depend on various factors: lithology, the depth of its stratification, a capillary rise zone presence and structural features of the column [10].

Most informative indirect interpretive features, implying an underflood, that are used include images of swamps, sinkholes, flat-bottom step depressions, floodplains, «low» terraces, underground water outputs, etc. The aforementioned objects and areas are easily interpreted via satellite images, available freely in high and very-high spatial resolution. However, there's a significant drawback, since the detection is reliable down to subterranean water stratification depth of 1 m only. According to [2], though, residential area underflooding occurs at depths smaller than 2.5 m.

where

$$U=\begin{bmatrix} u \\ \rho \\ E \end{bmatrix},\ A=\begin{bmatrix} u & 0 & 0 \\ 0 & u & 0 \\ 0 & 0 & u \end{bmatrix},\ B=\begin{bmatrix} -\frac{1}{\rho}p_x \\ -\rho u_x \\ -\frac{p}{\rho}u_x \end{bmatrix}.$$

Rewrite A in another form. For this end write u in A as

$$u=\frac{1}{2}(u+c)+\frac{1}{2}(u-c),$$

then

$$A=\begin{bmatrix} \frac{1}{2}(u+c)+\frac{1}{2}(u-c) & 0 & 0 \\ 0 & \frac{1}{2}(u+c)+\frac{1}{2}(u-c) & 0 \\ 0 & 0 & \frac{1}{2}(u+c)+\frac{1}{2}(u-c) \end{bmatrix}.$$

In this case the discrete equations are written similarly to (10) as

$$U_t + A_+U_x^+ + A_-U_x^- = B, \qquad (13)$$

where $A=T\Lambda^+T^{-1}+T\Lambda^-T^{-1}=A_+ + A_-$.

Here T^{-1} is a matrix with the left eigenvectors of A in the rows, T is reciprocal to T^{-1}, Λ^+ and Λ^- are diagonal matrices with the positive and negative eigenvalues of A, respectively.

The derivatives U_x^+ and U_x^- are approximated by finite differences similar to (11) and (12).

For strong shocks, formulas in (13) were modified by replacing B by

$$B=\begin{bmatrix} -\frac{1}{\rho}\tilde{p}_x \\ -\rho u_x \\ -\frac{\tilde{p}}{\rho}u_x \end{bmatrix}$$

with pressure $\tilde{p}$ calculated as

$$\tilde{p}=\begin{cases} p+\overline{p}, & \text{if compression} \\ p, & \text{if rarefaction} \end{cases}$$

where pressure $\overline{p}$ is calculated as proposed by V.F. Kuropatenko [2].

$$\begin{bmatrix} 0 & \frac{u+c}{2} & 0 \\ 0 & 0 & 0 \\ 0 & \frac{u+c}{\gamma-1} & 0 \end{bmatrix}\begin{bmatrix} 0 & 1 & 0 \\ 1 & 0 & \frac{\gamma-1}{2} \\ 0 & 0 & -\frac{\gamma-1}{2} \end{bmatrix}=\begin{bmatrix} \frac{u+c}{2} & 0 & \frac{(\gamma-1)(u+c)}{4} \\ 0 & 0 & 0 \\ \frac{u+c}{\gamma-1} & 0 & \frac{u+c}{2} \end{bmatrix}.$$

Similarly manipulate with A_- to obtain

$$A_- = \begin{bmatrix} \frac{u-c}{2} & 0 & \frac{(\gamma-1)(u-c)}{4} \\ 0 & u & 0 \\ -\frac{u-c}{\gamma-1} & 0 & \frac{u-c}{2} \end{bmatrix}.$$

Rewrite (3) with account for (9):

$$U_t + AU_x = U_t + A_+U_x^+ + A_-U_x^- = 0, \qquad (10)$$

where $U_t = \begin{bmatrix} u_t \\ \rho_t \\ c_t \end{bmatrix}$, $U_x = \begin{bmatrix} u_x \\ \rho_x \\ c_x \end{bmatrix}$. ($U_x^+ = \frac{\partial U}{\partial x}$ is the derivative related to the characteristic $\lambda = u + c$ and $U_x^- = \frac{\partial U}{\partial x}$ is the derivative related to the characteristic $\lambda = u - c$.)

Finite-difference approximation and the semi-splitting method

The derivative U_x is approximated as

$$U_x^+ \approx \frac{U_i - U_{i-1}}{x_i - x_{i-1}}, \text{ if } u_i + c_i > 0 \text{ and } U_x^+ \approx \frac{U_{i+1} - U_i}{x_{i+1} - x_i}, \text{ otherwise;} \qquad (11)$$

$$U_x^- \approx \frac{U_i - U_{i-1}}{x_i - x_{i-1}}, \text{ if } u_i - c_i > 0 \text{ and } U_x^- \approx \frac{U_{i+1} - U_i}{x_{i+1} - x_i}, \text{ otherwise.} \qquad (12)$$

The method uses information on the characteristics, and if $c = \frac{\tau}{h}$, where τ is time step and h is mesh step along the x axis, then the difference scheme satisfies the shift condition, i.e., it is a method of characteristics.

The full splitting implies that equations (1) can be presented in form (2). But it is not always possible. That is why we go from full splitting to semi-splitting. For this end we write (1) in the matrix form

$$U_t + AU_x = B,$$

As a result of the foregoing, it can be concluded that it is advisable to synthesize contact and remote sensing techniques to further their joint analysis and construction of the predictor. Additionally, it should be noted, that when constructing the decision rules, which determine the tendency of further modifications of the geometrical characteristics of potentially underfloodable zones, it is necessary to take into account the interval estimates under uncertainty.

III Results

A necessary step in obtaining the predictive assessment of potential underfloods' area change is determining the degree of influence for each of the perturbing factors. Additionally, as a result of joint analysis of the factors and the conditions causing underflooding, the degree of their combinatorial mutual influence and the influence directly on the area change of the analyzed territory must be determined. It should be pointed out, that determination of dependencies for such factors as excess above the watercourse level, impermeable layer depth, impact of water withdrawal from a chalk-marl (upper cretaceous) confined aquifer on the subterranean water level measuring [11] is possible only with large sample statistics. However, there are several factors, which are impossible to evaluate statistically due to geological structure diversity and insufficient field measurements. In order to solve this problem, using expert estimates was proposed [12]. Under conditions of limited a priori information, for operational decision making on the geometrical characteristics change of potentially underfloodable zones, during creation of decision rules, and consequently, of production models, using fuzzy linguistic statements was proposed. Following this approach, as a result of taking into account the interval estimates, even minor factors were considered. Such an approach allows elevating the accuracy of the constructed predictors.

To construct the rule base of a fuzzy inference system, during reception of quantitative characteristics of possible changes of the potentially underfloodable zones, it is advisable to use the classical mechanism of the fuzzy sets theory, specifically: formation of linguistic terms, fuzzification of input variables, aggregation, accumulation and defuzzification of output linguistic variables by the method of area centroid [13].

Generally, considering all stages of the product rules construction, the formation method of cartographic model of an underflood according to danger degree.

The first stage of the presented method is collecting freely available material about the site, including the object of study [14]. SRTM data with *.hgt extension was converted into *.shp, using «Global Mapper» software (fig. 1a). Identification of potentially underfloodable zones was carried out based on the fuzzy product rules results.

The result of implementing the aforementioned method on the terrain of Zidki village, Kharkiv region, is presented in fig. 1.

As a result, zones were classified according to the underflood danger degree into 5 categories:

- ED – extraordinary danger, characteristic of underflooded territories with subterranean water level at depths of 0-2,5 m;
- BD – great danger, characteristic of sites with subterranean water level stratification depth in the 2,5-4,0 m interval;
- MD – average degree of danger, for zones with possibly periodic rise of subterranean water;
- PD – possible danger. The territory is not underflooded, but there's a possibility of subterranean water level rising, associated with technogenic load.
- ZD – zero danger, corresponds to not underfloodable zones.

Based on product rules of decision making, a cartographic model of underflood was constructed according to SRTM (binding was performed in ArcGIS software) (fig. 1b).

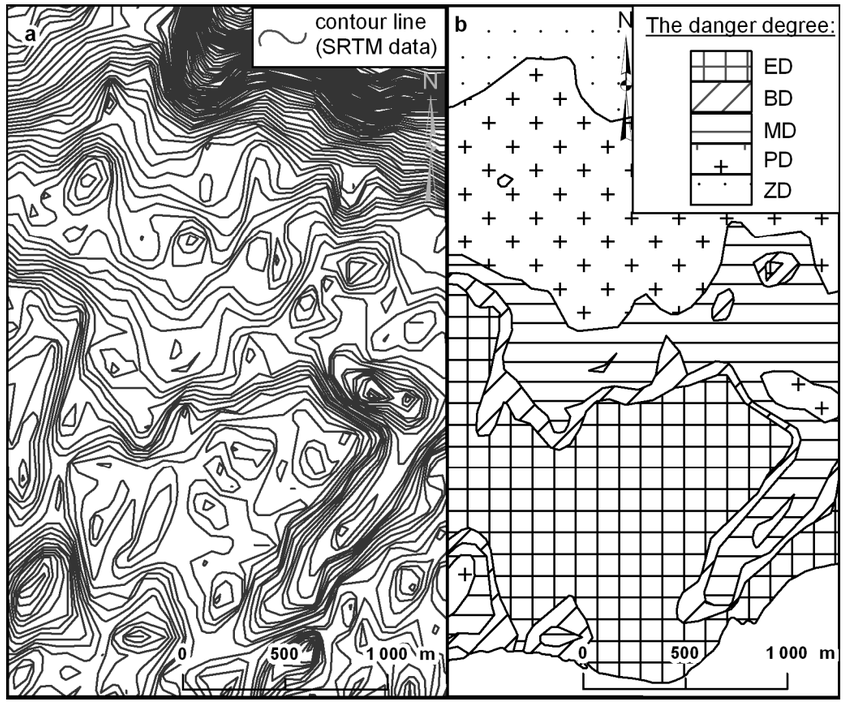

Fig. 1 – Formation of a cartographic model of potential underflooding of Zidki village, Kharkiv region, based on STRM data (a – horizontals, obtained during processing SRTM in *.shp, b – the acquired cartographic model according to danger degree)

It should be pointed out, that for the picking of a satellite image for an object of study (fig. 2a), it is advisable to use the free navigational system SAS.Planet. Herewith, one of the main requirements for the image is absence of snow cover. Pictures, taken in autumn or spring, are necessary for separating coniferous and deciduous forests. For

The matrix T^{-1} is taken to be so as to allow its rows to be the coordinates of the left eigenvectors:

$$T^{-1} = \begin{bmatrix} W_1 \\ W_2 \\ W_3 \end{bmatrix} = \begin{bmatrix} 0 & 1 & 0 \\ 1 & 0 & \frac{\gamma-1}{2} \\ 1 & 0 & -\frac{\gamma-1}{2} \end{bmatrix}.$$

The matrix T which is reciprocal to T^{-1} is

$$T = \begin{bmatrix} 0 & \frac{1}{2} & \frac{1}{2} \\ 1 & 0 & 0 \\ 0 & \frac{1}{\gamma-1} & -\frac{1}{\gamma-1} \end{bmatrix}.$$

Then, using (4), write the matrix A in (3) as $A = T\Lambda T^{-1}$, where Λ is a matrix with eigenvalues on the diagonal. We obtain

$$\begin{bmatrix} u & 0 & \frac{2}{\gamma-1} \\ 0 & u & 0 \\ \frac{2}{\gamma-1} & 0 & u \end{bmatrix} = \begin{bmatrix} 0 & \frac{1}{2} & \frac{1}{2} \\ 1 & 0 & 0 \\ 0 & \frac{1}{\gamma-1} & -\frac{1}{\gamma-1} \end{bmatrix} \begin{bmatrix} u & 0 & 0 \\ 0 & u+c & 0 \\ 0 & 0 & u-c \end{bmatrix} \begin{bmatrix} 0 & 1 & 0 \\ 1 & 0 & \frac{\gamma-1}{2} \\ 1 & 0 & -\frac{\gamma-1}{2} \end{bmatrix}.$$

Write the matrix Λ as $\Lambda = \Lambda_+ + \Lambda_-$ with

$$\Lambda_+ = \begin{bmatrix} 0 & 0 & 0 \\ 0 & u+c & 0 \\ 0 & 0 & 0 \end{bmatrix}, \ \Lambda_- = \begin{bmatrix} u & 0 & 0 \\ 0 & 0 & 0 \\ 0 & 0 & u-c \end{bmatrix}.$$

Now rewrite (4) as

$$A = T\Lambda_+ T^{-1} + T\Lambda_- T^{-1} = A_+ + A_-. \qquad (9)$$

Do some manipulation with A_+ and A_-.

$$A_+ = T\Lambda_+ T^{-1} = \begin{bmatrix} 0 & \frac{1}{2} & \frac{1}{2} \\ 1 & 0 & 0 \\ 0 & \frac{1}{\gamma-1} & -\frac{1}{\gamma-1} \end{bmatrix} \begin{bmatrix} 0 & 0 & 0 \\ 0 & u+c & 0 \\ 0 & 0 & 0 \end{bmatrix} \begin{bmatrix} 0 & 1 & 0 \\ 1 & 0 & \frac{\gamma-1}{2} \\ 1 & 0 & -\frac{\gamma-1}{2} \end{bmatrix} =$$

Find the left eigenvectors. For this end we need to solve the matrix equations

$$W_i\left(A-\lambda_i E\right)=0,\ i=2,3, \tag{6}$$

where W_i are eigenvectors.

Let $\lambda_2=u+c$ with the appropriate eigenvector $W_2=\left[\beta_1,\beta_2,\beta_3\right]$, then Eq. (6) in expanded form reads as

$$\left[\beta_1,\beta_2,\beta_3\right]\begin{bmatrix} -c & 0 & \frac{2}{\gamma-1}c \\ \rho & -c & 0 \\ \frac{\gamma-1}{2}c & 0 & -c \end{bmatrix}=0. \tag{7}$$

Equations (7) make a system of linear homogeneous algebraic equations for β_1,β_2,β_3. It reads as

$$\begin{cases} -c\beta_1+\rho\beta_2+\frac{2}{\gamma-1}c\beta_3=0 \\ -c\beta_2=0 \\ \frac{\gamma-1}{2}c\beta_1-c\beta_3=0. \end{cases} \tag{8}$$

It is seen from the second equation of (8) that $\beta_2=0$.

Note that we are seeking for a nontrivial solution. Equations one and three in (8) are interdependent. So, one of the unknowns β_1,β_2,β_3 is free. Now let $\beta_1=1$, then $\beta_3=\frac{\gamma-1}{2}$.

We have obtained the second left eigenvector corresponding to the eigenvalue $\lambda_2=u+c$

$$W_2=\left[1,0,\frac{\gamma-1}{2}\right].$$

In a similar manner we find the third eigenvector corresponding to the eigenvalue $\lambda_3=u-c$. It is

$$W_3=\left[1,0,-\frac{\gamma-1}{2}\right].$$

Having got the left eigenvectors W_1,W_2,W_3, write the matrices T and T^{-1}.

the biding and/or pre-binding of the satellite images, if required, additional photogrammetric processing is performed. During the interpretation of the images vegetation and geomorphologic element types must be necessarily identified. Those localized elements are the basis for the construction of a preliminary cartographic underflooding geo-model, formed only according to interpretive features (fig. 3a).

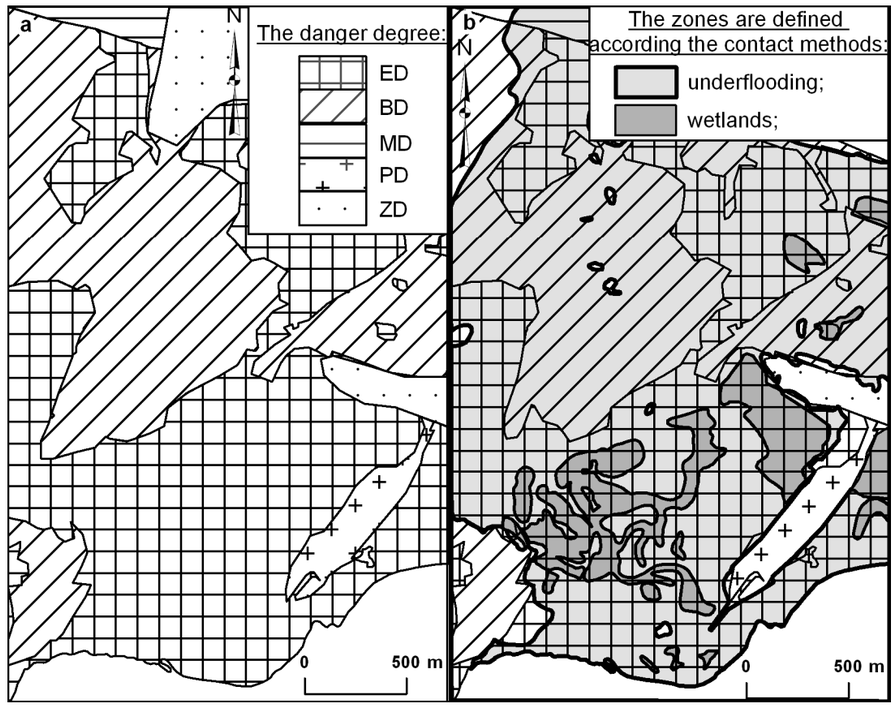

Fig. 2 – Creating the cartographic model of potential underflooding for Zidki village, Kharkiv region, according to interpreted data of a QuickBird satellite image (a – The satellite image, b – the result of thematic interpretation; I – 2nd «pine-forest terrace», II – floodplain; 1 – pine forest, 2 – non-turf-covered territory (sand), 3 – floodplain (meadow) vegetation, 4 – swamps, 5 – buildings (private sector)

When applying two cartographic models, acquired according to SRTM and interpretive features, taking into account statistical data of contact survey results, in order to clarify boundaries of potential underfloods and potentially hazardous and safe territories, overlaying all of the available layers is necessary (fig. 3b).

At the stage of localization of zones with increased technogenic load industrial buildings in enterprises with «wet» and «dry' processes of residential territories in the private sector, medium and high-rise buildings must be separated. Having private

building only and absence of enterprises allows combining the interpretation results of natural and technogenic zones within a single cartographic model (fig. 3a).

The resulting comprehensive cartographic model with definite potentially underfloodable zones according to their degree of danger, constructed taking into account the technogenic load using the example of Zidki village is presented in fig. 3b.

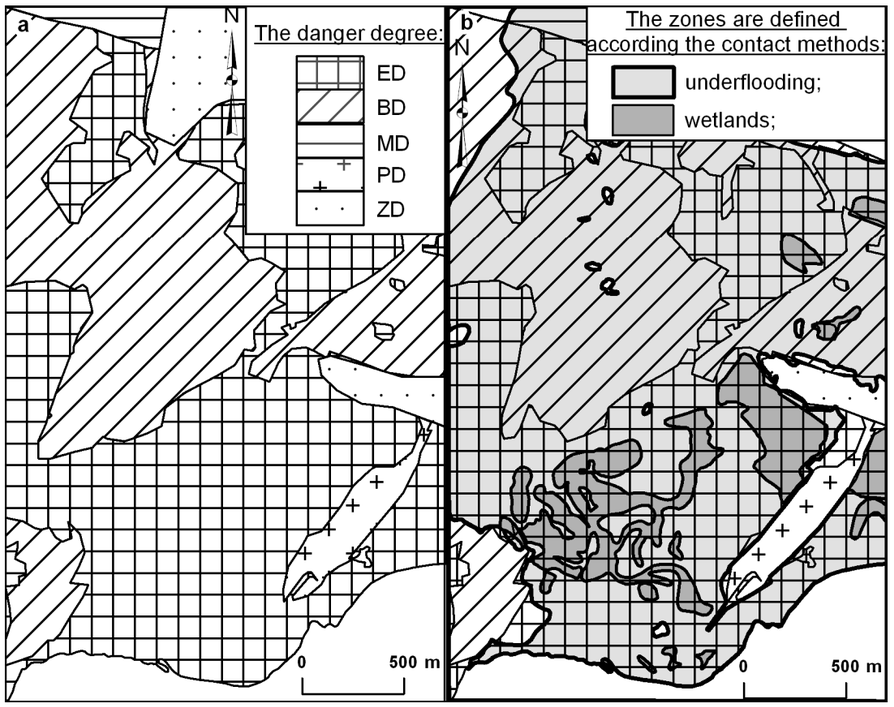

Fig. 3 – The resulting cartographic model of potential underflooding in Zidki village, Kharkiv region. (a – cartographic model according to danger degree, acquired from satellite image interpretation, b – the results cartographic model)

The predictive model, resulting from consequent overlay of all the layers of the available images, will allow quick detection of underflooded territories, their visual evaluation and timely decision on the underflood prevention in potentially hazardous zones.

To validate the model's adequacy, a comparative analysis of the acquired results with real data of contact survey for the period of 2007-2008 was carried out (fig. 3b).

Black thickened contour on fig. 4b emphasizes zones, determined by field surveys. According to contact method data the underflood area was 496,4 ha, geo-model's – 563,5 ha. Accordingly, the determination precision of potentially underfloodable

III. Results

Derivation of equations for the full splitting method

Derive finite difference equations and provide their justification.

We use staggered meshes: material velocity u is updated in nodes x_i, where i is node number, while density, pressure, energy and sound velocity are updated at the centers $x_{i+0,5}$ of intervals $(x_{i+1} - x_i)$.

Let begin with the fully split matrix coefficients for (2). Find an eigenvalue of A. For this end we need to solve the characteristic equation for A: $\det[A - \lambda E] = 0$, or, in expanded form,

$$\det\begin{bmatrix} u-\lambda & 0 & \frac{2}{\gamma-1}c \\ \rho & u-\lambda & 0 \\ \frac{\gamma-1}{2}c & 0 & u-\lambda \end{bmatrix} = 0. \qquad (5)$$

Expand determinant (5) with respect to its elements in the first row:

$$\det[A-\lambda E] = (u-\lambda)\det\begin{bmatrix} u-\lambda & 0 \\ 0 & u-\lambda \end{bmatrix} + \frac{2}{\gamma-1}c\det\begin{bmatrix} \rho & u-\lambda \\ \frac{\gamma-1}{2}c & 0 \end{bmatrix} = 0,$$

or

$$(u-\lambda)(u-\lambda)^2 + \frac{2}{\gamma-1}c\left(-\frac{\gamma-1}{2}c(u-\lambda)\right) = 0.$$

In the last equation, λ is unknown. Find the roots of the equation.

The root $\lambda_1 = u$ corresponds to the contact characteristic. The first left eigenvector corresponding to $\lambda_1 = u$ is

$$W_1 = [0,1,0].$$

To find the other two roots we need to solve the equation

$$(u-\lambda)^2 - \frac{2}{\gamma-1}c\left(\frac{\gamma-1}{2}c\right) = 0,$$

or

$$(u-\lambda)^2 - c^2 = 0.$$

Its roots are $\lambda_2 = u + c$ and $\lambda_3 = u - c$.

Equations (2) can be rewritten in matrix form. Denote

$$U = \begin{bmatrix} u \\ \rho \\ c \end{bmatrix} \text{ and } A = \begin{bmatrix} u & 0 & \frac{2}{\gamma - 1}c \\ \rho & u & 0 \\ \frac{\gamma - 1}{2}c & 0 & u \end{bmatrix}.$$

Then (2) takes the form

$$U_t + AU_x = 0, \tag{3}$$

where

$$U_t = \begin{bmatrix} u_t \\ \rho_t \\ c_t \end{bmatrix}, \quad U_x = \begin{bmatrix} u_x \\ \rho_x \\ c_x \end{bmatrix}.$$

Equations (3) can be solved with many numerical methods. They are listed in [1], including the method with split matrix coefficients.

The idea of the full splitting method

The splitting of matrix coefficients is based on the representation of the matrix A in the form

$$A = T\Lambda^+ T^{-1} + T\Lambda^- T^{-1}. \tag{4}$$

Here T^{-1} is the matrix of the left eigenvectors of A, T is reciprocal of T^{-1}, Λ^+ and Λ^- are diagonal matrices of, correspondingly, the positive and negative eigenvalues of A.

The method is advantageous in its consistency with the theory of characteristics and disadvantageous in the non-conservatism of difference equations.

In accord with [1], in order to apply the method to equations (2), we must rewrite them so as to allow the characteristics $\frac{dx}{dt} = u \pm c$ to appear explicitly. This cannot be done for a sophisticated or tabulated equation of state.

That is why we propose semi-splitting of matrix coefficients. For compression waves we use a method by V.F. Kuropatenko [2]. As a result, we obtain a simple and effective difference scheme for solving (1). The scheme is tested through comparison with exact solutions. The idea of using semi-split matrix coefficients was suggested in [3].

zones was 86,5%. The acquired result demonstrated the advisability of using the presented method of rapid identification of potentially underfloodable zones with their consequent localization for timely preventive decision making.

IV Conclusions

Construction of complex cartographic geo-models according to certain degrees of danger by the proposed method will allow, under condition of limited a priori information, sufficiently quickly identify potentially underfloodable zones, and localize potentially dangerous and safe territories. The process of geo-models' construction by the described scenario requires insignificant time and material costs.

Under conditions of insufficient a priori information and geological diversity of the structure, the given model is most adapted for identification of potentially underfloodable zones due to synthesizing of the given remote and contact methods.

References

1. Aref'eva A.V., Mukhin V.I., Mirmovich E.G. Podtoplenie kak potentsial'nyi istochnik ChS (Flooding as potential source of extraordinary situations), Tekhnologii grazhdanskoi bezopasnosti. 2007. Vol. 4. No 4. PP. 69-73.
2. Strizhel'chik G.G., Sokolov Yu.P., Gol'dfel'd I. A., Chebanov A.Yu., Nikolaenko N.S. Podtoplenie v naselennykh punktakh Khar'kovskoi oblasti (Underflooding in settlements of the Kharkov area). Kharkov: UkrNIINTIZ. 2003. 160 p.
3. Bakker W.H, Feringa W., Geiske S.M. and Gorte G.H. (eds) (2009) Princyples of Remote Sensing, 4th edn., Enschede: The International Institute for Geo-Information Science and Earth Observation.
4. Moran M.S., Peters-Lidard C.D., Watts J.M. and McElroy S. (2004) 'Estimating soil moisture at the watershed scale with satellite-based radar and land surface models ', Canadian Journal of Remote Sensing, 30(5), pp. 805-826.
5. James B. Campbell (2002) Introduction to remote sensing, 3d edn., New York: The Guilford Press A Division of Guilford Publication.
6. Levin N. (1999) Fundamentals of Remote Sensing, 1st edn., Tel Aviv: Remote Sensing Laboratory, Geography Department, Tel Aviv University.
7. Romanov A.N., Sutorikhin I.A. Distantsionnyi monitoring gidrologicheskogo rezhima pereuvlazhnennykh pochv (Remote monitoring of a hydrological mode of the rehumidified soils), Geografiya i prirodnye resursy. 2006. No 1. PP. 137-140.
8. Tsymbal V.N., Matveev A.Ya., Gavrilenko A.C., Bychkov D.M., Yatsevich S.E. Monitoring podtopleniya zemel' aviatsionnym kompleksom distantsionnogo zondirovaniya AKDZ-30 (Integrated monitoring of lands underflooding manifestationd by the aviation remote sensing complex

ACRS-30), Sovremennye problemy distantsionnogo zondirovaniya Zemli iz kosmosa. 2011. Vol. 8, No 3. PP. 199-207.
9. Vladov M.L. and Starovoitov A.V. (2002) Georadiolokatsionnye issledovaniya verkhnei chasti razreza (Georadio-location researches of overhead part of cut), 1st edn., Moscow: MGU.
10. Mundher Ali Seger and Ahmed Fouad Nashait (2011) 'Detection of Water-Table by Using Ground Penetration Radar (GPR)', Eng. & Tech. Journal, 29(3), pp. 554-566.
11. Gorelik S.I. Opredelenie zon vozmozhnykh podtoplenii v usloviyakh ogranichennoi apriornoi informatsii (Determination areas of possible underflooding in the conditions of limited a priori information), Sistemi obrobki informatsiї: zb. nauk. pr., Khark. un-t povitr. sil im. Ivana Kozheduba. 2014. Kh. Issue. № 114. PP 258-262.
12. Butenko O.S., Gorelik S.I. Metodika opredeleniya ekspertnykh otsenok dlya vyyavleniya zon vozmozhnykh podtoplenii (The deteremination technique of expert estimations for exposure of possible areas underflooding), Radioelektronni i komp'yuterni sistemi : nauk.-tekhn. zhurn. Kharkov, 2014. Issue. № 66. PP. 59–64.
13. McNeill F.M. and Thro E. (1994) Fuzzy logic: a practical approach, 1st edn., Chestnut Hill, MA. : ACADEMIC PRESS LIMITED 24-28 Oval Road, London NWI 7DX.
14. SRTM 90m Digital Elevation Data. Available at: http://dds.cr.usgs.gov/srtm [Accessed 12 Mar. 2014].

movement on the coast. Since the temporal and spatial scales of this sophisticated phenomenon are strongly different, it is currently impossible to reproduce them all in a unique physical model or a unique code.

In the paper we consider a problem of surface wave propagation in the ocean and its run-up on the coast. The problem is characterized by a large range (up to 1000 km) the wave covers and a long time (thousands of seconds) it takes the wave to reach the coast. This means that its numerical solution will require many cycles over time and hence the finite-difference scheme needs to have a minimal smoothing effect.

A semi-splitting finite-difference scheme is developed and used for solving the above problem.

II. Problem statement

Equations for the full splitting method

Consider 1D motions of ideal gas in Eulirian coordinates, which can be described by equations

$$\begin{cases} u_t + uu_x = -\dfrac{1}{\rho} p_x \\ \rho_t + u\rho_x + \rho u_x = 0 \\ E_t + uE_x = -\dfrac{p}{\rho} u_x, \quad p = (\gamma - 1)\rho E. \end{cases} \tag{1}$$

Here u is velocity vector component, ρ is volume density, p is pressure, E is internal energy per unit mass, and $\gamma = 1,4$ is adiabatic exponent.

Rewrite (1) in another form. Introduce sound velocity c such that

$$c^2 = \gamma \frac{p}{\rho} \text{ and } E = \frac{1}{\gamma(\gamma - 1)} c^2.$$

Using these to express pressure and energy in terms of sound velocity and their substituting into (1) yield

$$\begin{cases} u_t + uu_x + \dfrac{2}{\gamma - 1} cc_x = 0 \\ \rho_t + u\rho_x + \rho u_x = 0 \\ c_t + uc_x + \dfrac{\gamma - 1}{2} cu_x = 0. \end{cases} \tag{2}$$

Skorkin, N.A.,
PhD, Professor, Zababakhin RFNC-VNIITF, Snezhinsk, Russia
Simonenko, V.A.,
PhD, Professor, Zababakhin RFNC-VNIITF, Snezhinsk, Russia
Uglov, A.S,
Senior Researcher, Zababakhin RFNC-VNIITF, Snezhinsk, Russia

A SEMI-SPLITTING FINITE-DIFFERENCE SCHEME FOR 1D HYDRODYNAMIC EQUATIONS AND ITS APPLICATION TO TSUNAMI SIMULATION

Abstract

The paper presents a semi-splitting finite-difference scheme for solving 1D hydrodynamic equations. The scheme was implemented in a 1D code which was used to simulate mega-tsunami propagation and run-up.

Code verification shows that the proposed computational procedure works correctly.

The motion of a surface wave in the ocean is simulated and numerical results are compared with data obtained by C. Mader for a similar problem.

The code is shown to be applicable to the simulation of wave run-up on the coast. Further work implies the development of a 2D code for surface wave propagation simulation.

Keywords: *semi-splitting finite-difference scheme, shallow water theory, tsunami, coast, astronomical body*

I. Introduction

As a result of research taken in the recent decades, it has become widely understood that Earth collisions with small astronomical bodies – asteroids, comets and their fragments – involve great danger to our civilization. A rather high probability of such events stimulates further extended research into their consequences. The impacts of astronomical bodies on the ocean deserve special consideration because their probability is twice as high as that of impacts on earth. An astronomical body impacting on the ocean gives water considerable kinetic energy which transforms into the energy of a giant oceanic wave called tsunami. Tsunamis are very destructive. In this context it is of interest to investigate the effects of impacts on the ocean in more detail.

The impact of an astronomical body on the ocean and its effect can be considered to evolve in three phases: (1) impact and formation of a wave on the ocean surface, (2) propagation of the surface wave in the ocean and its run-up on the coast, and (3) – wave

Nosov Vladimir K.
Doctor of Sciences, Professor of Moscow Institute of Aviation Technology, Russian State Technology University, Stupino Branch Stupino
Nesterov Pavel A.
Associate professor of Moscow Institute of Aviation Technology, Russian State Technology University, Stupino Branch Stupino
Ermakov Evgeny I.
Post-graduate student of Moscow Institute of Aviation Technology, Russian State Technology University, Stupino Branch Stupino

3D MODEL OF THE STRUCTURAL CONSTRUCTION OF TITANIUM, A-TITANIUM ALLOYS AND A+B – TITANIUM ALLOY TI6AL4V

Abstract

3D models of structural construction of titanium, α-titanium alloys and α + β-titanium alloy Ti6Al4V were developed under the terms of the minimum surface free energy and full space-filling with isolated polyhedron – Kelvin`s tetrakaidecahedron. It was found an analytic dependence, which relates a size-defined crystallite with an average size of its planar reflection. Stereological characteristics of spatial structures of alloys were discovered. The dependence of the specific surface areas and the specific volumes of intergranular zones on the diameter of the crystallite in the micro-, submicro- and nanostructured levels were established.

Keywords*: titanium alloys, 3D model, stereological and stereometric parameters.*

Introduction

Theoretically sound and experimentally confirmed idea of a three-dimensional structure of one-phase and hetero-phase metallic materials increases the understanding of the processes of formation of volumetric structure during the plastic deformation, heat treatment, and their effect on mechanical properties. Three-dimensional model of a single-phase continuous polyhedral structure must meet the interrelated thermodynamic conditions of a minimum surface free energy and stereometric conditions of fulfilling of the space without gaps, overlaps and combinations with other polyhedrons with a crystallite (grain) in the form of an isolated polyhedron [1-4]. Three-dimensional simulation of a hetero-phase structure in addition to the single-phase should be taken into account to achieve the equilibrium phase composition of the alloy, determined by

theoretical and kinetic conditions of plastic deformation and heat treatment, form of a crystallite, a sequence of nucleation and filling crystal defects with the second phase in the process of its growth [1,2].

The purpose of this work is to develop a three-dimensional model of the structure of titanium, α-titanium alloys and α + β- titanium alloy Ti6Al4V at equilibrium condition.

The method of modeling

The approximation to the local equilibrium condition of the surface free energy of titanium and homogeneous α-solid solution is achieved on the conditions that three boundary planes at the rib are joined to each other at an angle of 120 °, and four ribs converging at the vertices – at an angle of 110 °. The truncated octahedron (Kelvin's tetrakaidecahedron) most satisfies such conditions. The ratio of the surface of tetrakaidecahedron to the surface of sphere of equal volume – 1,099. Choice of tetrakaidecahedron as an isolated polyhedron of an equilibrium polyhedral structure is caused by the fact that it is the only semiregular Archimedean solid, that can fill tridimensional space without gaps, superpositions and combinations with other polyhedra (Figure 1a), forming a space filling pack (SFP) (Figure 1b).

An arbitrary section of SFP monophase polyhedral structure (Figure 1c) displays a planar structure visible on the surface of the section in an optical microscope. This structure is typical for recrystallized conditions of technical titanium, homogeneous α- and β-solid solutions of titanium alloys and tempered α + β-alloys of the transitional class and pseudo-β alloys [5] (Figure 1d).

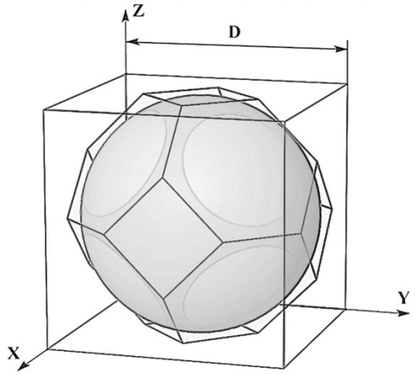

a)

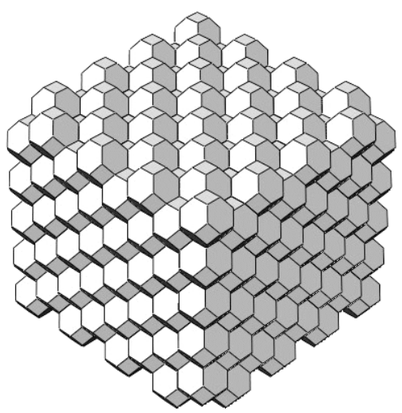

b)

3. Anokhin, VI The use of high-speed torque converters on crawler tractors / VI Anokhin – M .: Mechanical Engineering, 1972. – 304 p.
4. Anokhin, VI On the choice of the basic parameters of the converter for hydromechanical transmission speed tracked agricultural tractor / VI Anokhin, [et al.]. // Tractors and agricultural machinery. – 1985. – №10. – S. 11 – 15.
5. Kochkarev, AJ Hydrodynamic transmission / AY Kochkarev – L .: Mechanical Engineering, 1971. – 336 p.
6. Narbut, AN Torque converter / AN Narbut – M .: Mechanical Engineering, 1966. – 218 p.
7. Anisimov, VB Torque converters for building and road machines / VB Anisimov – M .: Stroyizdat, 1967. – 42 p.
8. panties, SM Automotive torque converters / SM Pants – M .: Mechanical Engineering, 1977. – 211 p.

Transparency – property impeller change the amount of torque when changing the gear ratio torque converter. If the change gear ratio of torque on the pump wheel remains constant, the torque converter is called the «opaque.»

3. Torque converter must convert the torque in the drive to the full range of workloads. Floating crane for maximum transformation ratio must be between 1.4 ... 1.6 [1]. Within the specified value ratio and maximum accepted level of transparency appropriate to use a single-stage torque converter having its greatest simplicity of design [4, 6, 7].

4. Torque converter should have a locking device in order to provide the drive with a constant low speed, i.e. have a freewheel.

5. For creating a drive mechanism for lifting torque converter is necessary to combine original characteristics of the induction motor and the torque converter, which is carried out by combining the rated torque of the motor with the zone of maximum efficiency torque converter. In this case, the converter convert properties used in all operating modes of the drive with the implementation of positive qualities, in relation to underwater mining.

On the basis of the formulated requirements necessary to select the following parameters converter mechanism for lifting floating crane.

Optimum is a single-stage torque converter with a comparatively simple design and the cheapest to produce.

The main requirement to the torque converter – high efficiency in the working area. This requirement may be more fully realized in integrated torque convertors (s centripetal turbine and the symmetrical arrangement of the pump and turbine wheel . Moreover, in a centripetal turbine torque converter when installed in the reactor wheels clutches realized efficient operation of the fluid coupling mode. The observed property is due to the fact that the output torque converters of this type of hydraulic fluid from the pump wheel is located on a larger diameter circle its circulation.

This analysis of the performance requirements and the design of the drive torque converters for floating cranes lifting mechanism, the relevant conditions and loads, suggests that they correspond to the most complex type torque converter with a centripetal turbine.

At the hoist drive, developed by the authors at the Department of handling machines Volga State Academy of Water Transport, received a patent for utility model №91999, and work is underway to further development and implementation of the actuator.

References.

1. Nikitaev, IV Ship power grab installations for the extraction of ore materials on the continental shelf / IV Nikitaev – Nizhniy Novgorod: VSAWT, 2000. – 26 p.
2. CAD / CAE system APM WinMachine

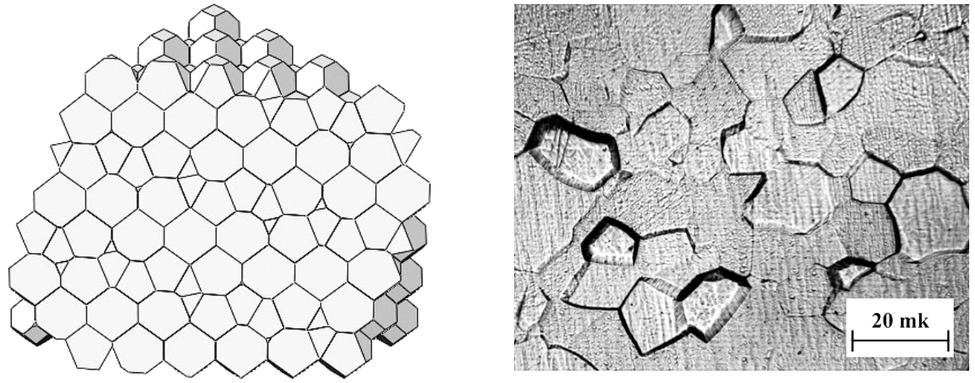

c) d)

Figure 1. Isolated semiregular polyhedron in the form of tetrakaidecahedron (a), SFP (b), any of its cross-section (c) and microscopic section (d).

The Ti6Al4V alloy belongs to the α + β-titanium alloys of average strength where volume fraction of β-phase is 10-15% in the equilibrium recrystallized condition [6]. *The d*evelopment of three-dimensional model of the structural Ti6Al4V alloy is also based on stereometric and thermodynamic conditions. The first condition consists in an absolute space filling with a single for two-phase α + β-structure of the alloy isolated polyhedron tetrakaidecahedron that is typical for monophase structures. The second condition suggests striving for infill with β-phase the volume with free energy of maximum level under conditions of a high-temperature recrystallized α + β annealing, that is, sequentially vertices and ribs of insulated crystallite (grain) α-phase – tetrakaidecahedron as a continuous frame in compliance with the dimension of nucleation [1]. The fulfilment of these conditions is achieved by truncating the vertices and ribs of a semiregular polyhedron tetrakaidecahedron in volume equal to the volumetric fraction of β- phase. Computer 3D modeling, visualization of constructing a dimensional model, the necessary measurements and accounts were performed in the software package of solid modeling «Solid Works Education Edition».

Modeling results

On the first level of 3D modeling structural composition of single-phase homogeneous structure includes: crystal (α-grain) in the shape of a truncated Kelvin`s tetrakaidecahedron and intergranular zone (grain boundaries) with a crystallographic thickness divisible by interatomic distance of titanium. Each structural component is a continuous, homogeneous, isotropic, deformable medium.

Random section SFP of one-phase equilibrium polyhedral structure (Figure1c) shows a planar structure visible on the surface of the section in an optical microscope

and applied in practice to calculate the average grain diameter $\overline{d}_{\alpha}$. As follows from (Figure 1c) in a planar section of the SFP trihedral and octagonal polygons with different areas, the size of the angles and their relation to each polygon are formed. The ratio between the average diameter of α-crystallite in the three-dimensional model and its arbitrary sections enclosed volume of a homogeneous single-phase polyhedral structure composed D = 1,53 $\overline{d}_{\alpha}$.

With the passage of intersecting planes equivalent to (001) plane of isolated tetrakaidecahedron its section consistently changes their shape from square to octagon (Figure 2a, b). The cross section of an isolated tetrakaidecahedron by the planes equivalent (110) in the sequence from the center gives the initial image of the hexagon, followed by changes in the shape of an octagon, and to finally rectangle (Figure 2c, d). Tetrakaidecahedron sectional planes in general position further illustrate the variety of forms derived polygons in the planar reflection (Figure 2e, f).

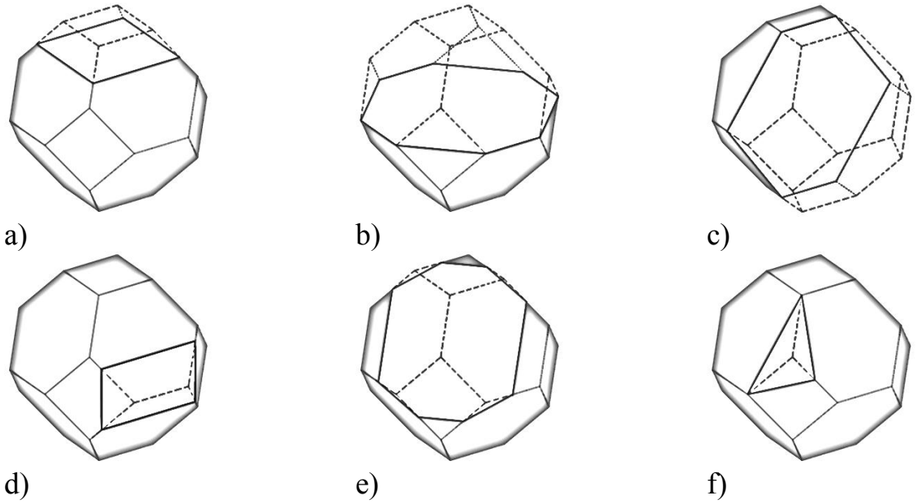

Figure 2. Cross-sections of tetrakaidecahedron with quotient planes equivalent to (001) plane (a, b); (110) (c, d) and planes in general position (e, f).

The simulation results of three-dimensional spatial structure of the two-phase α + β-titanium alloy Ti6Al4V presented in Figure 3. The result of truncation the edges and vertices of tetrakaidecahedron – «truncated tetrakaidecahedron» as an isolated irregular polyhedron (Figure 3a) of the crystal (grain) α-phase, characterized by the following stereometric parameters: the total number of vertices – 72; the total number of faces – 74 (of them are hexagonal – 8, square – 6, triangular – 24, long square – 12, and trapezoidal – 24). The ratio between the surface of «truncated tetrakaidecahedron» and the surface of a sphere of equal volume is 1.03.

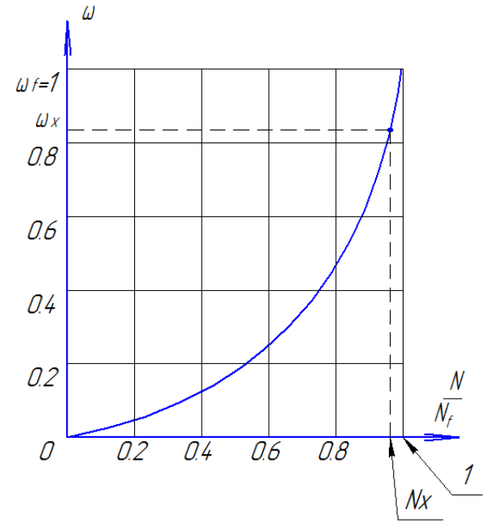

Fig. – 3 – Curve damage.

2. A method for increasing the reliability of steel structures and the drive mechanism for lifting floating crane clamshell.

The torque converter allows you to automatically adjust the speed of lifting and closing the grab by creating a feedback between the load on the ropes and speed scooping and lifting the grab. They allow you to smoothly change the gear ratio from the motor to the gearbox by 3.5 times in the direction of increasing and correspondingly increasing the torque on the shaft of the gearbox, which will overcome the effect of «peak» loads. Additionally, a means, which prevents the actuator from any overload, since the torque transmission therein through the liquid, rather than through a rigid kinematic linkage.

Analysis of the properties and characteristics of the existing torque converters [3, 4] allows us to formulate requirements for them to be installed in the mechanism of lifting floating crane:

1.Torque converter possessing high speed, must have the appropriate damping properties to avoid the effect of his work on the high-frequency oscillations in the hoisting ropes.

2. Torque converter must ensure operation of the motor drive in optimal conditions, will not enter when all the input power is spent on «myatie» fluid. Such requirements are met completely «opaque» torque converters [3, 5, 6], but the creation of torque converters of this type is problematic [6, 8], so it is advisable to apply torque converters with a low degree of «transparency» in the range of 1.0 ... 1.1 in the main working area.

Table 1 – Results of calculation.

№	Stress	mPa	Strans	m
1	Σ	149	e	$0.964x10^{-3}$
2	σ_X	32,5	e_X	$0.8x10^{-3}$
3	σ_Y	52,6	e_Y	$0.426x10^{-4}$
4	σ_Z	65,0	e_Z	$0.484x10^{-3}$
5	σ_{XY}	36,6	e_{XY}	$0.227\ x10^{-3}$
6	σ_{YZ}	46,7	e_{YZ}	$0.29\ x10^{-3}$
7	σ_{XZ}	18,0	e_{XZ}	$0.112\ x10^{-3}$

Results of calculation of the maximum deformations and stresses in the critical elements of the framework presented in Figure 2. It is seen that the stress state is triaxial (volumetric) character.

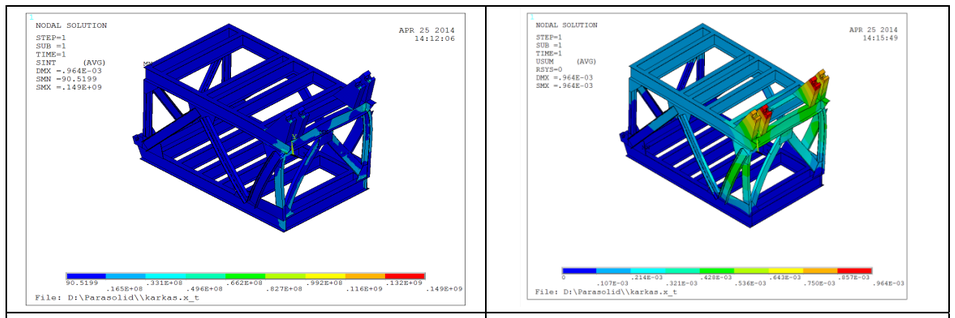

a) the equivalent stresses | b) the total deformation

Fig. 2 – The results of the calculation.

From the analysis of solutions of the problem (see Table 1) shows that the stress level does not exceed the yield strength. Figure 3 shows the curve of damage ω relative to the number of loading cycles $\frac{N}{N_f}$, where N_f – number of cycles to macrocrack formation. Analyzing the results of the maximum strain and stress can be concluded that the amount of accumulated damage is in the danger zone (close to the «critical» value ($\omega_x = 1$).

The evaluation of durability of the floating crane CPL 5-30 Head. №2040 concluded that the development of the resource metal frame of the engine room (residual life is within the error calculation) and is necessary to overhaul with replacement metal bearing loaded elements, or the reconstruction of the crane.

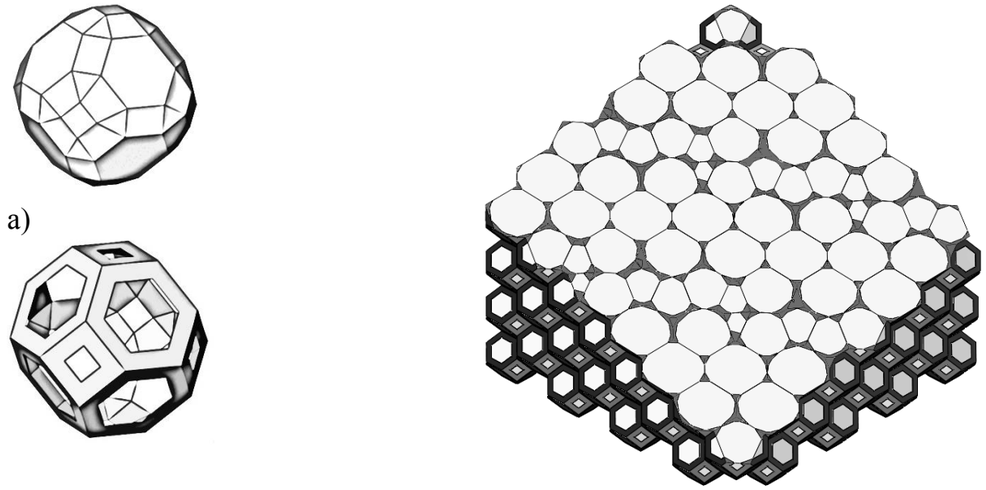

Figure 3. Isolated irregular α-phase polyhedron in the form of «truncated tetrakaidecahedron» (a) a continuous β-phase frame (b), an arbitrary section SFP(c) of two-phase Ti6Al4V alloy with 10% of volume fraction of the β-phase in the three-dimensional space.

Continuous reinforcing isolated spatial «β-phase frame» (Figure 3b) which has a volume equal to the volume fraction of β-phase in the alloy and supplementing the scope of the «truncated tetrakaidecahedron « to a volume of tetrakaidecahedron is represented as tunicary polyhedron that contains 36 ribs in the form of a triangular prism, obtained by truncating the ribs of tetrakaidecahedron and 24 vertices in the form of a triangular pyramid.

Thus, αα, αβ and ββ boundary surfaces are formed in SFP of the proposed three-dimensional model α + β-titanium alloy Ti6Al4V with isolated polyhedron as «precast tetrakaidecahedron» consisting of «truncated tetrakaidecahedron», α-phase and the continuous spatial «β-phase frame « (Figure 3c). It is necessary to distinguish between internal and external boundary surface toward the «precast tetrakaidecahedron».

To quantify the structure of the alloys following notation of spatial stereological parameters are used [7]:

V – the α-grain volume of single-phase polyhedral structure in the form of tetrakaidecahedron, which corresponds to the volume «precast tetrakaidecahedron» with α + β-structure;

S – surface area of the grain boundaries of α-single-phase polyhedral structure corresponds to the external αα and ββ-boundary surfaces of «precast tetrakaidecahedron»;

$\delta_\alpha = na_\alpha$ – crystallographic thickness of the α-boundary with the interatomic distance $a_\alpha = 2{,}9\times10^{-4}$ μm [8], where n – repetetition factor of thickness αα- border to the interatomic distance;

$V_b = S\delta_\alpha$ – the volume of α-grain boundaries of single-phase polyhedral structure;

V_α – α-grain volume in a two-phase structure in the form of «truncated tetrakaidecahedron»;

V_β – β-phase volume in two-phase α + β structure in the form of a continuous spatial «β-phase frame»;

$S_{\alpha\alpha}$ – surface area of α-phase grain boundaries in two-phase α + β structure that are in contact with adjacent grains of α-phase in SFP;

$S_{\beta\beta}$ – surface area of continuous frame of β-phase grain boundaries in two-phase α + β structure that are in contact with adjacent grains of β -phase in SFP;

$S_{\alpha\beta}$ – surface area of the internal interfacial αβ-faces between «β-phase frame» and «truncated tetrakaidecahedron» in SFP;

$S_\alpha = S_{\alpha\alpha} + S_{\alpha\beta}$ – area of the outer and inner boundary surface of «truncated tetrakaidecahedron», i.e. α-grains in a two-phase α + β structure;

$S_\beta = S_{\beta\beta} + S_{\alpha\beta}$ – area of the outer and inner boundary surface of β-phase in the continuous «β-phase frame» in the two-phase α + β structure;

$\delta_\beta = na_\beta$ – crystallographic thickness of the β -boundary with the interatomic distance $a_\beta = 2{,}86\times10^{-4}$μm [8], where n – repetetition factor of thickness ββ – border to the interatomic distance;

$V_{\beta\beta} = S_{\beta\beta}\times\delta_\beta$ – ββ-boundaries volume in SFP;

$V_{\alpha\alpha} = S_{\alpha\alpha}\times\delta_\alpha$ – αα-boundaries volume in SFP;

$\delta_{\alpha\beta} = (\delta_\alpha + \delta_\beta)/2$ – crystallographic thickness of the interfacial αβ-border;

$V_{\alpha\beta} = S_{\alpha\beta}\times\delta_{\alpha\beta}$ – the volume of interphase αβ-boundaries in the SFP of two-phase α + β structure;

$\bar{d}_\alpha$ – the average diameter of α-grain in a planar section of the «truncated tetrakaidecahedron»;

D – the average diameter of α-grain in a spatial model equal to the diameter of a sphere inscribed in tetragonal faces of tetrakaidecahedron.

The results of calculations stereological parameters of spatial single-phase polyhedral structure in the form of tetrakaidecahedron and two-phase structure in the volume of «prefabricated tetrakaidecahedron» with different D in the micro-, sub micro- and nanostructural scale levels (1-100 μm) and n = 1-5 are shown at Figures 4 and 5.

According to the calculations, it follows that the specific cross-boundary surfaces S/V and volumes V_b/V of the homogeneous equilibrium polyhedral structure increase with decreasing of the actual grain size D and characterized with the linear dependence in the coordinates lg S/V – lg D and lg V_b/V – lg D (Figure 4).

wind load working condition – wind speed of 15 m / s, the maximum inertia load and a maximum roll pontoon – 30.

2. For the second case selected peak operation of the crane, this mode occurs when using the grapple in water-saturated material under water, when scooping and lifting raises additional hydrostatic forces, «suction», filtration, hydrostatic and viscous flow of the material, depending on the speed scoop up material and separation of the grapple, which leads to stress the rope hoist and crane metal. This effect occurs in a short period of time and may exceed 30% allowable load on the crane and a «peak».

Lifting speed of cargo: m / s, the maximum weight of the load lifted kN. For a general idea of the nature of deformation of the frame and identify the location of the nodes that are critical in terms of durability, the first stage was carried out by elastic analysis account code [2].

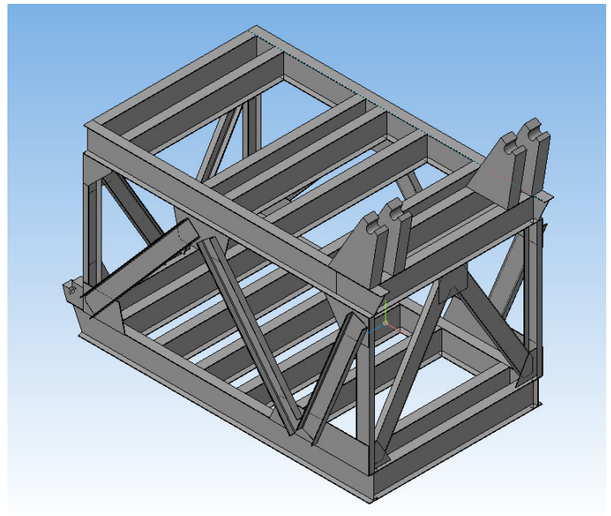

Fig. 1. – The model of the engine room carcass floating crane.

Physical and mechanical characteristics of St3 were adopted as follows: Young's modulus of elasticity $E = 1.94\times10^5$ mPa, Poisson's ratio ν=0,28, yield point σ_T = 230 mPa, density ρ=7820 kg/m^3. The frame was modeled in full size in compliance with specified characteristics and geometry. Each compound was replaced by a rigid – welded. Modeling supports the frame also been conducted, but in places bearing frame on the turntable imposed boundary conditions precluding movement of nodes in all directions and turn them into these nodes. Based assortments used profiles idealization carcass structure into finite elements was carried out using 8, 10, 20 – the final nodal elements are symmetric in cross section.

The calculation results are shown in Table 1, which shows the maximum values of the stresses and strains in the elements of metal carcass floating crane CPL 5-30.

Yablokov A.S.

THE METHOD OF RECONSTRUCTION OF THE DRIVE MECHANISM FOR LIFTING FLOATING CRANE BUCKET BASED ON AN ASSESSMENT OF DURABILITY METAL FLOATING CRANE

Key words: cycle fatigue experiment, damage, material parameters, the torque converter, impeller, turbine, reactor wheel, grab

The article discusses the problem of assessing the durability of metal structures of the engine room of the floating crane. Examined the effects of the phenomenon of «suction» grab for floating cranes involved in subsea production. The solution of the problem – including in the drive mechanism for lifting the torque converter, as well as the requirements to specifications and design for such a converter.

Introduction.

When subsea floating cranes as a lifting body uses grapple. Hoist and scoop grab the floating crane is not different from the hoist gantry crane, which when overloaded bulk materials as well as the lifting body uses grapple. However, when operating in the water-saturated material of the grapple under water when scooping and lifting raises additional hydrostatic forces «suction» filtering hydrostatics and viscous flow of the material in the grapple, which depend on the speed of separation and scooping material grapple, which leads to stresses in the hoisting ropes and metal crane. This effect, which occurs in a short period of time, may exceed the 50% allowable load on the crane and a «peak» [1].

Currently 90% of floating cranes have a lifespan of 15 years or more, which makes their use problematic in underwater mining, as their metal worn and are not designed for such loads.

1. Evaluation of the durability of metal floating crane CPL 5-30.

To assess the durability of metal floating crane CPL 5-30, was calculated metal frame floating crane engine room CPL 5-30, Head. №2040, made in 1974 by the «ship» Bor. To date, the floating crane was committed 902,467 cycles and handled 2,256,168 tonnes (according to the organization of the operator). Material metal crane St3kp. Determination of stress-strain state of a floating crane performed depending on the operating conditions of the crane:

1. For the first case, the calculation was chosen nominal mode of operation of the crane, the corresponding maximum permissible load capacity – 5 tons, the marginal

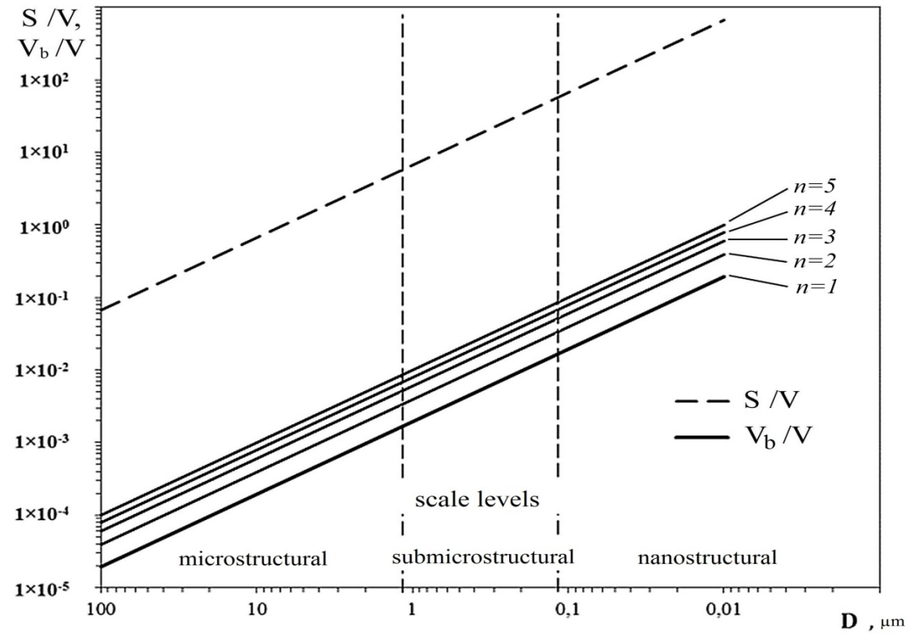

Figure 4. The dependence of the specific cross-border surface areas S/V and volumes V_b/V on the diameter of the inscribed sphere of tetrakaidecahedron for single-phase equilibrium polyhedral structure of titanium and α-titanium alloys.

The specific surface area S/V of the isolated polyhedron sharply increases with parameter D decrease. If in ultra fine-grained material with D=10μm, that meet the implementation requirement of superplastic deformation, this ratio is 0.67, then with the nanometeric grain size D=100nm and D=10nm the ratio increases to 67 and 670 respectively. The calculation results are evidence that the specific cross-boundary volumes V_b/V changed similarly. Thus, when the thickness of cross-boundary layer is two interatomic distances n = 2 and the values of D=10; 0.1 and 0.01μm of V_b/V is $3{,}88\cdot10^{-4}$; $3{,}88\cdot10^{-3}$ and $38{,}8\cdot10^{-1}$ μm^{-1}. This means that with D=10nm and the thickness of cross-boundary layer δ_α=0,58nm, volumetric fraction of the cross-boundary layer is 38.8%, and with the same D=10nm and n=5 (δ_α = 1,45nm) – 97.1% (Figure 4).

We obtained the similar results with 3D modeling of structural composition α + β – Ti6Al4V titanium alloy where β-phase volumetric fraction is 10%, which total specific volumetric fraction of interfacial $V_{\alpha\beta}/V$ and cross-boundary $V_{\alpha\alpha}/V$ and $V_{\beta\beta}/V$ is 28.7% even when the effective thickness of intergranular αα (ββ) and interfacial αβ layer equals to one interatomic distance α- and β – phases [7]. With the thickness of intergranular and interfacial layers equal to two interatomic distances their total specific volumetric fraction of the Ti6Al4V alloy with V_β =0,1 increases to 76.5%, while the alloy with V_β = 0,15 it increases to 81.5% (Figure 5).

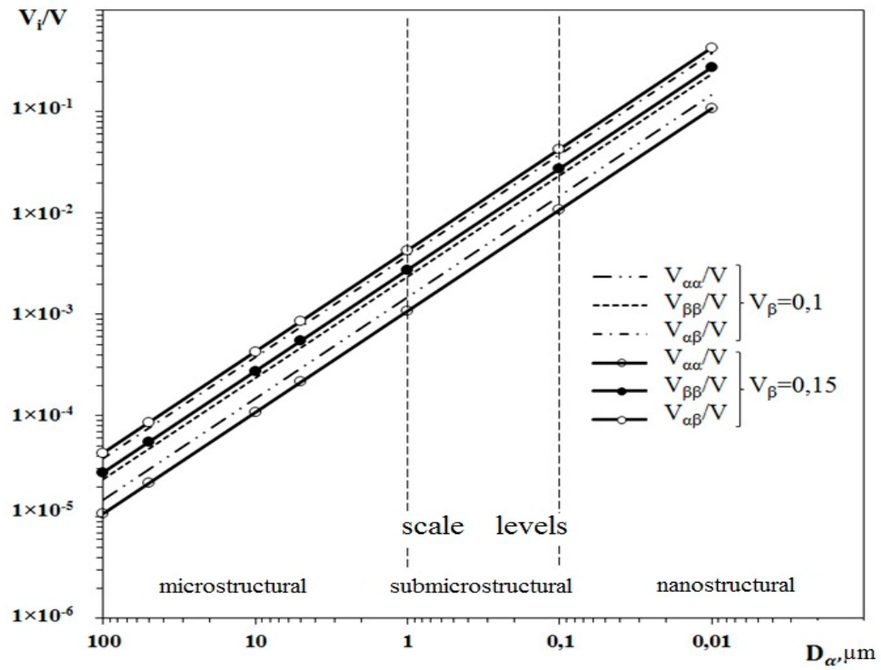

Figure 5. The dependence of the volumetric fraction of the interphase Vαβ and cross-boundary Vαα, Vββ components of VT6 alloy with a thickness of α- and β- boundaries is equal to two interatomic distances on the grain size at V_β=0,1and 0,15.

Such structural state with nanosized grain D=10nm and volumetric fraction of intergranular zones to 76-97% either absurd and almost unattainable, or is a specific structural state characterized by the primary crystalline structural state of «nonequilibrium boundary phase» with unpredictable today properties and colossal thermodynamic fluctuation.

Conclusions

1. The stereological parameters of mono-phase homogeneous polyhedral structure with the isolated polyhedron in the form of tetrakaidecahedron in 3D model have been denoted and calculated.

2. Three-dimensional model of microstructural state of α+β-titanium Ti6Al4V alloy where β-phase volumetric fraction equals 10 and 15% has been suggested in the form of «precast tetrakaidecahedron» consisting of α-phase crystallite in the form of truncated tetrakaidecahedron by the vertices and ribs and continuous volumetric «β-phase frame», that fills truncated volumes.

3. The principal stereometric parameters of α-phase crystallite of «truncated tetrakaidecahedron» and continuous volumetric «β- phase frame» have been determined.

located in the countryside, the use of ion-exchange water treatment unprofitable. However, in addition to saving money on water treatment, there are indicators that magnetic water treatment compares favorably with other methods [4,5]. Subject to the technological scheme and parameters of the magnetic field, the method allows water to get rid of scale formation on the walls of heating equipment, as well as remove a previously formed scale [6]. Technological scheme of water using AMOV allegedly based on the real circuit with the addition of mud in it – sludge trap [7]. It is also necessary to take into account the special regime purges the system and monitor the effectiveness of water treatment.

List of References

1. SN Antonov The unit of magnetic water treatment for boiler greenhouses // thesis for the degree of candidate of technical sciences / Stavropol State Agrarian University. Stavropol, 2003.
2. Antonov SN The unit of magnetic water treatment for boiler greenhouses // thesis abstract on scientific degree of candidate of technical sciences / Stavropol State Agrarian University. Stavropol, 2003.
3. Antonov SN, Atanov IV Efficiency magnetic water treatment systems for heating / mechanization and electrification of agricultural – 2011.-№9. – S.15-16.
4. SN Antonov, AV Ivashina Device magnetic water treatment / mechanization and electrification of agricultural – 2009.-№8. – S.31-32.
5. Gurnitsky VN Nikitenko GV, Atanov IV Antonov SN results of the study of magnetic water treatment unit for 2001. // Proc. Scien. tr .: Methods and means of improving the efficiency of electricity in agricultural – SGSKHA, 2002. – P.73
6. Gurnitsky VN Nikitenko GV, Atanov I. In Antonov SN Magnet on water. // Inventor. – M., 2001. – P.12
7. Devices magnetic water treatment. Design, modeling and research: monograph / SN Antonov, AI Adoshev, IK Sharipov, VN Shemyakin. – Stavropol: Agrus Stavropol State. Agricultural University, 2014. – 220 p.

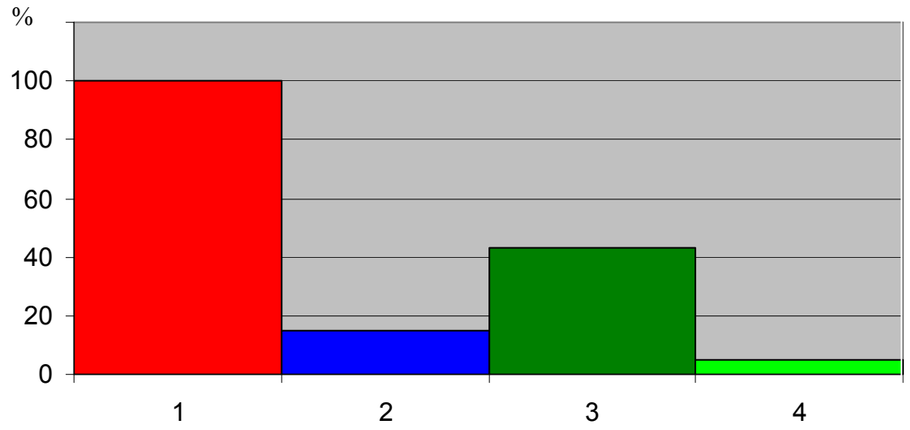

Figure 5 – Histogram of the cost of preparation of 1m3 of water: 1 – two-stage Na- cation exchange; 2 – Preparation kompleksonatov in hot water boiler; 3 – Preparation kompleksonatov in steam boiler; 4 – Preparation of water in the boiler with the magnetic treatment

Preparation of 1m^3 of water using Na- cationization costs are currently 17-21 rubles., And water treatment kompleksonatov worth 2.03 rubles. The cost price of the magnetic treatment of 1m3 of water does not exceed 0.1 rubles. Statistical study of the use of different methods for boiler water treatment Stavropol Territory and Karachay-Cherkess Republic gave the results shown in Figure 6.

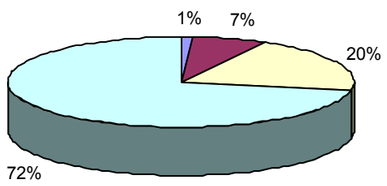

Figure 6 – The pie chart on the boiler water treatment methods of the Stavropol Territory and Karachay-Cherkess Republic: 1% – HEDP-Zn, 7% – magnetic water treatment, 20% – chemical water treatment, 72% – without preparation

At the moment, broad experience of magnetic water treatment in hot water and heating. The need for an economical and simple method of water treatment for these systems is high. Statistical studies of the use of water treatment methods have shown that, in the Stavropol region and KCR 72% of boilers do not use pre-water treatment. It is used only on the boiler subordinate gostehkotlonadzoru. Since the bulk of boilers

4. The stereological parameters, that characterize the ratio of internal and external cross-boundary αα, ββ and interfacial αβ surfaces and volumes have been denoted and calculated in relation to «precast tetrakaidecahedron» of α-phase crystallite.

5. The analytical ratio of α-grain volumetric diameter with its surface reflection has been determined.

List of references

1. J.W. Christian The theory of transformations in metals and alloys. Second edition. Part 1. Equilibrium and General Kinetic Theory. Oxford : Pergamon Press. 1975. 806p.
2. J.W. Martin, R.D. Doherty Stability of microstructure in metallic systems. Cambridge : Cambridge University Press. 1976. 280p.
3. A.S. Saltykov Stereometric metallography. Training manual for institutes of higher education. M.: Metallurgy, 1977. 279p.
4. K.S. Chernyavskiy Stereology in metal technology. M.: Metallurgy, 1977. 279p.
5. E.A. Borisova, G.A. Bochvar, M.YA. Brun and others Titanium alloys. Metallography of titanium alloys. M.: Metallurgy, 1980, 464p.
6. A.A. Ilyin, B.A. Kolachev, I.S. Polkin Titanium alloys. Composition, structure, properties. Technical reference handbook. M.: VILS-MATI, 2009, 520p.
7. V.K. Nosov, P.A. Nesterov, O.A. Polyakov 3-D model of microstructural structure of α+β titanium VT6 alloy// Materials science, №4. 2014. p.26-27.
8. U. Zwicker Titanium and its alloys. Translation from German. M.: Metallurgy, 1979, 512p.

Grigor'ev S.M. [(1)], Ivanov V.I. [(2)], Nesterenko T.N. [(2)], Kovalev A.M. [(3)]
[(1)] Zaporozhe national university
[(2)] Zaporozhe state engineering academy
[(3)] Zaporozhe national technical university

TO CALCULATION OF ECONOMY AT TECHNOGENIC WASTE PROCESSING OF PRECISION ALLOYS ON THE NICKEL BASIS

It is refined the methods of estimation of through economic efficiency for processing of high-alloy waste on the nickel basis as it applies to direction of making up in nickel deficit and other accompanying alloying elements at the production of precision alloys.

Keywords: through economic efficiency, estimation, production of precision alloys, nickeliferous basis, processing of waste

I. Introduction.

The high rates of growth of production for special steels and alloys on the nickel basis can be provided at condition of output simultaneous increase for alloying materials accompanying to them and improvement of their quality. Thus for the substantial spreading of assortment the above-stated steels build-up volume of alloying materials output must be carried out by advanced.

A large economic interest is presented by utilization of basis metals (nickel, molybdenum, cobalt and chrome) from waste of precision alloys on the basis of nickel [1].

II. Statement of task.

The main purpose of work is development of method for estimation of through economy at technogenic waste processing of precision alloys on the nickel basis.

III. Basic part of researches.

At smelting of corrosion-resistant chromium-nickel steels and alloys on the nickel basis the requirement in this metals makes 8-12 and 40-45 % accordingly [2]. The through degree of the use of this metal at processing of nickelcontaining raw material in the non-ferrous metallurgy and engineering does not exceed 0.36-0.42.

The perspective approach to the decision of a problem completion of nickel deficiency is processing of production waste of precision alloys on the basis of the given metal for the receipt of new ligatures compositions satisfying for high-quality metallurgy.

In general, Figure 2 shows the classification of methods of water treatment.

Figures 3, 4, 5 are bar graphs that allow you to assess the degree of scaling, corrosion and cost of preparation of 1 m3 of water.

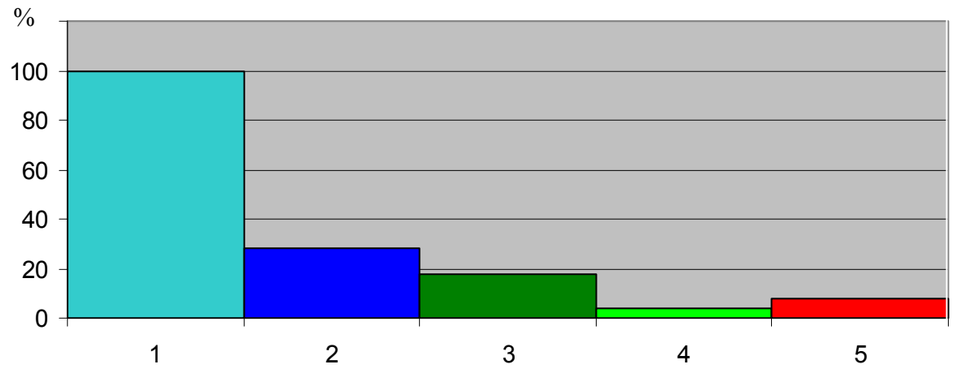

Figure 3 – Histogram scaling relative to the origin of water: 1 – scaling the application of source water; 2 – deposition of scale in the preparation of water for a single-stage scheme Na- cationization; 3 – scale water treatment as a result of two-stage scheme Na- cationization; 4 – Allocation of scale in the preparation of the initial water kompleksonatov; 5 – scale layering with magnetic water treatment

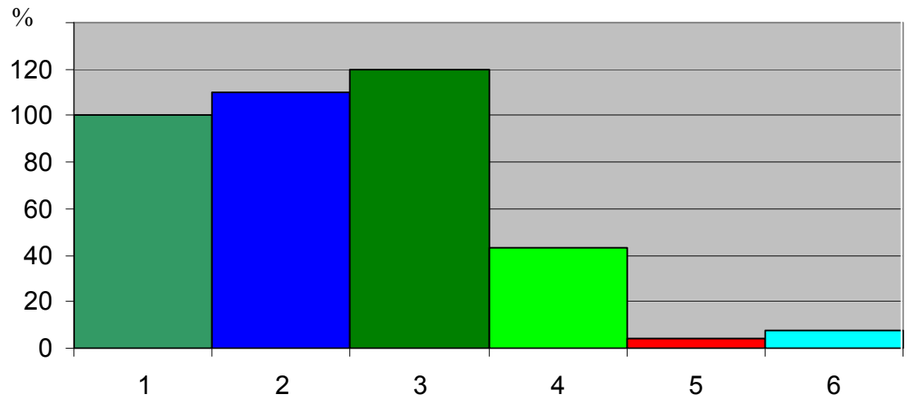

Figure 4 – Histogram corrosion relative to the origin of water: 1 – corrosion when using raw water; 2 – corrosion due to water treatment scheme for a single-stage Na- cationization; 3 – corrosion at the water treatment scheme for the two-stage Na- cationization; 4 – corrosion in preparation for the two-stage scheme Na- cationization + deaeration; 5 – corrosion in the preparation of water kompleksonatami; 6 – corrosion in magnetic water treatment

hydrogen ions. It is used in conjunction with other schemes ionirovaniya processes for the preparation of water from artesian or surface water if necessary to reduce the relative alkalinity. Recently became popular method of water treatment kompleksonatov. For treating water used corrosion inhibitor HEDP-Zn. Its use allows to obtain the following results: – Protect steel from corrosion; – Gradually wash existing deposits; – Prevent the formation of new deposits. This technology has spread in the Rostov Region and Stavropol Territory. In currently attracting attention in water treatment application magnetic field. Magnetic water treatment method is based on the phenomenon that the water after exposure to a magnetic field during its subsequent heating in the boiler does not crustose deposits on the heating surface. Some compounds crystallize on the surface of the heating, forming scum. Scaling centers are heating surface roughness [2,6]. As a result, the stiffness of the magnetic treatment of the salt precipitated as sludge and must be removed continuously from the low points of the boiler.

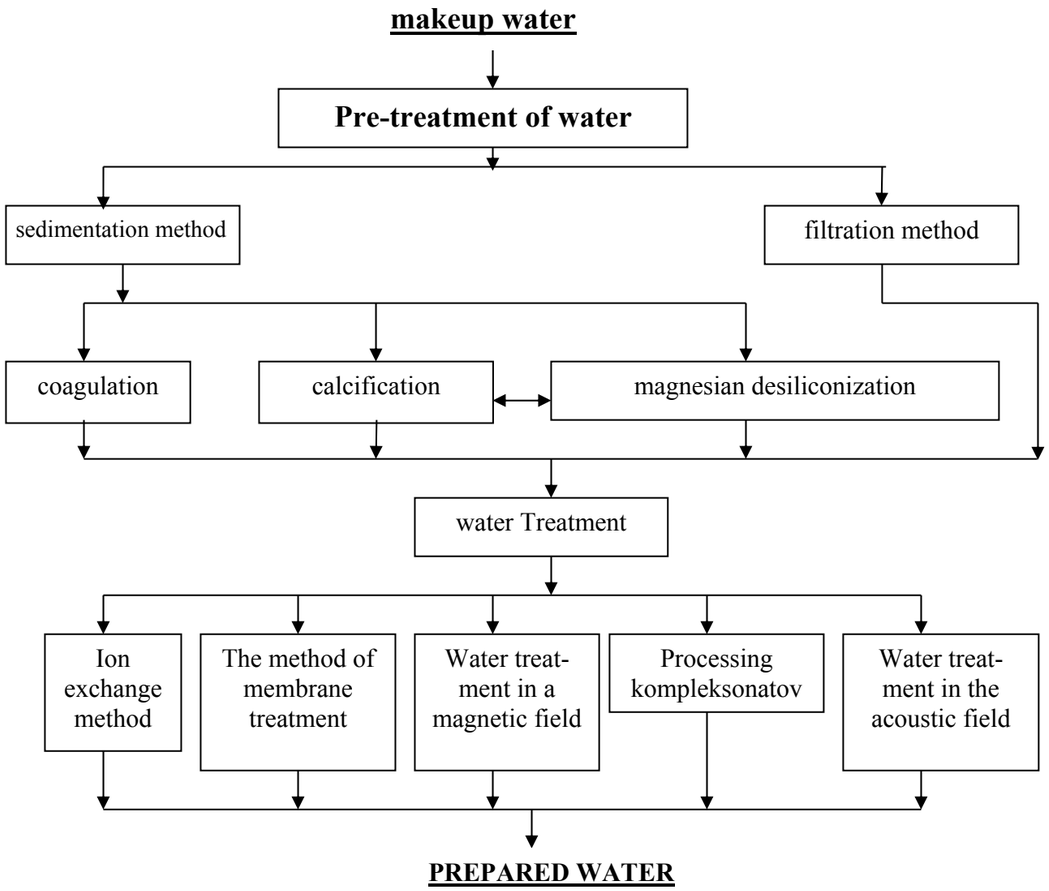

Figure 2 – Classification of methods of water treatment

At processing of waste for production of precision alloys on the nickel basis the obtaining of base contents (60-85 %) of this metal is fixed in ligature at rational correlation of active elements (aluminum, silicon, titan, zirconium), and also some additions of refractory elements (molybdenum, tungsten and cobalt) [3]. It is necessary to take into account only the form of presence for elements in waste, and also presence and concentration of accompanying admixtures, reducing the practical value of refractory elements.

Size of economy from introduction of one separately taken technical decision, directed on use of new ligatures compositions (instead of traditionally applied metallic nickel and molybdenum of high-cleanness) at the production of precision alloys on the nickel basis, is calculated by the formula

$$E_{o.t.d} = \sum_{i=1}^{n} \left\langle E_{b.m} + E_{\ell.d} + E_{t.e} + E_{e.f} \right\rangle \cdot U_i \quad , \qquad (1)$$

where i = 1,2,3…n is a number of grades of precision alloys, melted with use of new ligatures, differing by the contents of alloying and active elements; $E_{b.m}$ is a amount of economy of accompanying expense burden materials at the production of precision alloys, mon. of acc./t; $E_{\ell.d}$ is a amount of economy of accompanying alloying and deoxidizing elements from the decrease of metal discharge coefficients on the subsequent repartitions, mon. of acc./t; $E_{t.e}$ is a amount of economy from the cut-back of the technological expenses (fuel, energy, water and other) at decrease of a melting temperature and speed increase of dissolution of refractory elements in fused alloy, mon. of acc./t; $E_{e.f}$ is an economy (overdraft) from the change of external factors and their influence on the rate of turnover of circulating assets, mon. of acc./t; U_i is an annual volume of production for i grade of precision alloy with use of new ligature, t.

The calculation of amount of burden materials economy $E_{b.m}$ for melting of precision alloy is carried out with use of the formula

$$E_{b.m.i} = \sum_{i=1}^{n} U_i \cdot \sum_{j=1}^{m} \left\langle H_{0.j} - H_{i.j} \right\rangle \cdot P_j \quad , \qquad (2)$$

where j = 1,2,3 … m is quantity of burden materials components for melting; $H_{0.j}$, $H_{i.j}$ are expenses of j component of burden materials for melting of one ton of alloy before and after application of technology of precision alloy smelting with the use of ligature, t, accordingly; P_j is a price of j component of burden materials, mon. of acc./t.

It is known that major factors, defining efficiency of smelting process for precision alloys on the nickel basis, at other equal terms, there are the price and technological properties of this metal and other refractory elements. In this connection at the calculation of through economy it is necessary to take into account reserves of its increase at the stage of

reception of alloying materials on the nickel basis, alloyed by molybdenum and other refractory elements. Calculations are should be carried out by the formulas:

$$P_j = \Pi_j + F_{c.j} \; ; \tag{3}$$

$$P_j = \sum_{j=1}^{m} P_{i,j} \cdot K_1 \cdot K_2 \; , \tag{4}$$

where Π_j is an profit obtained at ligatures production with use of technogenic waste of precision alloys on the nickel basis, mon. of acc./t; $F_{c.j}$ is a full cost price of production of the given ligature, mon. of acc./t; $P_{i,j}$ is a price of separately taken standard component of charge, received on operating technologies (for example, metallic nickel, molybdenum, chrome), mon. of acc./t; K_1 is a coefficient, taking into account the increase of degree of each element use at its input in fusion by ligature; K_2 is a coefficient, taking into account technological advantages of complex ligature as compared to the use of each metallic element separately.

For the estimation of amount of profit, obtained at production of precision alloys on nickeliferous basis, alloyed by refractory elements because using of trouble-free technology of ligature smelting, it is necessary to consider nonconventional factors which are materialized at formation of structure of cost price by articles.

Then the full cost price of ligature smelting can be calculated by the formula [4]:

$$F_{c.j} = G_{t.p} + G_{e.\ell} + G_{o.e} \; , \tag{5}$$

where $G_{t.p}$ are expenses on the article «there are taken in a production», mon. of acc./t; $G_{e.\ell}$ are expenses on processing taking into account expenses on the lease of capital assets and secondary equipments, mon. of acc./t; $G_{o.e}$ are overhead expenses, mon. of acc./t.

Taking into account technological factors the formula (5) can be written down in a kind:

$$P_j = \frac{\left\langle G_{t.p} + G_{e.\ell} + G_{o.e} \right\rangle \cdot K_{im} \cdot \omega}{\eta \cdot y_\eta + z_{\beta-\gamma} \cdot y_z + \ell_{\xi-f} \cdot y_\ell} \; , \tag{6}$$

where η, y_η are base content of main alloying element in technogenic waste of production, %, and degree of it adoption by ligature; $z_{\beta-\gamma}$ is a concentration of corresponding elements in technogenic waste of production, %: β = 1,2,3, … γ is number of refractory and other useful elements in waste of production; y_z is adoption degree of accompanying (β = 1, 2,3 ... γ) elements in ligature from waste; $\ell_{\beta-\gamma}$ is a concentration of active elements (or deoxidizers) in technogenic waste or burden components for ligature smelting; y_ℓ is a

when a once-through system, the movement of water (boilers, heat exchangers). In the circulating cooling systems with multiple contact of water with the magnetic field presence of aggressive carbon dioxide noticeable effect on the magnetization does not have any effect. The need for pre-decarbonization address specific for each installation. If during the production process a reduction of carbon dioxide concentration, the magnetic device installed in a place where there is no aggressive carbon dioxide or its minimum amount. Reducing the total amount of carbon dioxide, including aggressive, may be achieved by blowing air through the water or heated to a temperature of 40-50 C. In those cases where such treatment is not possible to carry out, then the change in the concentration of carbon dioxide can occur when water is heated in a closed system. A prerequisite for the treatment of water is carbonate hardness. For values of up to 1.5 mEq / L application of a magnetic field is ineffective and is not advisable. Reduced antiscaling effect observed in the spring, when the surface water diluted meltwater. During the summer, the effect is improved and reaches a maximum in the winter – in the period of greatest concentration of salts, which is associated with the state of the system is close to supersaturation. For industrial boilers with a working pressure up to 15 atm. when dokotlovoy treatment, total hardness feedwater must not exceed 0.7 mEq / L. When vnutrikotlovoy treatment, total hardness feed water should not exceed 5 mEq / L. The variety of impurities in natural water is the reason that cleaning up water according to [dissertations] for boiler feed water treatment plant to be organized in several stages. In the first stage, the method of deposition of the water allocated coarse material. Final cleaning of the sediment carried by the process of filtration: – Through the single-layer mechanical filters downloading anthracite particle size 0.5-1.2 mm for water containing suspended solids up to 50 mg / kg; – Through two-layer mechanical filters downloading quartz sand grain size of 0.5-1.2 mm and anthracite with grain size 0.8 to 1.8 mm water containing suspended solids up to 100 mg / kg. If the purification of water from the coarse impurities have appreciable gravitational effect may be achieved by conventional sedimentation, the selection of dispersed colloidal substances from the process water requires coagulation. Under coagulation understand the physico-chemical process of adhesion of colloidal particles and the formation of coarse phase with subsequent separation from water. Liming of water is used to improve the performance of the ion-exchange water treatment devices. Currently, the main purpose of liming – reduction of bicarbonate alkalinity of water. Simultaneously decreasing stiffness TDS concentration of coarse impurities. Water subjected to pretreatment, practically does not contain suspended solids, and is largely exempt from the colloid. However, the bulk of the impurities remain in solution in water and must be removed therefrom. Currently this is used for ion exchange. Summary ion exchange is the ability to use some special materials (ion exchange resins) in a desired direction to change the ionic composition of water impurities. In water treatment technology for removing ions from water, as specified in [1,5,6] employs two processes: cation exchange – and removing cations anionirovanie – removing anions. Ionirovaniya processes carried out in different devices, but the most widely used bulk ionite filters. Na-cation exchange – a process used for water softening and has independent significance in the preparation of water with low alkalinity for low-pressure boilers and heating systems feeding. Water was passed through the cation layer. In this process, water is removed from the ions Ca2 + and Mg2 + in exchange for an equivalent amount of ions Na +. H-cation exchange – the process of removing all of the water with the cations replacing them with

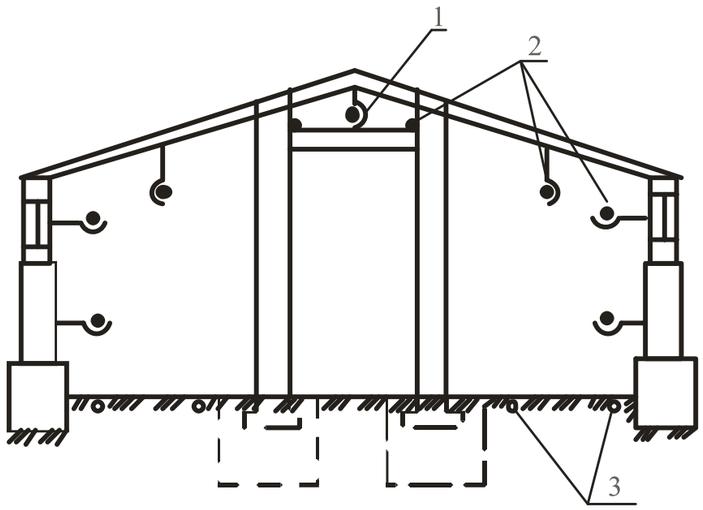

Figure 1 – Dirt greenhouse with water heating: 1 – the main supply pipe; 2 – heating pipes airspace; 3 – subsurface heating pipes

Sources of water heating boiler rooms in buildings protected ground can serve as surface water from lakes, rivers and artificial reservoirs and underground water from artesian wells. Surface water always contains dissolved substances and undissolved impurities. Groundwater is usually transparent and substantially free of impurities. Salinity of groundwater is usually higher than the surface. The greatest value for water boiler plants are the surface waters of rivers and lakes. Flow and river water quality varies cyclically not only on the time of year, but in the long-term perspective. Depending on the nature of water use by different users are defined and indicators necessary for the qualitative and quantitative characteristics of the water. One such indicator of water for use in water-heating equipment is rigidity. Total water hardness Jo called the total concentration of calcium and magnesium ions, expressed in mEq / kg, and for small znacheniyah- in mg-eq / kg. By defining Cationics total hardness of water is divided into calcium and magnesium ZhCa ZhMg [1,2,3,4]. On the other hand, part of the overall stiffness of the equivalent concentration of bicarbonate – ions in water, the carbonate hardness Hk is called, and the remainder is contained in the water equivalent of other anions (Cl-, SO42-, etc.). Uncarbonate called stiffness EFAs. By value of total hardness, meq / kg, natural waters are classified as follows: Jo <1.5 – low water hardness; Jo = 1.5-3.0 – with an average water hardness; Jo = 3-6 – water with high rigidity; Jo = 6-12 – water with high rigidity and Jo> 12 – water with very high stiffness. The possibility of using magnetic treatment, a place to install the machine and achieves the effect depends on the quality of the source water. The quality of water to be treated, must meet certain requirements. Water should not contain mechanical impurities more established norms and aggressive carbon dioxide. The presence of water in an aggressive carbon dioxide reduces antiscaling effect is proportional to its concentration due to lower supersaturation. When the concentration of carbon dioxide aggressive 10-15 mg / kg, antiscaling effect is reduced by several percent, and at a concentration of 30 mg / kg reduced the effect of not less than twice. The greatest reduction effect occurs

degree of adoption of active elements (or deoxidizers) at ligature smelting; K_{im} is a coefficient, considered the concentration of detrimental or useful impurities, improving or lowering consumer properties of ligature; ω is an output of suitable ligature.

The formula (6) allows to calculate the production cost of complex of alloying and active elements for ligature on the nickel basis from technogenic waste of precision alloys production, as opposed to the proportional cost of each element at the complex processing of ore raw material or utilization of useful components from the collected dust.

The economy from decreasing of the technological expenses $E_{t.e,i}$ determine by comparison of corresponding articles of cost calculation of precision alloy before and after application of ligature on the basis of technogenic waste:

$$E_{t.e,i} = G_{t.e,1} - G_{t.e,2} \ , \qquad (7)$$

where i = 1,2,3 ... is quantity of variant number of smelting technology for precision alloys, differing composition of burden materials, method of their putting and technological units for production; $G_{t.e,1}$, $G_{t.e,2}$ are technological expenses at the precision alloys production without and with the use of ligature, under variants, mon. of acc./t.

Indexes of the costs of technological fuel (electric power), water, slag-forming additions and fluxes reducing are determinant for these articles that is provided by technological advantages of ligature as compared to separately taken burden components to melting. The economy from the decrease in carbon-monoxide wastes of alloying elements and deoxidizers at smelting can be defined by the formula:

$$E_{d.c-m} = G_1 - G_2 \ , \qquad (8)$$

where G_1, G_2 are costs of alloying and deoxidizing elements for smelting of precision alloys before and after application of ligature on the basis of technogenic waste, mon. of acc./t, accordingly.

For operating factors after substitution of above-stated expressions received the formula:

$$E_{\ell.d} = \left\langle C_1' \cdot y_\eta' + C_2' \cdot y_z' + C_3' \cdot y_\ell' \right\rangle - \left\langle C_1'' \cdot y_\eta'' + C_2'' \cdot y_z'' + C_3'' \cdot y_\ell'' \right\rangle \ , \qquad (9)$$

where C_1', y_η' is cost of nickeliferous basis in alloy at use of metallic nickel, mon. acc./t, and is degree of it passing to alloy accordingly; C_2', y_z' are cost of other alloying elements at use of them in a metallic state, mon. acc./t; and degree of their adoption in precision alloy accordingly; C_3', y_ℓ' are costs of clean deoxidizers at smelting of alloy, mon. acc./t, and their discharge coefficients at smelting of alloy by base technology, t/t; C_1'', C_2'', C_3'' are expenses to the nickeliferous basis, alloying elements and deoxidizers at the use of ligature for smelting of precision alloy, mon. acc./t; y_η'', y_z'', y_ℓ'' are degrees of the use of nickeliferous basis, alloying elements and deoxidizers at smelting of alloy from ligature accordingly.

The expected economy from the change of external factors is calculated with use coefficients, taking into account the rate of turnover of circulating assets, conjecture of market prices and other unrecorded factors. Size of this economy it is possible to define by the formula [4]:

$$E_{e.f} = C_1 - C_2 \quad , \tag{10}$$

where C_1, C_2 are prices of precision alloy, made with the use of clean elements and complex ligature, received on the basis of technogenic waste, accordingly, mon. acc./t.

Price of precision alloy, made with the use of complex ligature, is calculated by the formula:

$$C_2 = D_1 \cdot D_2 \cdot D_3 \cdot G_0 \quad , \tag{11}$$

where D_1 is a coefficient, taking into account decrease of trade price for a precision alloy in the conditions of market; D_2 is a coefficient, taking into account the rate of turnover of circulating assets at the conditions of direct contractual deliveries; D_3 is a coefficient of other unrecorded factors; G_0 is a total expense on production and realization of precision alloy, made with the use of complex ligature, mon. acc./t.

The most acceptable values of discharge coefficient for the application of complex ligature at smelting of precision alloy of 29NC are within from 20 to 450 kg/t alloy [8].

IV. Conclusions.

The method of estimation of through economy of material resources at processing of technogenic waste of production of precision alloys on the nickel basis with the purpose to use of ligature for alloying and deoxidizing of fused metal is specified. The further researches of a method will allow to reveal ways of decrease in expenses for production of precision alloys on the nickel basis and consequently, to save means and to redirect them on enterprise development**.**

Reference

1. Gasik M. I. Theory and technology of production of ferroalloys / M. I. Gasik, L. N. Lyakishev, B. I. Emlin. – Moscow : Metallurgy, 1988. – 784 p.
2. Grigor'ev S. M. Extraction of refractory elements from the dross of high-speed steel / S. M. Grigor'ev // Steel. – 1994. – No 3. – P. 63-66.
3. Grigor'ev S. M. Economic strategy and tactic/pl of resource- and energy-savings in metallurgy of refractory materials / S. M. Grigor'ev // Metallurgy: scientific studies of ZGIA. – Zaporozhe: ZGIA, 1988. – Vol. 1. – P. 17-23.
4. Gasik M. I. Electrometallurgy of ferroalloys, special steels and alloys / M. I. Gasik. – Dnepropetrovsk: MagFund, 2009. – 116 p.

Sergey Antonov –
Ph.D., Associate Professor
the Department «Application of electrical energy in agriculture»
Stavropol State Agrarian University

WATER TREATMENT IN THE BOILER ROOM FOR THE CONSTRUCTION OF THE PROTECTED GROUND

In water and steam boilers and other heat and power, the surface heating as a result of a number of physical and chemical processes form solid deposits – scum. Protection of boilers and other thermal units of scale achieved mainly in two ways: by removing nakipeobrazovateley before entering the water in the boiler (water pretreatment) and the creation of conditions inside the boiler to form a slurry (vnutrikotlovaya processing). Evolved slurry is intermittently or continuously removed and thus the harmful effects associated with scale to a greater or lesser extent prevented. Cleaning equipment from scale very time-consuming and expensive process that is associated with a change in the mode of operation of thermal devices, using chemicals that alter the salt composition of the aqueous solution. Magnetic water treatment chemicals and does not require large capital investments in equipment and in contrast to the chemical, is environmentally friendly.

Keywords*: water, magnetic field, water, salt crystals, scale, magnetic system, water treatment, magnetic water treatment device, an electromagnet, scale, hardness salts, magnetic water treatment, magnetic induction, magnetic flux.*

The greatest practical application in industrial horticulture has a technical heating, as it allows to obtain products in the off-season time of year. Local heating systems is carried out by boiler built specifically for the greenhouse complex. Water heating is the most common, as it allows to use automated systems control the temperature of air and soil. Water heating is divided on hot water heating systems and heating the tent of the soil. The temperature of the coolant in the heating system of the tent from its own boiler is taken not more than 130 C, and return water temperature is 70 C [1, 2]. The temperature of the soil in the root zone should be from 18 C to 25 C. The temperature of the coolant, the flow of 40-45 C, and in the opposite 30C.

3. Joint access to «hypersound» http://vpk-news.ru/articles/3901
4. Karachun, V. V., Mel'nick, V. N. (2012) Influence of Diffraction Effects of the Inertial Sensors of a Gyroscopically Stadilized Platform: Three – Dimensional Problem. Int. Appl. Mech., 48 (4), 458-464.
5. Karachun, V.V., Mel'nick, V. N., Shybetskiy, V.Y. (2013) Gyro error due to developing pumped fuselage during flight operation. East European Journal of advanced technologies, 5/7 (65), 45-47.
6. Shybetskiy, V.Y. (2012) The influence of the Gaussian curvature of suspension of floating gyroscope on the elastic compliance in the acoustic field. Young scientist. Monthly magazine, 12, 116-120.
7. Kuz'michev, Y.M., Makarov, V.M. (1958) Excitation of a cylindrical shell with ultrasound. Acoust. Magazine, 3, 282-283.
8. Makarov, V.I., Fadeev, N.A. (1960) On the radiation waves shells in the sound field. Acoust. magazine, 2, 261-263.
9. Karachun, V.V., Trivaylo, M.S., Mel'nick, V. N., Rudenko O.S. (2011) Float gyroscope. Patent of Ukraine № 66311 G01C19 / 20.
10. Shenderov, E.L. (1972) The wave of hydroacoustic. USSR, Leningrad: Shipbuilding.
11. Zaborov, V.I. (1962) The theory of sound insulation walling. USSR, Minsk: Stroyizdat.

Varden Khvedelidze
Doctor of Technical Science, Professor
Ketevan Sirbiladze
postgraduate student
Akaki Tsereteli State University, Department of Chemical Technology, Kutaisi, Georgia

THE CHEMISTRY AND TECHNOLOGY FOR PRODUCING HYDROPHILIC LIQUID EXTRACT FROM GRAPE STONES

Abstract. *It has been established that after wine making process, the grape stones contain an appreciable quantity of valuable biologically active substances of current interest to pharmaceutical industry. There is developed the technological scheme and determined parameters for producing liquid hydrophilic extract from grape stones of* ***Saperavi*** *variety.*

Key words: *grape stones; chemical composition; hydrophilic extract; technology.*

It is known that epicatechin-gallateand various procyanidins, including catechin monomers, produced from grape stones are superoxide radicals and sorbents of hydroxyl radicals in the aqueous solutions.

It was experimentally shown that antioxidant synergism, which is typical of foods containing total polyphenols of grapes. Consequently, when producing biologically active foods from grape stone, it is advantageous to use extraction of dissoluble total polyphenols in the liquid phase.

Ground and pre-defatted grape stones of Saperavi variety were used for an experiment. Herewith, the defatted ones have been produced by using four-fold extraction of grape stones with a petroleum ether at room temperature. The ratio of extracting agent and raw material at all extraction steps was 3:1. After extraction from the grapestone cake, the extracting agent was distilled off until an outright loss of a smell.

Quantitative determination of tanning agents was carried out by extraction of pre-defatted cake of grape stones by water according to the methodology GF XI [1]. The obtained data are presented in table 1.

Table 1 Quantitative content of tanning agents in grape stones

Raw material variety	The content of tanning agents, %	Metrological characteristics
Saperavi	2,60 ±0,05	Sx = 0,02; є,%= 1,92

Quantitative determination of flavonoids was carried out by using nitrate-aluminum colorimetric method, during which aluminum nitrate is activated with a keto-group of flavonoids with forming of a stable acidic complex, which is an indicator of sustainable absorptive power at 415 nm [2].

The obtained data are presented in Table 2.

Table 2 Quantitative content of flavonoids in Saperavi variety grape-seeds

Raw material variety	The content of flavonoids, %	Metrological characteristics
Saperavi	0,0210 ±0,005	Sx=0,02; є,%=2,38

Quantitative determination of anthocyans was carried out by colorimetric method, at A_{max} = 540 нм. The obtained data are presented in Table. 3.

Table 3 Quantitative content of anthocyans in Saperavi variety grape-seeds

Raw material variety	The content of anthocyans, %	Metrological characteristics
Saperavi	0,028±0,0008	Sx=0,0003; є, %=2,86

Quantitative content of free organic acids was made by using titrimetry; as a titrant we have taken sodium hydroxide solution (0,1 mole/l), using as indicators 0,5 ml of 1% alcohol solution of phenolphthalein and 0,5 ml of 1% solution of methylene blue, and then we titrated until the appearance of lilac-red coloration. Concurrently the control titration (V_K) was carried out, in which the purified water was used instead of aliquot of the extract. The results of six determinations were processed statistically and presented in Table 4.

Table 4 The content of free organic acids in grape stones

Raw material variety	The content of organic acids, %	Metrological characteristics
Saperavi	2,605 ± 0,07	Sx=0,03; є, %=3,10

The content of glucose was determined by iodometric method. The results are presented in Table 5.

Table 5 The content of glucose in grape stones

Raw material variety	The content of glucose in grape seeds, %	Metrological characteristics
Saperavi	6,92 ± 0,17	Sx = 0,06; є,% = 2,99

Thus and so, it has been established that from defatted grape stones of Saperavi variety it is possible to extract hydrophilic biologically active substances, as tanning

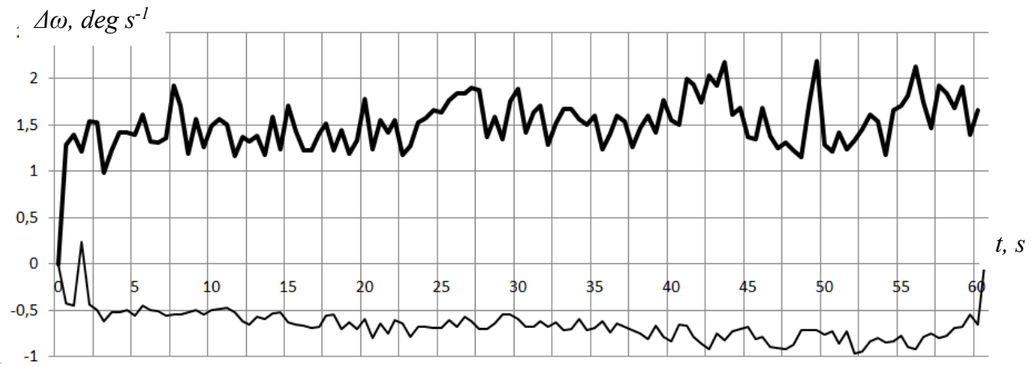

Fig. 3 Output signal of DUSU at $\varphi = 0°$ thin line – $\theta = 0°$; contour line - $\theta = 10°37'$

It is obvious that on the output signal, except for the suspension, began to affect also the gyroscopic response. And its impact is so significant that casts doubt on the performance of the device under these conditions.

Here are reviewed several solutions. Or develop a passive soundproofing techniques device, or use schematics to eliminate (or partially suppress) the effect on the instrument ultrasonic radiation hypersonic flight.

VI. Conclusions

The seminatural stand tests of the angular velocity sensor on the functional ability of the ultrasonic field in hypersonic flight provide an opportunity to draw some conclusions about the compliance characteristics of the passport requirements:

- For the first time was found that in the operation of the sensor of DUSU class the external ultrasound beam creates additional errors of DUSU at the resonance level in the presence of the wave coincidences, that size exceed permissible Passport requirements;
- Set the cause of the appearance of acoustic energy concentration zones (*zone kaustikos*) in state liquid suspension device and calculated radius of the zones of caustics. Designated areas of acoustic shadows in the suspension;
- Constructed computational models allow us to generalize the results to other objects that require *«acoustic transparency»* and *«invisibility»* in the search beam.

References

1. Shybetskiy, V.Y., Karachun, V.V. (2013) Float suspension gyroscope under Flight Operations. News of SAC. Aerospace Instrumentation: scientific. Magazine, 4, 41-44.
2. Hypersound: third party race (2014) http://rus.ruvr.ru/2014_01_17/Giperzvuk-tretij-uchastnik-gonki-8178/

The *«zero offset»* of the device, with switched off gyromotor, on the diagram of the output signal of the sensor of the angular velocities is indicated by the thin line, when $\theta = 0°$. The output signal is represented by contour lines, when the ultrasound beam direction $\theta = 10°37'$ (see Fig. 2).

At perpendicular incidence of the ultrasonic beam on the shell portion of body ($\theta = 0°$), as shown, the suspension hardly ever reacts on the acoustic disturbance. The output signal can be set equal to zero (see Fig. 2, thin line). Quite a different picture is observed at an angle of incidence of the ultrasonic beam is $\theta = 10°37'$. Theoretical calculations have shown that this occurs when the angle of incidence is $\theta = 10°$.

The difference between the analytical determination of the angle of coincidence and stand measurements is only *37 arc minutes*, that is permissible.

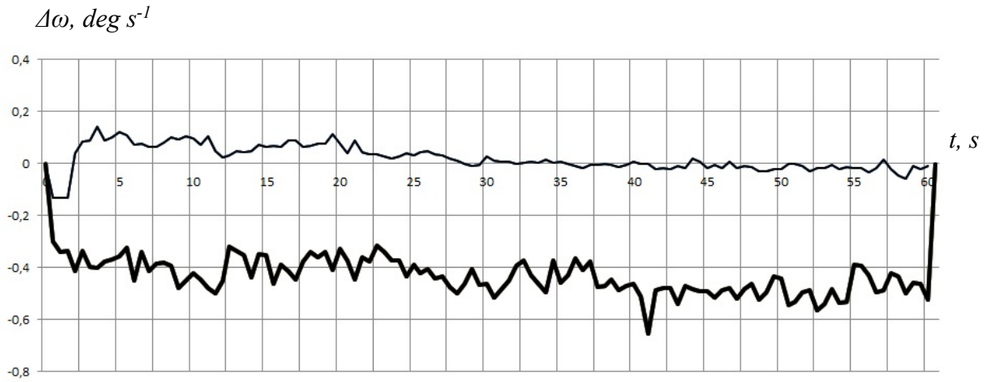

Fig. 2 Reaction of the suspension of the gyroscope on action of the ultrasound ($\varphi = 0°$): beam thin line – $\theta = 0°$; contour line – $\theta = 10°37'$

Implementation of output signal of DUSU shows that it has a sufficiently significant constant component (about *0.5 deg s*$^{-1}$) and a stochastic component (see Fig. 2). Moreover, the maximum output value reaches *0.65 deg s*$^{-1}$, which is much larger than the threshold value for the appliance (DUSU2-30V threshold is *0.45 deg s*$^{-1}$).

When the gyromotor is on, the gyro, naturally, bring a significant effect on the output signal of the device.

Thus, for angles of incidence of the ultrasonic beam that is not equal to the angle of coincidence θ_c, the output only slightly exceeds the threshold (see Fig. 3). Conversely, when the angle of coincidence is θ_c, the output signal increases sharply, reaching *2.19 deg s*$^{-1}$. Its average value is *1.6 deg s*$^{-1}$. Moreover, the sign of the output signal is changed too.

agents – up to 2,5%; as flavonoids – up to 0,21%, anthocyans – up to 0,028%; organic acids – up to 2,6%; glucose – up to 6,9% and so on that testifies advisability of industrial application of Saperavi grape stones for producing valuable hydrophilic extracts.

When developing technology for producing hydrophilic liquid extract from grape stones, it is necessary to pre-set the drying schedule of initial material – fresh stones. As the objects of research the grape stones of Georgian variety Saperavi have been taken. We have examined three three variants of their drying: I. At temperature of 50-55°C with intensive supply of air; II. At temperature of 100-105°C, convection drying; III. At temperature of 130-135°C, convection drying. The results of determining chemical composition of grape stones are presented in Table 6.

Table 6 The phenol compounds of grape stones dried out at different temperatures (Saperavi variety stones, 2013)

Variant of drying	The content of tanning agents, %	Total content of flavonoids, %	Total content of anthocyans, %
I	2,350 – 2,400	0,019 – 0,020	0,0260 – 0,0270
II	2,155-2,165	0,0035 -0,0045	0,0013 – 0,0015
III	1,255-1,265	0,0030 – 0,0035	0,0034 – 0,0036
Initial content	2,61 ± 0,05	0,0210 ± 0,005	0,028 ± 0,0008

The obtained results confirm that grape stones of Saperavi variety represent a rich source of hydrophilic biologically active substances. Maintaining the level of initial content of tanning agents, flavonoids, anthocyans and others could only be possible during permissive drying of fresh stones at a low temperature. At the same time, rise in temperatures causes destruction of almost all antioxidant active substances.

When developing technology for experimentation, we have taken the stone, obtained from the sweet septum of Georgian grape variety – Saperavi. The samples were dried in a drying oven at temperature not higher than 50 °C to humidity of 8-10%. There were used the ground and pre-defatted stones. Defatting was made by using four-fold extraction of stones with a petroleum ether at room temperature. Duration of the first three extractions was 1 hour each, but of the forth one – 24 hours. The ratio of extracting agent and raw material at all extraction steps was 3:1. After extraction from the grape-stone cake, the extracting agent was distilled off until an outright loss of a smell.

Dispersing or homogenization of the defatted stone until micro-particles was implemented in hammer-type mill (TP2 Hammer Mill). The equipment enabled to grind raw material until particles of a size up 50-100 microns. The activation product was used for the extraction.

The complex hydrophilic solvent – As an extracting agent – 40%-ethanol solution in a drinking mineral water of Borjomi-Utsera with mineralization 5-15 g/l and pH=3333,5-6,5, was taken as an extracting agent. The mentioned waters contain sodium (potassium) and boric acid bicarbonate, and, as is shown by trial experiment, they can successfully substitute ethanol aqueous solution oxidized by hydrochloric acid.

The optimal mass ratio micro-dispersed raw material and hydrophilic solvent is established experimentally and makes up 12 l/kg.

The following extraction parameters have been also experimentally determined: temperature – 50-55°C; duration – 120 minutes and pulsing mode of the extractive mass – vibration frequency – 4 m^{-1}; amplitude – 2 mm.

The obtained extract is subject to filtration, first by deposition, and then by centrifugation. Then the extract is concentrated in a vacuum-evaporating apparatus until 65%-concentration at temperature not higher than 50 °C.

After sanitary disposal of the production (production shop, technological equipment, maintenance staff uniform), the pre-processed raw material – defatted cake of grape stones with extracting agent – is moved into periodically acting extractor. During the process of extraction, with a purpose of process intensification, every 10 minute, the pulsing of extractive mass was implemented during one minute.

The technological scheme of producing biologically active liquid hydrophilic extract from grape stones is shown in Fig. 1.

Filtration of the obtained extract comprises two steps: first by deposition in a special-purpose vessel-precipitators at temperature of + 4°C during 8-10 hours by sediment discharge, and then by filtration in the wine layered filters.

The obtained filtered out extract has a concentration not higher than 3,2-3,5% of dry substances, and it has to be concentrated.

Drying-concentration of filtered out extract comprises two steps as well: first it is implemented in a continuously acting double-casing vacuum-evaporating apparatus of «Lang»-type, to a concentration of dry substances in the extract – 30-32%, and then in a periodically acting vacuum-evaporating apparatus with mixer to a final concentration of dry substances in the extract -65%. In both cases, the drying-concentration temperature was not higher than 50°C.

By means of pump units, the concentrated liquid preparation is pumped into the enameled collecting tanks, from which the sampling and quality control of target product are implemented.

The final product in kind of hydrophilic liquid extract of grape stones produced in such way, is packed in hermetic vessels for further use in compliance with Pharmacopoeia reference standards.

Regerences:

1. N.I. Grinkevich. Chemical analysis of medicinal plants/N.I. Grinkevich, L.N. Sofronich. – M.,: Medicina, 1983.-346 p. (in Russian)
2. Mojca Skerget, Petra Kotnik, Majda Hadolin, Andreja Rizner Hras, Marjana Simonic, Zeljko Knez. // Phenols, proanthocyanidins, flavones and flavonols in some plant materials and their antioxidant activities. Food Chemistry. 2005. Vol. 89. N 1. P. 191-198.

$$\sin\alpha = \frac{c_0}{V_{np}}.$$

As a consequence, a significant fraction of the energy of the sound wave will concentrate near the circle with radius r_1.

For example, if taken for a particular size of the internal radius of the DUSU body equal $R = 2{,}5\,cm$, body material assume like aluminum ($V_{np} = 6400 - 5200\,m/s$, $V_{nn} = 3080\,m/s$), a static liquid suspension – glycerin ($c_0 = 1923\,m/s$ at $t = 20°C$), and the sound radiation of frequency $f = 42\,kHz$, then the wave size of the inner surface of the DUSU body $kR = \frac{\omega}{c_0}R = \frac{2\pi f}{c_0}R \approx 3{,}43$, i.e. rather more than 1. Means $\alpha = 21°40'$.

Where (see Fig. 1, a):

$$r_1 = 2{,}32\ (cm).$$

For the same reason, the *transverse* wave (the flexural wave in the radial direction) will result in a concentration of energy near the circumference of radius r_2:

$$\sin\beta = \frac{c_0}{V_{nn}};$$

$$r_2 = 1{,}68\ (см).$$

The radius of float is *2 cm* so, obvious, that in the device the caustic surface of radius r_2 will not occur, and the surface of radius r_1 – will remain (see Fig. 1, b).

Caustic surface of radius r_1 clearly divides the acoustic shadow of the static liquid suspension.

It is clear, that by choosing appropriate material of the body and the fluid we can affect the nature of the surface *areas of caustics*. In particular, for example, we can make them discrete-continuous [9].

If you use the methods of ray acoustics, then it is possible to classify the phenomenon in question as a kind of *aberration* of sound waves. Are known that in the aberration-free designs the caustic surface is transformed into a straight line, and thus in this case they will be located on the longitudinal axis of the float body of gyro [10, 11].

V. Stand testing of the angular velocity sensor by acoustic beam

Comparative analysis of the implementation of the output signal of the sensor allows, on the one hand, to establish the degree of influence of the ultrasonic beam, in fact, to a polyaggregate suspension of gyroscope, and on the other – to determine the effect of gyroscopic moments and Euler inertial forces on the measurement accuracy $\Delta\omega$ of the angular velocity of the aircraft during hypersonic flight.

form of dark (acoustic shadow) and light areas that alternate, but not of such intensity as the surface of the *caustic* radius r_1 and r_2 [8].

The computational model, which gives the opportunity to discover the nature of this phenomenon, based on the assumption of significant wave *kR* body size, where appropriate, consideration of the elementary portion of the inner cavity of the body in the form of a plate.

For the purpose of clarity, comment on the event in the middle of the frames (see Fig. 1). To simplify, first imagine that the float inside is absent. Thus, externally acting on the cylindrical body of angle velocity sensor by the sound wave P will generate on the material *circumferential*, along the parallel, elastic vibrations $U_\varphi(t, z, \varphi)$, that propagate velocity V_{np} in a direction of parallel. That is, along a side surface of the body. Furthermore, there are bending, *radial* vibrations $W(t, z, \varphi)$ in the plane of the frame (in the transverse plane) with velocity V_{nn}

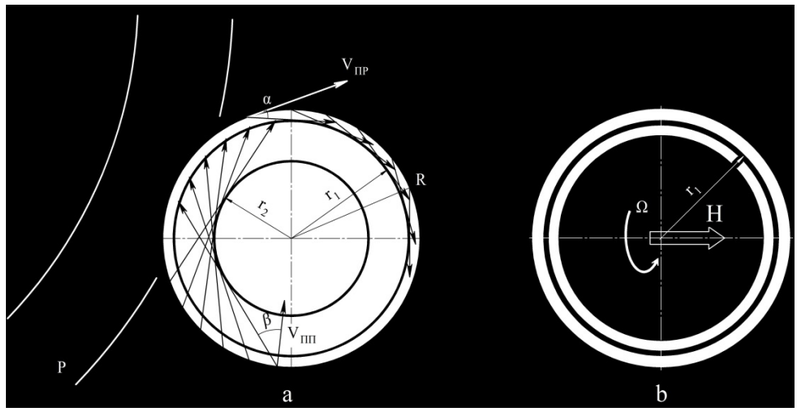

Fig. 1. a – Focusing of acoustic radiation energy in the envelope with the fluid; b – Focusing of the energy of penetrating radiation in a static liquid suspension of the float – a dark circle

Circumferential waves. Considering the side of the body shell angle velocity sensor with large wave sizes, that is, one where the property is shown $kR>>1$ ($k = \frac{\omega}{c}$ – wave number), it is permissible to consider separately taken circular element of the inner surface as plate with approximately zero curvature, velocity of *longitudinal* waves in which coincides with the *circumferential* velocity along the parallel shell, i.e. V_{np}.

If the velocity of the *longitudinal* wave V_{np} more than the speed of sound c_0 in the fluid, i.e.

$V_{np} > c_0$,

then wave, which runs along the parallel, will emit a sound wave in the liquid, and the direction of its makes the angle α with vector of velocity V_{np}. This angle can be defined by the expression (see Fig. 1, a):

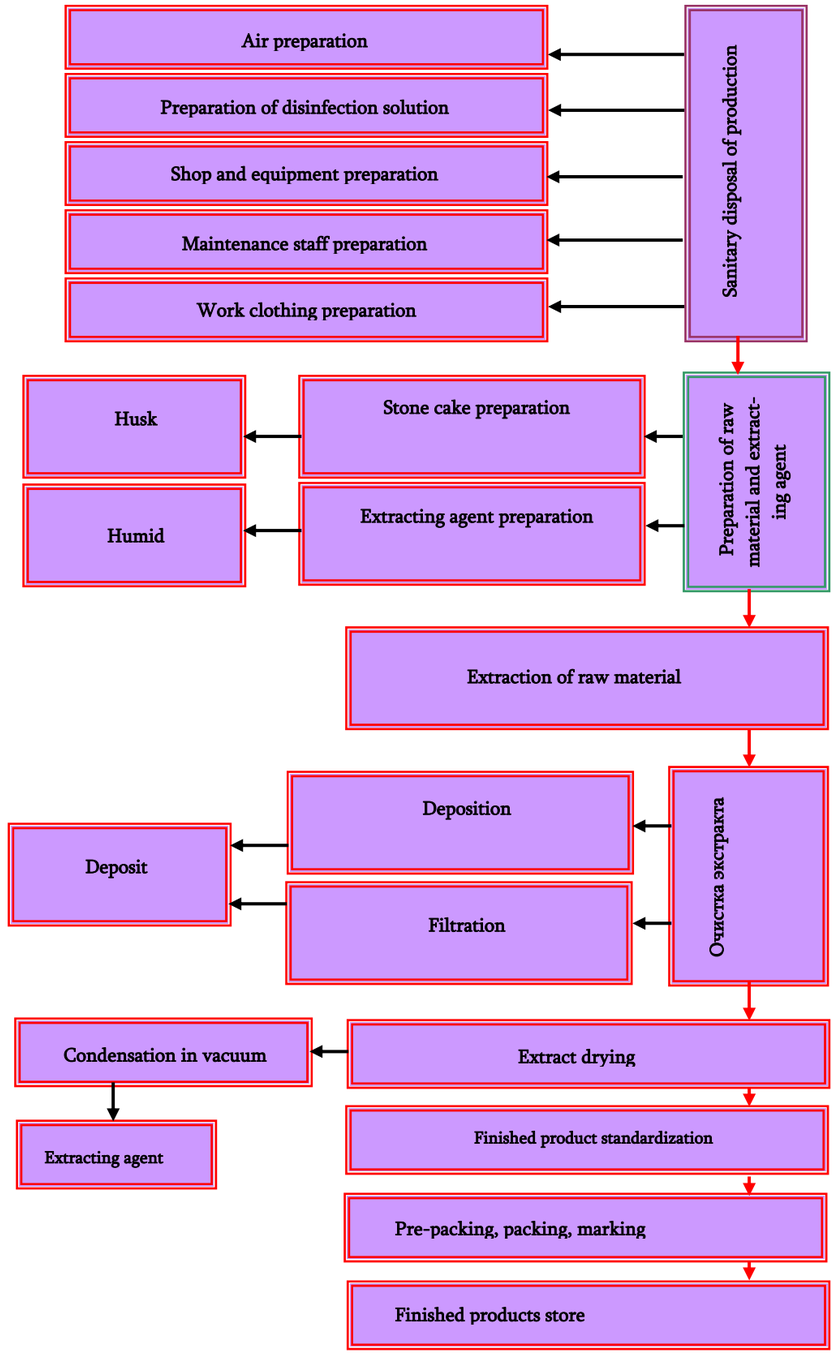

Fig.1. The technological scheme of producing biologically active liquid hydrophilic extract from grape stones of Saperavi variety

Doctor of Technical Sciences, Prof. V. Karachun, V. Shybetskij
National Technical University of Ukraine «Kyiv Polytechnic Institute»

WAVE COINCIDENCE AND ERRORS OF FLOATING GYROSCOPE AT THE RESONANCE LEVEL

Abstract: *The computational model of additional errors, which occur from interaction of intense shock N-wave with in-ertial positioning devices of hypersonic aircraft was built. Angles of coincidence for the industrial design of the an-gular velocity sensor were fitted. A comparative analysis of the experimental data for seminatural conditions for the two cases (gyroscope ON, gyroscope OFF) was made. The ways of solving problems of additional measurement errors were proposed. Conclusions about the possibility of use of the results were made.*

Key words: *N-wave, hypersonic aircraft, the area of caustics, wave of coincidence*

I. Introduction

At the conclusion of analysts, in the near future hypersonic technology is able to protect the strategic interests of any country in the world.

Value of *hypersonic technology* cannot be overstated. Battle hypersonic aircraft (A) has a huge tactical advantage over existing combat systems, becoming almost invulnerable to modern air defense systems. [1] Even at a velocity of 4 *Max* hypersonic cruise missile is capable to fly over Atlantic in less than an hour.

Until recently, the development and testing of hypersonic aircraft was performed by only two countries – USA and Russia. But now China joined them, with own hypersonic technologies. Testing of apparatus, according to Chinese sources, have only scientific value. However, in the future, cruise missiles can be created on the base of this design [2].

Despite the fact that China does not have such a long history of hypersonic aircraft as the United States and Russia, its aircraft, according to the media, overcame speed of 10 *Max*, when such aircraft in Russia are moving at a speed of 4.5 *Max*, and in the United States – 5 *Max* [3].

The interest in the development of active hypersonic atmosphere flight is growing rapidly in a world. However, the work that had been started in the Soviet Union and the United States in the 60's do not have a convincing continue. The reason is not only a financial component. The greatest difficulty lies in solving technical problems, which generated a huge amount of scientific and technical barriers [4].

Large-scale studies of hypersonic technologies implemented in five mainline areas: *aerodynamics; thermal protection; guidance; navigation and traffic management; equipment and motors.*

II. Formulation of the research problem

In supersonic aircraft control systems have found wide use floating gyros, which are structurally deprived of the main drawbacks of «dry» devices, namely large in size (and, more importantly, the variables in sign) moments of dry friction forces on the reference axis, as well as unacceptably high sensitivity to shock and vibration effects, particularly adverse for integrating gyroscopes [5, 6]. To illustrate the effect of stringent conditions of hypersonic flight on gyro navigation and flight instruments we select, as a research object, the specific technical implementation of serially produced aircraft industry float device, as the part of the on-board equipment of long-acting agents.

Considering super rigid operating conditions of hypersonic motion it's become extremely **actual** task to analyze the elastic interaction of inertial navigation devices with a penetrating acoustic radiation, which has place during the operation, and serving the cause of errors in the aircraft positioning. First of all, it concerns the shock N-wave.

III. Features of computational models constructing of phenomena

Research shows that under certain conditions the body of floating gyroscope can be «acoustically transparent» and shock N-wave with virtually no loss will be held inside the device and lead to a sharp increase in the measurement error. This phenomenon can be classified as a space (geometric) response, or both wave coincidence. At frequencies above the cutoff, at a certain angle of coincidence θ_c, that corresponding to a different frequency, the flexural wave in the unit formulate local features of resonant type, which will serve to appearance of Euler inertial forces in the float, which will lead to a sharp increase in the measurement error [7, 8].

In turn, at frequencies below the cutoff f_{lim}, circumferential wave in body also will cause the wave of coincidence, but its angle of coincidence θ'_c. This take place when the trace of incident and circumferential waves will be equal.

By the way, at low frequencies, the circumferential wave can lead to another resonance – when the track of circumference of the frame and the length of the wave generated by circumferential on a plane incident wave front will coincide. In this case, the body also becomes *«acoustically transparent»*, and acoustic radiation, passed into, will also improve the measurement errors of the gyro.

IV. The occurrence of zones of concentration of acoustic energy in the static liquid part of the suspension. *Zone of the caustic*

In the static liquid part of the suspension, in operating conditions, there may be areas of energy concentration in the form of a confocal surfaces and the form of flat strips. This phenomenon is a consequence of the interference processes. They take the